



MINISTRY OF EDUCATION AND RESEARCH
University POLITEHNICA of Bucharest
Doctoral School of
Industrial Engineering and Robotics

Mihai-Alin M. STAMATE

DOCTORAL THESIS

**Constructive-functional
improvement of hexacopter
drones to ensure dynamic
stability**

SUMMARY

PhD supervisor,
Prof.univ.dr.ing. Cristina PUPĂZĂ (UPB)

- 2023 -

Contents

Introduction	4
List of abbreviations	6
<i>Chapter 1. Current status of the research on the constructive-functional optimization of hexacopter drones.....</i>	<i>7</i>
1.1 Introduction	7
1.2 Conclusions and objectives of the PhD thesis	7
1.3 Research methodology	9
<i>Chapter 2. Contributions on mathematical modelling of hexacopter drones.....</i>	<i>10</i>
2.1 Introduction	10
2.2 Chapter objectives	10
2.3 Overview of the original hexacopter platform developed within the Thesis	11
2.3.1 CAD model of the developed hexacopter.....	11
2.4 Mathematical model of the hexacopter developed in the thesis	11
2.4.1 The hexacopter structure	11
2.4.2 Coordinate systems associated to the drone	12
2.4.3 Drone attitude. Axis of rotation	12
2.4.4 Rotation matrices	13
2.4.5 The hexacopter equations of motion	14
2.4.5.1 Forces acting on the hexacopter	14
2.4.5.2 Moments acting on the hexacopter	15
2.5 Calculation algorithm for determining the dynamic characteristics of the hexacopter	16
2.6 Conclusions, original contributions and published articles	20
<i>Chapter 3. Research on the constructive-functional improvement of hexacopter drones</i>	<i>22</i>
3.1 Introduction	22
3.2 Chapter objectives	22
3.3 Theoretical aspects on drone flight autonomy	22
3.4 Theoretical and practical aspects on choosing optimal combinations for the propulsion system	22
3.4.1. BLDC – Brushless DC Motor	23
3.4.2 The propeller	24
3.4.3 ESC – Electronic Speed Controller	25
3.4.4 The battery	26

3.5 Simulations carried out using specialized online platforms	27
3.5.1 Simulations carried out with the <i>xcopterCalc</i> platform	27
3.5.2 Simulations carried out with the <i>flyeval.com</i> platform	29
3.5.3 Simulations carried out with the <i>drivecalc.de</i> platform	30
3.6 Laboratory tests carried out to determine propulsion system performance	31
3.6.1 Determination of traction force	31
3.6.2 Determination of maximum rotor speed	31
3.6.3 Determination of the motor operating temperature range	32
3.7 Interpretation of results obtained from analytical calculations	33
3.8 Interpretation of the results on choosing of the optimal motor-propeller combination	33
3.9 Conclusions, original contributions and published article	33
<i>Chapter 4. Experimental tests on hexacopter behavior during hover flight</i>	<i>35</i>
4.1 Introduction	35
4.2 Chapter objectives	35
4.3 Equipment variants of the hexacopter developed and tested	35
4.4 Hexacopter tests and results analysis	40
4.4.1 Ground tests	41
4.4.2 Hover flight tests	42
4.4.3 Interpretation of the results	43
4.5 Conclusions, original contributions and published article	49
<i>Chapter 5. FEM analysis of the hexacopter drone using advanced simulation procedures.....</i>	<i>50</i>
5.1 Introduction	50
5.2 Chapter objectives	51
5.3 Aerodynamic study of the hexacopter drone employing numerical methods (CFD)	51
5.3.1 CFD simulation	52
5.3.2 The flow model	53
5.3.3 Simulation scenarios and discussion of results	53
5.4 Static analysis of hexacopter structural elements	55
5.5 Dynamic analysis and hover stability conditions	56
5.5.1 Discussion of the modal analysis results	57
5.6 Impact analysis of the hexacopter	59
5.6.1 Objectives	59
5.6.2 Drop test	59
5.7 Conclusions, original contributions and published articles	60

Chapter 6. Final conclusions, original contributions, and directions for further research 63

 6.1 Final conclusions 63

 6.2 Original contributions 64

 6.2.1 Theoretical contributions 64

 6.2.2 Experimental contributions 64

 A. Laboratory experiments 64

 B. Experiments on flight simulators 65

 C. Field tests 66

 6.2.3 Contributions regarding FEM/CFD modelling and simulation 66

 6.3 Other original contributions 67

 6.4 Further research topics 68

References 69

Introduction

Multicopter UAVs have seen continuous development over the last 10 years as the need for this type of platform has grown continuously and they are used in a wide range of activities and fields such as: inspection of large industrial installations, large buildings and constructions, oil and gas pipelines, inspection of continuous flow machinery in quarries (to monitor temperatures in the area of high friction pits using thermal imaging cameras), inspection of petrochemical installations (to detect cracks, fissures, leaks that may occur in pressure vessels using thermal imaging cameras), etc. , can be equipped with a range of electromagnetic spectrum sensors, gamma ray sensors, biological sensors and chemical sensors, which provide remote sensing functions.

Electromagnetic sensors typically include visual spectrum, infrared or near-infrared cameras as well as radar systems. Other electromagnetic wave detectors such as microwave and ultraviolet spectrum sensors may also be used but are less common. Biological sensors are sensors that can detect the presence of various micro-organisms and other biological factors in the air. Chemical sensors use laser spectroscopy to analyze the concentration of each element in the air.

A UAV possesses almost all the characteristic strengths of a manned aircraft, in addition to overcoming some of the physiological and physical limitations of the pilots and completely avoiding human risk. The absence of the pilot from the cockpit allows UAVs to be operated at their performance limit, thus increasing endurance, payload, altitude ceiling and maneuverability.

Also, advances in micro-electronics and proximity/optical sensors, coupled with the availability of detailed GIS mapping, has led to the development of micro-UAVs that can operate autonomously at very low altitudes in a dense urban environment and provide unbelievable intelligence.

Given the upward trend in the aviation industry in the field of Unmanned Aerial Vehicles (UAVs), especially in the field of multicopter drones, whose advantage over fixed-wing aircraft (airplanes) is that they can hover at a fixed point, which obviously allows their use in remote surveillance applications of different types of targets (industrial, strategic, governmental, public order, etc.), the use of UAVs in the field of surveillance is also a key issue.) and, at the same time, taking into account that the market for components for this type of vehicle is constantly growing and at increasingly low cost, I considered it appropriate to develop such a research topic in my PhD thesis.

* * *

The PhD thesis studied the category of hexacopter drones with rotors arranged in a plane parallel to the ground (flat configuration).

Chapter 1 (State-of-Art) presents the research in the following areas: mathematical modelling, development, based on derived equations, of controllers and command and control systems for multicopter drones in general, with emphasis on hexacopter platforms; constructive solutions for hexacopter platforms; command and control of drones out of direct line-of-sight, some solutions for improving the autonomy of drones, respectively FEM/CFD analysis using the ANSYS FLUENT environment.

Chapter 2 presents the mechanical structure of the physically developed hexacopter, elements of mathematical modelling theory, based on matrix formalization, adapted for a hexacopter drone with rotors mounted in a plane parallel to the ground (flat configuration), and an analytical computational algorithm adapted for the realized hexacopter, starting from the input data of the hexacopter presented in the first sub-chapter, and concluding with the results concerning the dynamic characteristics of the drone (lift force, drag force, moments) during the fixed stationary flight. The study focuses exclusively on the study of the behavior of the drone in stationary flight at a fixed point, these results are then used, in chapter 5, in the FEM/CFD analysis of the hexacopter, using the specialized ANSYS/FLUENT software, to compare the results and validate the simulations performed.

Chapter 3 aims to present in a new practical approach, through comparative analyses, the performance of a hexacopter drone in different equipment variants, starting from theoretical elements

of preliminary calculations and using specialized online platforms. It starts from the hexacopter variant developed in the thesis and analyses four different equipment variants in terms of battery, propellers or engines used. For comparison, simulations are also carried out for two variants of multicopter quadcopter and octocopter drones. With the help of theoretical computational elements, analytical calculations are carried out to determine the theoretical performance of the hexacopter, in particular: flight range, propeller thrust, maximum speed, motor efficiency, motor operating temperature, propeller efficiency. Some of the parameters will be determined using a propulsion system test stand, in particular thrust.

Chapter 4 presents the results of tests carried out both in the laboratory and in the field, during engine start-stop maneuvers, to check that the engines are operating in optimum parameters, stationary flight maneuvers at a fixed point, and roll, pitch and yaw maneuvers, when moving in different flight directions, under atmospheric conditions suitable for these types of activities (temperature: 10°-30°, wind: 1-2 m/s, no precipitation). The flight parameters extracted from the tests were analyzed and corrective action was taken where necessary. All these tests were carried out using the physically realized hexacopter platform used in the thesis. At the end, conclusions were drawn from the tests performed and the interpretation of the flight parameters obtained, i.e., solutions for improving the drone parameters. At the same time, flights with the hexacopter will be carried out, in different battery versions, in order to analyze the flight range.

Chapter 5 presents a complete and complex FEM/CFD analysis study. An aerodynamic study of the hexacopter is performed through CFD simulations, the modelling strategy and the mathematical model used in the turbulence study are presented, CFD simulation scenarios for different wind speeds and directions are analyzed and the simulation results are interpreted, then the CFD simulation results are transferred to the structural elements of the drone and the displacements that occur as a result of the speeds and pressures created by the turbulence occurring when the drone is stationary at a fixed point are analyzed. At the same time, a study of the free vibrations of the hexacopter with implications for the stability of the drone is also performed, and finally a dynamic impact analysis is performed for a scenario of the hexacopter falling from a height of 20 m. And here the results are analyzed in relation to observations during flight tests.

List of abbreviations

No.	Abbrev.	Significance
01	BLDC	Brushless DC Motor
02	BVLOS	Beyond Visual Line-of-Sight
03	CAD	Computer Aided Design
04	CAE	Computer Aided Engineering
05	CFD	Computational Fluid Dynamics
06	CCW	Counterclockwise
07	CW	Clockwise
08	DRONE	Dynamic Remotely Operated Navigation Equipment
09	ESC	Electronic Speed Controller
10	FEM	Finite Element Modeling
11	FFT	Fast Fourier Transform
12	FPV	First Person View
13	GCS	Ground Control Station
14	GIS	Geographic Information System
15	GPS	Global Positioning System
16	HUT	Hexacopter Under Test
17	IMU	Inertial Measurement Unit
18	KV	Parameter of BLDC motor, expressed in RPM/V
19	MOSFET	Metal–Oxide–Semiconductor Field-Effect Transistor
20	OSD	On-Screen Display
21	PA	Automated Pilot
22	PID	Proportional-Integral-Derivative
23	PD	Proportional-Derivative
24	PMU	Power Module Unit
25	ROAV	Remotely Operated Air Vehicle
26	RPAS	Remotely Piloted Aircraft System
27	RPM	Revolutions per Minute
28	RTL	Return to Land
29	R _x	Receiver
30	SBUS	Serial Bus
31	SVTOL	Short Vertical Takeoff and Landing
32	T _x	Transmitter
33	UAV	Unmanned Aerial Vehicle
34	UGV	Unmanned Ground Vehicle
35	UUV	Unmanned Underwater Vehicle
36	VTOL	Vertical Takeoff and Landing

Chapter 1. Current status of the research on the constructive-functional optimization of hexacopter drones

1.1 Introduction

DRONE is a generic name for a whole family of aerial, land, water, and underwater platforms. The term **DRONE** is an acronym from the English language, one of the definitions identified being: **D**ynamic **R**emotely **O**perated **N**avigation **E**quipment. The following main categories of vehicles belong to the DRONE family: UAV - Unmanned Aerial Vehicle, UGV - Unmanned Ground Vehicle and UUV - Unmanned Underwater Vehicle. Aerial drones are also found under other names: UAV - Uninhabited Aerial Vehicle, UAS - Unmanned Aerial System, RPAS - Remotely Piloted Aircraft System, ROAV - Remotely Operated Air Vehicle. UAVs fall into two main categories: fixed wing (aeroplane) and rotor borne (single rotor - helicopter or at least two rotors - multicopter). In the latest period (2020-2022) a third category of UAVs has seen rapid development: fixed-wing UAVs with Vertical Takeoff and Landing (VTOL) capabilities, which combine the capabilities of an aeroplane with those of a multicopter UAV, with either electric or combined propulsion (electric with internal combustion motor) to extend flight range and develop superior flight performance to carry large payloads over long distances. The main purpose for which UAVs were originally developed was their use in military applications and special operations. Subsequently, they have been widely developed and used in an increasing number of civilian applications: law enforcement surveillance missions, firefighting assistance, securing borders, strategic and governmental targets, detecting illegal hunting, measuring landslides, monitoring incidents involving crowds of people, inspecting large industrial facilities, large buildings and constructions, oil and gas pipelines, inspection of continuous-flow machinery in quarries (to monitor temperatures in the area of high-friction pits using thermal imaging cameras), inspection of petrochemical facilities (to detect cracks, fissures, leaks in pressure vessels using thermal imaging cameras), and more recently (2020-2022) home parcel delivery, warehouse stock management using specialised software, passenger transport, air travel, etc.

The PhD thesis deals with the category of rotor-supported UAVs (multicopter), specifically the category of hexacopter drones. Due to their low-cost efficiency and numerous possibilities for use in a wide range of civil, commercial, and industrial applications (inspection of power lines, inspection of road infrastructure, bridges, inspection of oil pipelines, inspection of industrial facilities of strategic interest - oil refineries, nuclear power plants, inspection of disaster areas), multicopter UAVs have already been the subject of study for more than a decade. Since then, numerous research studies have been carried out on the modelling and development of actuation, command and control systems and the development of various design solutions for them. Chapter I aims to present the research in the areas of: mathematical modelling, equation-based development of controllers and command and control systems for multicopter drones in general, with a focus on hexacopter platforms; constructive solutions for hexacopter platforms; command and control of drones out of line-of-sight, some solutions for improving drone autonomy, and FEM/CFD analysis using the ANSYS FLUENT environment. At the end of the chapter, conclusions are drawn regarding the issues presented and directions for further work in the following chapters of the thesis.

In this summary only the conclusions of the extended state of art study regarding hexacopter drones were included. The Thesis comprises more than 40 pages with a synthetic review of recent and important published perspectives on this topic.

1.2 Conclusions and objectives of the PhD thesis

Conclusions

- the reviewed articles presented theoretical and experimental research, either through the use of simulation environments or through practical laboratory or field tests, demonstrating their effectiveness according to derived mathematical relationships. These will form the fundamentals for the development of the mathematical model of the hexacopter.

- in terms of autonomy, in the initial test version the hexacopter is equipped with a LiPo battery with a capacity of 6600 mAh, which gives the drone, at a take-off mass of about 2.77 kg, an operating time of about 10-12 minutes. For a long-distance mission, 10-12 minutes is extremely short. It is therefore necessary to present some aspects of LiPo batteries and how they can be coupled together, so that, by equipping drones with different battery variants of different capacities and voltages, it is possible to extend the operating time of the drone, obviously taking into account the total mass of the drone. A high-capacity battery also has a high mass, therefore the more high-capacity batteries are fitted, the greater the total take-off mass of the drone. That is why a trade-off between amperage-voltage-total mass of the drone must be made in order to find the best solution for powering the drone for as long as possible.
- in the case of the hexacopter used in the Thesis, modeling and simulation will be carried out using the computer aided environments appropriate for the study of the influence of the variability of atmospheric factors on the flight behaviour of multicopter drones in automatic and manual operation respectively. For the FEM/CFD analysis stage, the 3D virtual model of the hexacopter developed in SolidWorks will be employed. In this stage, studies carried out with finite element analysis utilities will allow modelling the influence of airflow regimes, which influence the flight regime and functional stability of the hexacopter, for different sets of specific values of atmospheric parameters. Having also the physical prototype (model) of the hexacopter, some of these influencing factors on the drone behaviour will be tested experimentally. The conclusions drawn from this step will help to define the optimal operating regimes of the hexacopter under different conditions of atmospheric parameter variability.

Objectives of the PhD thesis
A. Main objectives
- Design and upgrading of a hexacopter UAV platform for monitoring, surveillance and inspection of industrial facilities.
- Fundamentals of mathematical modelling of hexacopter drones.
- Improving the construction and performance of hexacopter drones, with a focus on extending flight autonomy and payload carrying capacity, depending on the equipment variant.
- Experimental testing of hexacopter behaviour during fixed-point flight manoeuvres on the original experimental model.
- FEM analysis of the hexacopter drone using advanced simulation procedures.
B. Secondary objectives
- Improved CAD model of the hexacopter prototype.
- Construction of the hexacopter and its upgrade in two versions.
- Development of the mathematical model and extraction of the equations of motion of the hexacopter.
- Presentation of the aspects of rotor dynamics and the geometrical elements of the propeller.
- Adaptation of a calculation algorithm for determining the dynamic characteristics of the hexacopter developed in the Thesis.
- Research on the determination of the best battery combinations - Electronic Speed Controller (ESC) - Brushless DC motor (BLDC) - propeller propulsion system, depending on the size of the drone frame, to achieve maximum efficiency (range vs. payload carried).

- Simulations of hexacopter performance using dedicated online platforms.
- Laboratory tests to determine the performance of the propulsion system and interpret the results.
- Carry out ground tests on the hexacopter in the two different configurations.
- Carry out flight tests on the hexacopter in the two equipment variants to determine the best performance parameters during fixed-point flight in certain atmospheric conditions.
- Determine the flight autonomy of the hexacopter by carrying out flights in the field in different equipment variants with batteries of different capacities.
- Ground and in-flight verification of the command and control chain using the Mission Planner ground control station.
- Ensuring the stability of the drone during stationary flight manoeuvres;
- Perform a complete and complex simulation model for all types of CAE analysis;
- Validate the FEM computational model;
- Synchronisation of analytical, experimental and numerical results;
- Use the results of the FEM study to improve flight parameters (e.g., rotor speeds).

1.3 Research methodology

The research methodology has been summarized in the following diagram.

The diagram in Figure 1 follows the sequence of the research and it illustrates through representative images the most important aspects of the research. Its structure follows the chapters of the thesis, and it is focused on the most important achievements, especially on the achievement of the PhD thesis objectives, starting with the state-of-art study regarding hexacopter drones, followed by the constructive approach of the hexacopter and the mathematical modeling. It continues with the simulations and laboratory test performed, then the upgrade of the drone, followed by ground and flight test, and culminating with the CFD/FEM approach.

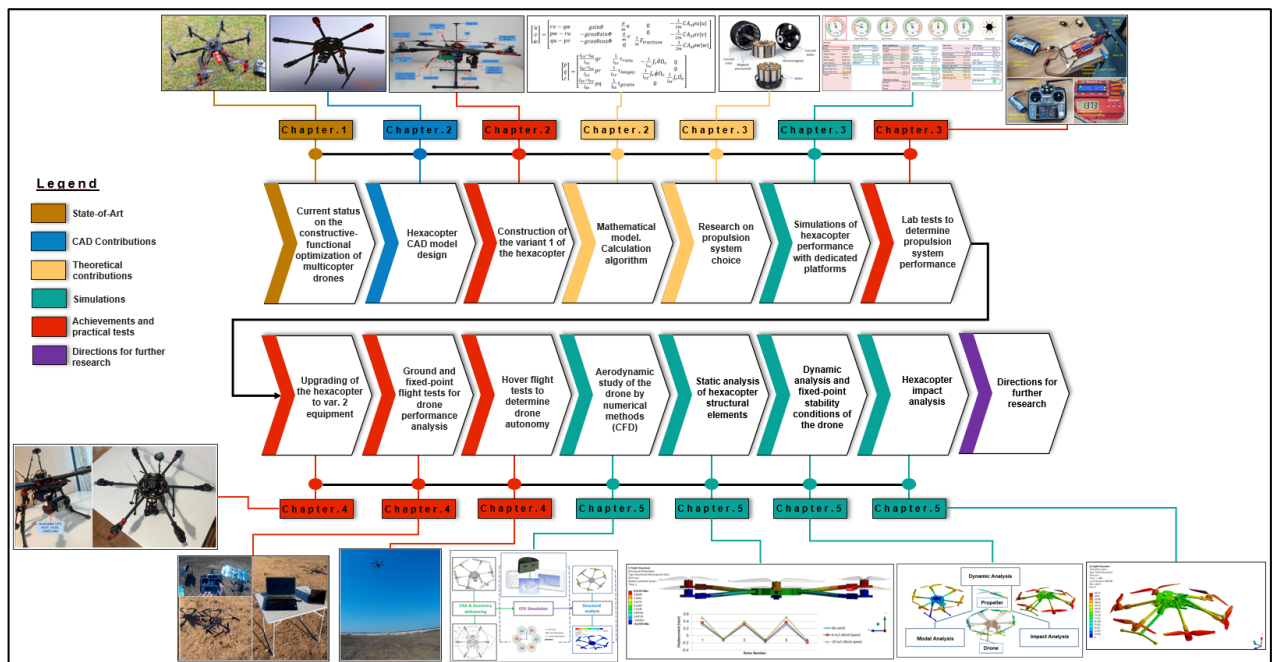


Fig. 1 The research methodology

Chapter 2. Contributions on mathematical modelling of hexacopter drones

2.1 Introduction

Chapter 2 presents, in the first part, the **mechanical structure of the physically developed hexacopter**, as presented in the paper **Stamate et. al [22]**, together with its equipment with the avionics components for the command and control of the drone, the video subsystem consisting of the gimbal with three-axis stabilization and the photo-video camera, respectively the radio control used by the operator to send commands from the ground to the hexacopter. At the end of the first subchapter, the technical data sheets of these components are included. In the second part, **elements of mathematical modelling theory, based on matrix formalization, adapted for a hexacopter drone with the rotors mounted in a plane parallel to the ground (flat configuration)**, as presented in the article **Stamate et. al [23]**, mathematical relations describing the movements performed in three-dimensional space by the drone, forces and aerodynamic moments occurring during flight are presented. In the case of the hexacopter studied in this Thesis, operation is based solely on varying the rotor speed. Concepts of rotor dynamics are explained, in order to highlight the main forces and moments that develop on the propeller blade, respectively the geometrical elements of the propeller, necessary further for the calculation methodology presented in the third subchapter. In the third part of Chapter 2 the analytical calculation algorithm is developed, starting from the input data of the hexacopter presented in the first subchapter, which ends with the results concerning the dynamic characteristics of the drone (lift force, drag force, moments) during the fixed-point hover flight. The study focuses exclusively on the behavior of the drone in stationary flight at a fixed point. These results are then used, in Chapter 5, in the FEM/CFD analysis of the hexacopter, to compare the results and validate the numerical simulations.

The **analytical calculation methodology** developed in this chapter has been adapted for the hexacopter version of a computational model applied to a quadcopter presented in a published work by Rotaru [19]. In recent years, numerous studies have been carried out on the mathematical modelling of multicopter UAVs, analyzing their behavior for different flight regimes. In general, the studies have focused on multicopter drones with rotor blades whose propellers are mounted at a fixed angle of incidence (so-called fixed-pitch blades), where the operation is mainly based on the variation of the speed of the electric motors, depending on the chosen configuration. Since this type of aerial vehicle belongs to the VTOL (Vertical Take-Off and Landing) family, the study of the mechanical structure, forces, moments, laws of motion, kinematics and dynamics of these aerial vehicles differs from that of conventional aircraft, but not radically and entirely. Among the many challenges faced by conventional UAVs, such as short flight duration, limited ability to carry a payload, instability in operation in the outdoor environment under the action of certain atmospheric factors, one extremely important element is their under-actuation, i.e., the inability to exert certain forces in some directions of the drone frame.

2.2 Chapter objectives

- CAD model design of the hexacopter prototype.
- Improvement of the hexacopter construction in version 1
- Development of the mathematical model and extraction of the equations of motion of the hexacopter.
- Presentation of the rotor dynamics and propeller geometry.
- Adaptation of a computational algorithm for determining the dynamic characteristics of the hexacopter developed in the Thesis.

2.3 Overview of the original hexacopter platform developed within the thesis.

The solution designed for the practical development is a hexacopter in X-configuration, with the arrangement of the rotors as shown in Fig. 2.1. The arrangement of the rotors and the operation of the hexacopter are described in subchapter 2.4.

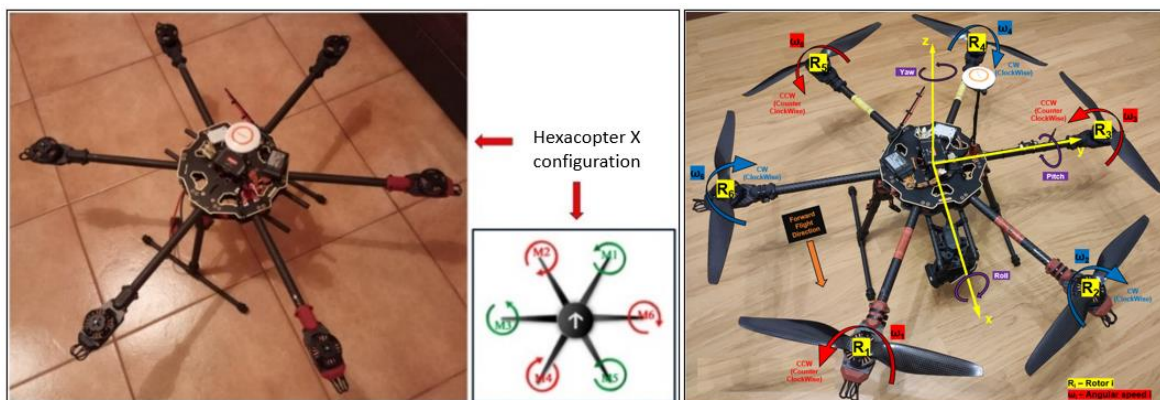


Fig. 2.1 Adopted solution - hexacopter in X configuration.

2.3.1 CAD model of the developed hexacopter

The CAD model of the hexacopter was built using SolidWorks software (Fig. 2.2).

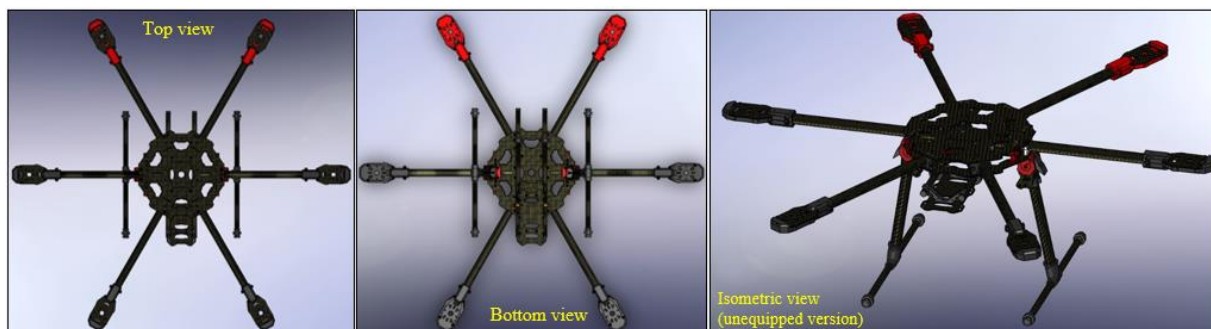


Fig. 2.2 CAD model of the hexacopter - top view, bottom view

2.4 Mathematical model of the hexacopter developed in the Thesis.

2.4.1 The hexacopter structure

A multicopter drone is an under-actuated, dynamically unstable aerial vehicle, having a six degrees of freedom system, which requires flight stability control. The six degrees of freedom consist of translational and rotational motions in three dimensions. Translational motion is created by changing the direction and magnitude of the propeller thrust (oriented in the opposite direction to gravity). For fixed rotor blades (such as those fitted to the hexacopter in this Thesis) the rotational motion required to tilt the thrust vector is achieved by individually changing the propeller speed in order to create torques around the center of rotation. The hexacopter designed in the Thesis is built in an X-configuration, with the 6 motors mounted on 6 support arms, arranged, in groups of 3 (R1, R3, R5), respectively (R2, R4, R6), at 120° to each other, on a symmetrical frame, constructed of carbon fiber, with three sets of CW and CCW propellers mounted respectively.

2.4.2 Coordinate systems associated to the drone.

To analyze the behavior of the drone, two coordinate systems are used to represent the position and orientation of the hexacopter in the three dimensions, namely: the coordinate system associated with the ground (inertial) and the coordinate system associated with the frame of the drone (Fig. 2.3a), presented also in the paper **Stamate et. al [23]**. In order to keep the hexacopter at a fixed point (hover) it is necessary to rotate the rotors in different directions, so that three rotors rotate clockwise (CW - Clockwise) and the other three rotate trigonometrically (CCW - Counterclockwise).

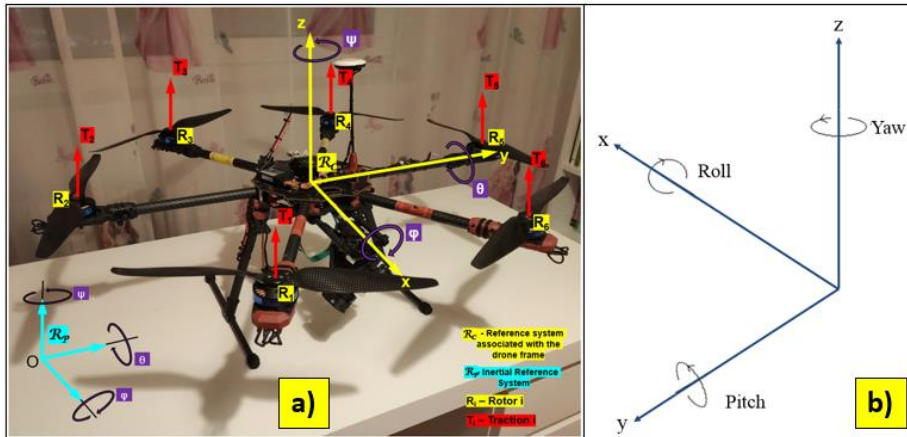


Fig. 2.3 a) Inertial and associated coordinate systems of the drone; b) Rotational motions on the three coordinate axes: roll (x-axis), pitch (y-axis) and yaw (z-axis)

2.4.3 Drone attitude. Axis of rotation

The attitude of the drone is the orientation of the drone's coordinate system relative to the inertial (ground-bound) coordinate system. It represents the rotation of the drone about its x, y, and z axes. In this case, using the right-hand rule, the three classic aircraft motions of roll, pitch, and yaw result (Fig. 2.3b).

2.4.3.1 Roll is the rotational movement about the x-axis achieved by increasing/decreasing the speed of 1, 2 and 3 and simultaneously increasing/decreasing the speed of rotors 4, 5 and 6. During this maneuver, a rotational torque is created about the x-axis and thus an angular acceleration occurs. The angle of rotation for the rolling motion is denoted by φ and measured in rad/s (Fig. 2.4a).

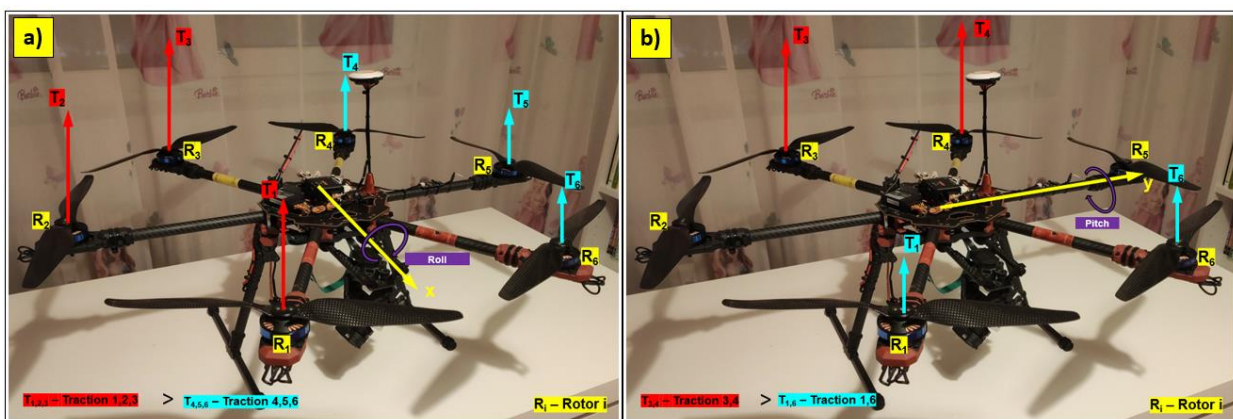


Fig. 2.4 a) Rolling motion (φ); b) Pitch motion (θ)

2.4.3.2 Pitch is the rotational movement about the y-axis and is achieved by increasing/decreasing the speed of rotors 1 and 6 and simultaneously increasing/decreasing the speed of rotors 3 and 4.

Since the direction of the y-axis coincides with the position of rotors 2 and 5, they do not affect the pitch. The pitch angle is denoted by θ and is also measured in rad/s (Fig. 2.4b).

2.4.3.3 Yaw is the rotary motion about the z-axis. In this motion each propeller creates a rotational torque about the z-axis as it rotates. Thus, this torque is directed in the opposite direction to the direction of rotation of the rotor. If the propeller rotates clockwise, it will create a trigonometric rotation about the z-axis. The spinning motion is achieved by decreasing/increasing the speed of rotors 1, 3 and 5 and simultaneously increasing/decreasing the speed of rotors 2, 4 and 6. The angle of rotation for the gyration motion is denoted by ψ and measured in rad/s (Fig. 2.5).

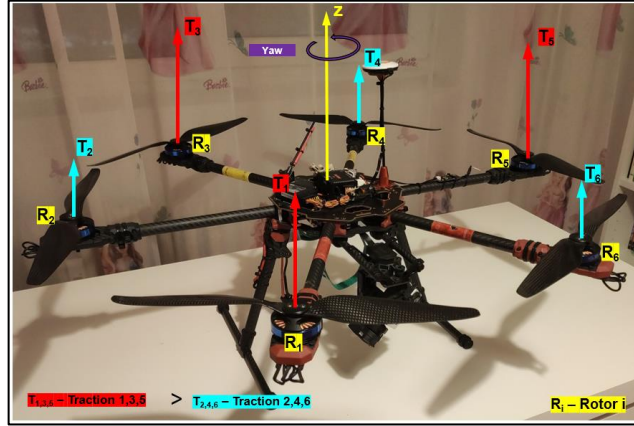


Fig. 2.5 Yaw motion (ψ)

2.4.4 Rotation matrices

The inertial coordinate system is a fixed reference system, so when defining a route that the drone is going to follow, this coordinate system has to be employed to express the movement of the drone relative to a fixed body. The coordinate system associated with the drone frame (RC) is chosen to be aligned with the sensors mounted on the drone, so that the x-axis will be oriented in the forward direction (red motor mounting heads), the y-axis oriented to the left and the z-axis oriented upwards, perpendicular to the plane determined by the x- and y-axes. To represent the rotational motions of the coordinate system associated with the drone frame (RC) relative to the coordinate system associated with the ground (RP - inertial reference system), one of the most common transformation methods will be used, namely the rotation matrix. The rotation matrix, when rotating the drone on the three axes, is composed of a series of three rotation matrices, one for each rotation axis.

2.4.4.1 Yaw rotation matrix (z-axis)

$$R_C^P(\psi) = \begin{bmatrix} \cos\psi & \sin\psi & 0 \\ -\sin\psi & \cos\psi & 0 \\ 0 & 0 & 1 \end{bmatrix} \quad (2.1)$$

2.4.4.2 Pitch rotation matrix (y-axis)

$$R_C^P(\theta) = \begin{bmatrix} \cos\theta & 0 & -\sin\theta \\ 0 & 1 & 0 \\ \sin\theta & 0 & \cos\theta \end{bmatrix} \quad (2.2)$$

2.4.4.3 Roll rotation matrix (x-axis)

$$R_C^P(\phi) = \begin{bmatrix} 1 & 0 & 0 \\ 0 & \cos\phi & \sin\phi \\ 0 & -\sin\phi & \cos\phi \end{bmatrix} \quad (2.3)$$

By performing the three rotations in the order shown above, the drone - earth (inertial) frame rotation matrix is obtained R_C^p .

$$R_C^p = R_C^p(\psi)R_C^p(\theta)R_C^p(\phi) = \begin{bmatrix} \cos\psi \cos\theta & \cos\psi \sin\theta \sin\phi - \sin\psi \cos\phi & \cos\psi \sin\theta \cos\phi + \sin\psi \sin\phi \\ \sin\psi \cos\theta & \sin\psi \sin\theta \sin\phi + \cos\psi \cos\phi & \sin\psi \sin\theta \cos\phi - \cos\psi \sin\phi \\ -\sin\theta & \cos\theta \sin\phi & \cos\theta \cos\phi \end{bmatrix} \quad (2.4)$$

R_C^p is an orthogonal matrix, which means that its inverse matrix is equal to its transpose, so the transformation of the rotation matrix earth (inertial) - drone frame is done with the relation:

$$(R_C^p)^{-1} = (R_C^p)^T = R_p^C \quad (2.5)$$

2.4.5 The hexacopter equations of motion

In the following, the hexacopter is considered to be a rigid solid with a symmetrical structure, with the center of gravity located in the center of the drone. Taking this into account, the Newton-Euler formulation has been used to describe the dynamics of a rigid solid (the hexacopter in this case) on which external aerodynamic forces and moments act.

The forces F^C (forces acting on the drone frame [N]) and moments τ^C (moments acting on the drone frame [Nm]) will be defined accordingly in the relationships below. The two main forces acting on the drone are the force of gravity (G) and the thrust force generated by the rotation of the rotors, through the entrainment of air currents. Also acting on the multicopter in a negative direction, which tends to oppose forward or upward motion, is the drag force, or friction with atmospheric air.

The gravitational force will always have a direction along the z-axis and a downward direction and can be expressed as follows [13]:

$$F_{gravity}^C = R_p^C \begin{bmatrix} 0 \\ 0 \\ -mg \end{bmatrix} = \begin{bmatrix} mg \sin\theta \\ -mg \cos\theta \sin\phi \\ -mg \cos\theta \cos\phi \end{bmatrix} \quad (2.6)$$

2.4.5.1 Forces acting on the hexacopter.

Traction (lift force) is the horizontal lift force that allows the hexacopter to fly horizontally and hover. During the hover maneuver this thrust force can be approximated by equation [13]:

$$F_{traction}^C = b \sum_{i=1}^6 \Omega_i^2 \quad (2.7)$$

where: b - traction constant, measured in Ns^2

During flight, a drag force is applied to the frame of a drone to resist movement. This force will affect the accelerations on x and y, and can be expressed, during the flight maneuver at constant altitude, by the equation below [13]:

$$F_{drag}^C = \begin{bmatrix} -\mu u \\ -\mu v \\ 0 \end{bmatrix} \quad (2.8)$$

where: μ - constant, measured in kg/s.

Air resistance is proportional to the square of the velocity, shape, and size of the object, according to the relation [13]:

$$F_{air}^C = \begin{bmatrix} -\frac{1}{2} CA_x \rho u |u| \\ -\frac{1}{2} CA_y \rho v |v| \\ -\frac{1}{2} CA_z \rho w |w| \end{bmatrix} \quad (2.9)$$

where: C - dimensionless friction constant; A_i - cross-sectional area, measured in m^2 ; ρ - air density, measured in kg/m^3 ; w - linear velocity along the z-axis (relative to the drone frame coordinate system).

2.4.5.2 Moments acting on the hexacopter.

By varying the speed of the rotors, rotational moments of the x, y, and z axes can be obtained, resulting in gyration, roll, and pitch maneuvers. Figure 2.6 shows the lengths and angles of the motor support arms arranged relative to the center of gravity of the drone, which is the distance from the rotor to the axis of rotation, where Ω [rad/s] is the rotational speed of the propeller, l [m] is the length of the support arm of the motor-propeller assembly and d [Nms^2] is a drag factor.

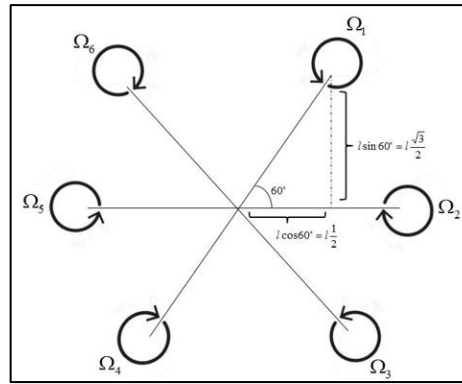


Fig. 2.6 Rotor distances from the center of gravity of the drone [13]

Decreasing $\Omega_1, \Omega_2, \Omega_3$ and increasing $\Omega_4, \Omega_5, \Omega_6$ will result in a positive rolling moment [13].

$$\tau_{roll} = bl(-\Omega_2^2 + \Omega_5^2 + \frac{1}{2}(-\Omega_1^2 - \Omega_3^2 + \Omega_4^2 + \Omega_6^2)) \quad (2.10)$$

Decreasing Ω_1, Ω_6 and increasing Ω_3, Ω_4 will result in a positive pitching moment [13].

$$\tau_{pitch} = bl \frac{\sqrt{3}}{2} (-\Omega_1^2 + \Omega_3^2 + \Omega_4^2 - \Omega_6^2) \quad (2.11)$$

Decreasing $\Omega_1, \Omega_3, \Omega_5$ and increasing $\Omega_2, \Omega_4, \Omega_6$ will result in a positive yawing moment [13].

$$\tau_{yaw} = d(-\Omega_1^2 + \Omega_2^2 - \Omega_3^2 + \Omega_4^2 - \Omega_5^2 + \Omega_6^2) \quad (2.12)$$

The rotational motion of the propellers leads to the production of a gyroscopic effect defined by the relation [13]:

$$\tau_{gyroscopic.effect} = \begin{bmatrix} -J_r \Omega_r \dot{\theta} \\ J_r \Omega_r \dot{\phi} \\ 0 \end{bmatrix} \quad (2.13)$$

$$\Omega_r = -\Omega_1 + \Omega_2 - \Omega_3 + \Omega_4 - \Omega_5 + \Omega_6 \quad (2.14)$$

Where: J_r - moment of inertia of the propeller, measured in $[Nms^2]$; Ω_r - total propeller speed $[rad/s]$.

The different values of the rotational accelerations of the propellers produce an anti-inertial torque moment, defined by the relation [13]:

$$\tau_{anti-torque} = \begin{bmatrix} 0 \\ 0 \\ J_r \dot{\Omega}_r \end{bmatrix} \quad (2.15)$$

The final equations of motion of the hexacopter are given in rel. 2.16÷2.17, and their relationships with the angular velocities of the propellers are described by rel. 2.7, 2.10, 2.11, 2.12, and 2.14, respectively [13].

$$\begin{bmatrix} \dot{u} \\ \dot{v} \\ \dot{w} \end{bmatrix} = \begin{bmatrix} rv - qw & g \sin \theta & \frac{\mu}{m} u & 0 & -\frac{1}{2m} C A_x \rho u |u| \\ pw - ru & -g \cos \theta \sin \Phi & \frac{\mu}{m} v & 0 & -\frac{1}{2m} C A_y \rho v |v| \\ qu - pv & -g \cos \theta \cos \Phi & 0 & \frac{1}{m} F_{traction} & -\frac{1}{2m} C A_z \rho w |w| \end{bmatrix} \quad (2.16)$$

$$\begin{bmatrix} \dot{p} \\ \dot{q} \\ \dot{r} \end{bmatrix} = \begin{bmatrix} \frac{I_{yy} - I_{zz}}{I_{xx}} qr & \frac{1}{I_{xx}} \tau_{roll} & -\frac{1}{I_{xx}} J_r \dot{\theta} \Omega_r & 0 \\ \frac{I_{zz} - I_{xx}}{I_{yy}} pr & \frac{1}{I_{yy}} \tau_{pitch} & \frac{1}{I_{yy}} J_r \dot{\phi} \Omega_r & 0 \\ \frac{I_{xx} - I_{yy}}{I_{zz}} pq & \frac{1}{I_{zz}} \tau_{yaw} & 0 & \frac{1}{I_{zz}} J_r \dot{\Omega}_r \end{bmatrix} \quad (2.17)$$

After the presentation of the geometrical elements of the propeller, respectively the aspects concerning the rotor dynamics, the analytical calculations to determine the dynamic characteristics of the hexacopter are performed.

2.5 Calculation algorithm for determining the dynamic characteristics of the hexacopter.

The dynamic performance of the hexacopter will be determined analytically by implementing the presented computational algorithm. The analytical method involves certain approximations and simplifying assumptions which, when added together throughout the calculation algorithm, ultimately influence the results obtained. Inconsistencies may also occur if there are differences between the technical data of the hexacopter components, provided by the manufacturer, and the actual technical data of the components, calculated or measured with specific instruments, or if the technical data of the components are insufficient. In the calculation algorithm, the technical characteristics of the components of the hexacopter designed in the thesis shall be entered as initial data. The initial data shall be chosen from manufacturers' specifications or laboratory measurements or from tables of international constants.

2.5.1 Calculation of motor speed loss

During the operation of the hexacopter part of the electrical voltage from the battery to the motors is lost due to the internal resistance of the electric motor windings. This leads to a decrease in the working speed of the motors and a decrease in their efficiency.

In the ideal case the motor speed at 14.8 V operating voltage is given by the relation:

$$\mathbf{rpm}_{ideal} = KV \cdot U_i = 620 \cdot 14.8 V = 9176 \text{ RPM} \quad (2.18)$$

The lost voltage is calculated with the relation:

$$U_p = R_s \cdot I_i = 0.126 \Omega \cdot 14A = 1.746 V \quad (2.19)$$

The loss per spiral is determined as follows:

$$P_s = R_s \cdot I_i^2 = 0.126 \Omega \cdot 14^2 A = 24.696 W \quad (2.20)$$

In the real case the motor speed is given by the relation:

$$rpm_{real} = KV \cdot (U_i - U_p) = 620 \cdot (14.8V - 1.746V) = 8082.32 \text{ RPM} \quad (2.21)$$

It follows that the loss of speed is:

$$rpm_{ideal} - rpm_{real} = 9176 - 8082.32 = 1093.68 \text{ RPM} \quad (2.22)$$

The maximum rotor speed will be determined experimentally in Chapter 3 on the test stand using the tachometer.

2.5.2 Calculation of the airflow velocity on the rotor blade profile (tangential velocity)

$$\text{According to rel. (2.21) } rpm_{real} = 8082.32 \text{ RPM} = rps_{real} = 134.7053 \text{ rot/s} \quad (2.23)$$

We calculate the angular velocity of the rotor:

$$\omega = rps_{real} \cdot 2 \cdot \pi = 134.7053 \frac{\text{rot}}{\text{s}} \cdot 2 \cdot \pi = 846.3786 \frac{\text{rad}}{\text{s}} \quad (2.24)$$

The tangential velocity at the blade tip is determined with the relation:

$$V_{tang.at.blade.tip} = \omega \cdot R_p = 846.3786 \frac{\text{rad}}{\text{s}} \cdot 0.1651 \text{ m} = 127.0414 \frac{\text{rad}}{\text{s}} \quad (2.25)$$

Determine the tangential velocity at the reference radius according to the relation:

$$V_{tangential} = \omega \cdot r = 846.3786 \frac{\text{rad}}{\text{s}} \cdot 0.1001 \text{ m} = 84.6943 \frac{\text{rad}}{\text{s}} \quad (2.26)$$

2.5.3 Determination of Reynolds number (Re) as a function of propeller profile

For the calculation of the thrust force and the drag force, it is necessary to find the Reynolds number (Re) in order to determine the thrust and drag coefficients from the analysis of the blade profile pole, based on the Reynolds number (Re) obtained. This is calculated with the relation:

$$Re = \frac{\rho \cdot \omega \cdot R_p \cdot c_{profil}}{\mu} = \frac{1.225 \cdot 846.3786 \cdot 0.1501 \cdot 0.034}{1.81 \cdot 10^{-5}} = 292335.6514 \quad (2.27)$$

Following the Reynolds number determination, the APC 13X55 MR propeller model was identified as having aerodynamic and construction characteristics close to the propeller equipping the hexacopter (Tarot 1355). The APC 13X55 MR propeller profile is APC12 (taken from the manufacturer's specifications) [2]. This APC12 profile is equivalent to the NACA 4412 profile (naca4412-il) whose performance, at different Reynolds numbers, could be identified for the extraction of the two coefficients mentioned above [1]. An incidence angle of 10° is considered for the hexacopter maneuvers. Thus, in Fig. 2.7, the characteristics of the NACA 4412 (naca4412-il) profile can be seen, for Reynolds numbers ≥ 200000 , from which the values for the lift coefficient (C_L) and the drag coefficient (C_D) can be extracted. At an incidence angle of 10° C_L has a value of about 1.3 and C_D has a value of about 0.025.

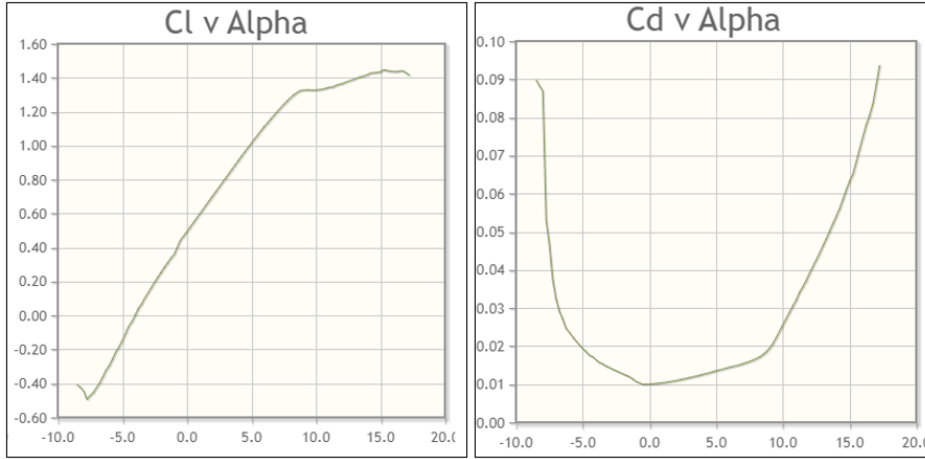


Fig. 2.7 C_L – Lift Coefficient and C_D – Drag Coefficient, as a function of angle of incidence, for Reynolds numbers ≥ 200000 [1]

2.5.4 Calculation of the pitch angle

2.5.4.1 Calculation of the ideal pitch angle

The ideal pitch angle is calculated by applying the relationship:

$$\varphi = \text{atan}\left(\frac{H_{pitch.angle}}{2 \cdot \pi \cdot 0.75 \cdot R_{blade}}\right) = \text{atan}\left(\frac{0.1397}{2 \cdot \pi \cdot 0.75 \cdot 0.1651}\right) = 10.1795 \text{ deg} \quad (2.28)$$

2.5.4.2 Calculation of the actual pitch angle

The actual pitch is calculated by applying the relation:

$$H_r = 2 \cdot \pi \cdot r \cdot \text{tg}(9.6) = 0.1113 \text{ m} \quad (2.29)$$

From relation (2.29) the actual pitch angle results

$$\varphi_r = \text{atan}\left(\frac{H_r}{2 \cdot \pi \cdot 0.75 \cdot R_{pala}}\right) = \text{atan}\left(\frac{0.1113}{2 \cdot \pi \cdot 0.75 \cdot 0.1651}\right) = 8.1417 \text{ deg} \quad (2.30)$$

2.5.5 Calculation of Lift and Drag Forces

After extracting the data for C_L and C_D , the two main aerodynamic forces acting on the rotor are calculated.

2.5.5.1 Calculation of Lift Force

To calculate the lift force, it is necessary to find the area of a blade with the relation:

$$S_p = R_p \cdot c_{profil} = 0.1501 \cdot 0.034 = 0.0051 \text{ m}^2 \quad (2.31)$$

The lift force of a rotor is determined with the relation:

$$L_{rotor} = \frac{1}{2} \cdot \rho \cdot V_{tangential}^2 \cdot S_p \cdot C_L = \frac{1}{2} \cdot 1.225 \cdot \left(84.6943 \frac{\text{rad}}{\text{s}}\right)^2 \cdot 0.0051 \text{ m}^2 \cdot 1.3 = 29.1486 \text{ N} \quad (2.32)$$

We can determine the theoretical maximum mass that can be lifted by a motor with the relation:

$$m_{rotor} = \frac{L_{rotor}}{g} = \frac{29.1486}{9.81} = 2.97 \text{ kg} \quad (2.33)$$

The value obtained according to rel. (2.33) is purely theoretical, its value may change considerably depending on the type of profile considered in the choice of C_L .

The theoretical maximum mass the hexacopter can lift can be written with the relation:

$$m_{hexacopter} = 6 \cdot \frac{L_{rotor}}{g} = 6 \cdot \frac{29.1486}{9.81} = 17.8279 \text{ kg} \quad (2.34)$$

2.5.5.2 Calculation of Drag Force

To calculate the drag force, it is necessary to find the area of the circle determined by the rotation of a propeller, with the relation:

$$A_{rotor} = \pi \cdot R_p^2 = 3.14 \cdot 0.1501^2 = 0.0708 \text{ m}^2 \quad (2.35)$$

The drag force of a rotor is determined with the relation:

$$D = \frac{1}{2} \cdot \rho \cdot V_{tangential}^2 \cdot S_p \cdot C_D = \frac{1}{2} \cdot 1.225 \cdot \left(84.6943 \frac{rad}{s}\right)^2 \cdot 0.0051 m^2 \cdot 0.025 = 0.5605 N \quad (2.36)$$

2.5.5.3 Calculation of traction force

In order to determine the thrust required by a motor to lift the drone in its current configuration, according to the input data, it is necessary to determine the thrust coefficient according to the relation:

$$C_T = \frac{Gravity}{no.rotors \cdot \rho \cdot A_{rotor} \cdot (\omega \cdot R_p)^2} = \frac{2.77 \cdot 9.8}{6 \cdot 1.225 \cdot 0.0708 \cdot \left(846.3786 \frac{rad}{s} \cdot 0.0051\right)^2} = 0.0032 \quad (2.37)$$

Using the value obtained in rel. (2.37) we find the thrust required by a motor to lift the drone:

$$Traction = C_T \cdot \rho \cdot A_{rotor} \cdot (\omega \cdot R_p)^2 = 0.0032 \cdot 1.225 \cdot 0.0708 \cdot \left(846.3786 \frac{rad}{s} \cdot 0.0051\right)^2 = 4.5274 N \quad (2.38)$$

2.5.6 Calculating the necessary power for a motor

For a maximum working voltage of 14.8V and a maximum current of 17.5A the maximum available motor power will be:

$$P_{maximum.available} = U \cdot I = 14.8 V \cdot 17.5 A = 259 W \quad (2.39)$$

In order to determine the maximum required mechanical power of a motor it is necessary to determine the total drag coefficient and the power coefficient.

2.5.6.1 Determination of the total resistance coefficient (C_X)

It is determined on the basis of the two coefficients C_L and C_D determined above. Thus, the relation for calculating the total resistance coefficient of the motor, and thus of the rotor, is given by the relation:

$$C_X = C_D \cdot (1 + C_L^2) = 0.025 \cdot (1 + 1.3^2) = 0.0673 \quad (2.40)$$

2.5.6.2 Determination of power coefficient (C_P)

For the calculation of this coefficient, it is necessary to determine the overall filling coefficient, according to rel.:

$$\sigma_{el} = \frac{n \cdot S_p}{A_{rotor}} = \frac{2 \cdot 0.0051}{0.0708} = 0.1442 \quad (2.41)$$

where: σ_{el} - the overall fill coefficient (is the ratio of the surface projection of the blades on the propeller disc to the propeller area); n is the number of blades; S_p is the area of a blade.

Thus, the power coefficient is determined with the relation:

$$C_P = C_T \cdot \sqrt{\frac{C_T}{2}} + \sigma_{el} \cdot \frac{C_X}{8} = 0.0013 \quad (2.42)$$

2.5.6.3 Determining the maximum required mechanical power of a motor.

After finding the power coefficient according to relation (2.42), we can calculate the maximum required mechanical power of a motor according to the relation:

$$P_{maximum.necessary} = \rho \cdot A_{rotor} \cdot (\omega \cdot R_p)^3 \cdot C_P = 1.225 \cdot 0.0708 \cdot \left(846.3786 \frac{rad}{s} \cdot 0.0051\right)^3 \cdot 0.0013 = 238.6415 W \quad (2.43)$$

2.5.6.4 Determining the useful power of a motor

Knowing the two power parameters of a motor, i.e., maximum available mechanical power and maximum required mechanical power, we can find the useful power of a motor, using the relation:

$$P_{useful} = P_{maximum.available} - P_{maximum.necessary} = 259 W - 238.6415 W = 20.3585 W \quad (2.44)$$

2.5.7 Calculation of (theoretical) climb rate at ground level.

After determining the useful power of a motor, we can calculate the rate of climb of the hexacopter at ground level according to the relation:

$$V_{ascensional} = \frac{6 \cdot P_{useful}}{Gravity} = \frac{6 \cdot 20.3585}{2.77 \cdot 9.8} = 4.4967 \frac{m}{s} \quad (2.45)$$

2.5.8 Determination of calculation relationships for forces and moments acting on the hexacopter in stationary fixed-point flight

The following are the computational relationships for hexacopter maneuvers in stationary fixed-point flight. For these maneuvers the forces and moments acting on the drone will be calculated analytically.

2.5.8.1 Moments acting on the rotor.

The following moments act on the rotor: the rotor resisting moment, the profile resisting moment and the induced resisting moment. The following relationships are used to calculate these.

2.5.8.1.1 Anti-torque resistant moment acting on the rotor.

It is determined with the relation:

$$M_{resistant} = n \cdot \int_0^{R_p} (C_D + \varphi_r \cdot C_L) \cdot \frac{\rho}{2} \cdot (r \cdot \omega)^2 \cdot c_{profil} \cdot r dr = 0.7941 Nm \quad (2.46)$$

2.5.8.1.2 Resistant moment of the profile

It is determined with the relation:

$$M_{resistant.profile} = n \cdot \int_0^{R_p} c_{profil} \cdot r \cdot C_D \cdot \frac{\rho}{2} \cdot (r \cdot \omega)^2 dr = 0.0947 Nm \quad (2.47)$$

2.5.8.1.3 Induced Resisting Momentum

It is determined with the relation:

$$M_{resistant.induced} = n \cdot \int_0^{R_p} c_{profil} \cdot (r \cdot \varphi_r \cdot C_L \cdot (r \cdot \omega)^2) dr = 0.6995 Nm \quad (2.48)$$

2.5.8.1.4 The anti-torque moment of the rotor

It is determined with the relation:

$$M_{anti-torque} = D \cdot R_p = 0.5605 N \cdot 0.1501 = 0.0841 Nm \quad (2.49)$$

2.5.8.1.5 Hexacopter hover flight

In the case of hover flight, the sum of forces and moments along the z-axis of the hexacopter is zero. Thus, we can write the mathematical relations for stationary flight at a fixed point, according to the relations below:

$$\sum F_{z.hover} = 0 \Leftrightarrow T_{1.hover} + T_{2.hover} + T_{3.hover} + T_{4.hover} + T_{5.hover} + T_{6.hover} = 0 \quad (2.50)$$

The thrust required of a motor for hover flight is:

$$Traction_{hover} = Traction = 4.5274 N \quad (2.51)$$

The total thrust required for hover flight of the hexacopter is:

$$Traction_{hover.total} = 6 \cdot Traction = 6 \cdot 4.5274 N = 27.1644 N \quad (2.52)$$

In the case of moments acting on the drone, the situation is similar:

$$\sum M_{z.hover} = 0 \quad (2.53)$$

$$M_{1.hover} = M_{2.hover} = M_{3.hover} = M_{4.hover} = M_{5.hover} = M_{6.hover} = M_{resistant} \quad (2.54)$$

The sum of the anti-torque moments in hover flight is zero:

$$M_{antitorque.total.hover} = M_{1.hover} - M_{2.hover} + M_{3.hover} - M_{4.hover} + M_{5.hover} - M_{6.hover} = 0 Nm \quad (2.55)$$

2.6 Conclusions, original contributions and published articles.

Conclusions:

- the **dynamic characteristics of the hexacopter developed in the Thesis** were determined, in order to further study the possibilities of improving the constructional-functional characteristics, a subject that will be dealt with in Chapter 3.
- in the case of the equations of motion of the hexacopter, only the forces and moments acting on the drone in stationary flight at a fixed point were calculated, without considering disturbing factors, in particular wind speed and direction. This issue will be studied in detail, in Chapter 5, in the FEM/CFD analysis.
- the computational model for the study of the drone equations of motion for climb flight, forward flight, sideways flight, and rotational motion about the z-axis (gyration), respectively, is formally prepared, but requires information of an experimental nature, which is not the subject of this thesis.

Original contributions:

- the CAD model of the hexacopter drone prototype.

- improvement of the original construction solution of the hexacopter platform, in version 1 of the equipment.
- adaptation of a mathematical model based on matrix formalization, resulting in the equations of motion of the hexacopter and the rotor dynamics equations.
- adaptation of the steps of the analytical calculation methodology to the mechanical structure of the hexacopter developed in the thesis, as follows:
 - o experimental mass that a motor can lift - was chosen from the manufacturer's specifications (later to be determined from tests performed on the test stand presented in chap. 3).
 - o the maximum rotor speed was calculated analytically - (later to be determined experimentally using the tachometer shown in Chapter 3).
 - o the maximum theoretical mass that can be lifted by a motor, i.e., the hexacopter, has been determined.
 - o the coefficient of lift CL and the coefficient of drag CD - have been obtained from the NACA 4412 (naca4412-il) airfoil polar, for an incidence angle of 10° . The NACA 4412 airfoil (naca4412-il) has similar characteristics to the APC12 airfoil of an APC 13x55 MR propeller, which is constructively similar to the Tarot 1355 propeller with which the hexacopter is equipped (diameter - 13", pitch - 5.5").
 - o the lift force and drag force were determined analytically.
 - o the total drag coefficient CX and the power coefficient CP were determined analytically, based on the previously obtained CL and CD .
 - o the (theoretical) rate of climb of the hexacopter at ground level was determined analytically.
 - o the forces and moments acting on the rotor during hover of the drone were determined analytically.

Published articles:

- **Stamate, M. A.**, Nicolescu, A. F., 2017, *Conceptual and functional study of a multirotor drone prototype used for security applications*, Research and Science Today (rstjournal.com), Supplement No. 2, p. 155-164, ISSN-p: 2247-4455 / ISSN-e: 2285-9632 / ISSN-e supplement: 2344-0007, [Google scholar](#)
- **Stamate, M. A.**, Nicolescu, A. F., Pupăză, C., 2017, *Mathematical model of a multi-rotor drone prototype and calculation algorithm for motor selection*, Proceedings in Manufacturing Systems (icmas.eu), Volume 12, Issue 3, 119-128, ISSN 2067-9238, [Copernicus](#).

Chapter 3. Research on the constructive-functional improvement of hexacopter drones

3.1 Introduction

Compared to a quadcopter, a hexacopter offers additional redundancy, i.e., *it can continue its flight and come in for a safe landing if a motor fails during flight*. Furthermore, the configuration of the frame and hence its dimensions directly influence the maximum size of the propellers that can be mounted on the motors, which is *one of the main factors in the efficiency of the drone during flight*. The efficiency of the propeller is strictly related to its surface area. For the same input power, a propeller with a larger diameter will ensure a higher lift compared to a propeller with a smaller diameter. As a general rule, in order to obtain the best performance during fixed-point flight - hover (necessary when inspecting a site, industrial installations, aerial photography, etc.), the drone should have a mass as low as possible and a propeller with a lift area as large as possible - in this case the best flight range is obtained, as presented in the paper by **Stamate et. al [24]**.

3.2 Chapter objectives

- To determine the criteria for choosing the optimum combinations of the propulsion system, consisting of battery - Electronic Speed Controller (ESC) - Brushless DC motor (BLDC) - propeller, depending on the size of the drone frame, to achieve maximum efficiency (range vs. maximum payload carried).
- to carry out, in a new practical approach, comparative studies of the performance of the hexacopter in four different equipment variants in terms of battery, propellers and motors used, based on theoretical elements of preliminary calculations, and employing specialized online platforms. For comparison purposes, simulations were also carried out for two versions of quadcopter and octocopter multicopter drones.
- analytical calculations of the hexacopter performance, in particular: flight range, propeller thrust, maximum speed, motor efficiency, motor operating temperature, propeller efficiency.
- laboratory tests to determine the performance of the propulsion system (thrust, maximum speed, working temperature range of the motors) and results interpretation.

3.3 Theoretical aspects on drone flight autonomy

One of the most important aspects regarding hexacopter drones to focus on is the **flight range**, **Stamate et. al. [24]**. Starting from the existing information in the online environment ([18], [30]), on the flight autonomy of electrically powered multicopter drones, i.e., the fact that most hexacopter drones have a rather low flight autonomy, between a minimum of 8÷10 minutes and a maximum of 20÷25 minutes, it is possible to increase this autonomy, under certain conditions, through a rigorous analysis and planning of the components to equip the drone. Biczyski et. al [6] presented a calculation methodology for choosing the optimal motor-propeller combination with parameterizations, ending with the transposition of mathematical models into MATLAB. Dai et. al [9] published a method for optimizing the design of multicopter drones to achieve a desired hover autonomy. Mathematical models with parameterizations for propulsion system components are also described. The works of Bershinsky & Haviland [5], Dai et. al. [10], and Gatti [14], respectively, address the problem of electric propulsion system sizing for multicopter drones to predict performance and optimize their design. For the optimization of the hexacopter operating regimes, equations for the best configurations are presented. After explaining the computational relations regarding the autonomy of the drone, theoretical elements concerning the choice of the optimal combination of propulsion system components are described.

3.4 Theoretical and practical aspects on choosing optimal combinations for the propulsion system.

In order to find the optimal configuration that provides the desired flight range, not only theoretical computational elements are required, but also a comprehensive analysis of the compatibility and integration of various electronic and mechanical components that equip the drone

is essential. From the design perspective, the electric propulsion system is composed of the following sub-assemblies: brushless electric motors, battery, electronic speed controller (ESC) and propeller.

3.4.1 BLDC – Brushless DC Motor

The motors employed to power multicopter drones are mainly brushless DC motors for their advantages: high efficiency, potential for size reduction and low manufacturing costs. They are most commonly used because of their high efficiency and the high value of the torque constant (KT), which allows direct coupling of the propeller (without gearbox). Depending on the position of the rotor, brushless DC motors can be *outrunner* (see Figures 3.1-3.2) and *inrunner*. Outrunner motors have a larger rotor diameter, which allows them to produce more torque and operate at higher speeds. Inrunner motors have a smaller rotor diameter and can operate efficiently at higher speeds, although they produce less torque.

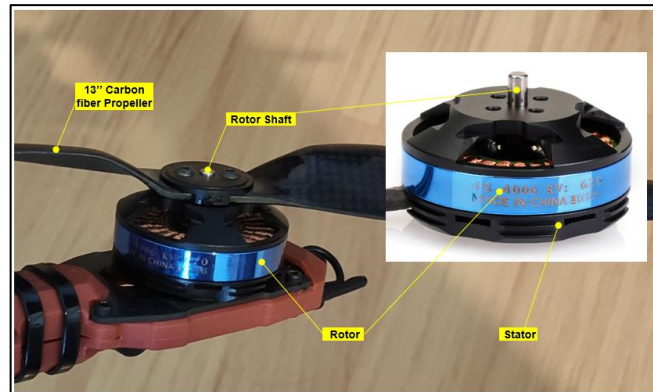


Fig. 3.1 Brushless electric motor powering the outrunner hexacopter

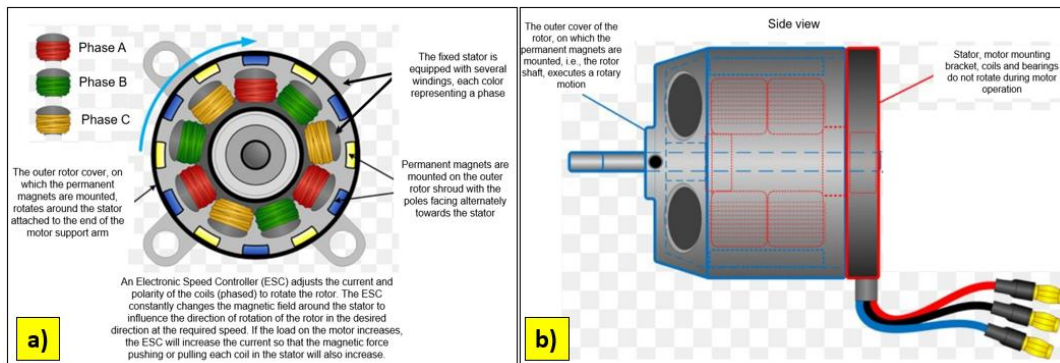


Fig. 3.2 a) Overview of an outrunner brushless electric motor.

b) Side view of an outrunner brushless electric motor [15].

BLDC outrunner motor parameters (fig. 3.3):

- **size** - is given by the size of the stator and is expressed as a 4-digit number. The first group of two digits represents the stator size (mm) and the second group of two digits represents the stator height.
- **KV** - is the most important parameter of this type of motor. This parameter indicates the number of revolutions per minute the motor rotates when a voltage of 1V is applied to the motor terminals, when the motor is rotating at no load. When a motor is supplied with a voltage, it spins. As the voltage increases, the speed of rotation will also increase. Thus, the speed of the motor can be determined according to the relationship:

$$RPM = KV * U_B \quad (3.1)$$

where: RPM - motor speed, expressed in revolutions per minute; KV - brushless electric motor parameter. The hexacopter drone developed and tested in the thesis is equipped with 6 BLDC outrunner motors, model Tarot 4006/620KV 24N22P (fig. 3.3b).



Fig. 3.3 a) Brushless DC electric motor with external rotor (outrunner); b) Tarot 4006/620KV 24N22P motor with which HUT is equipped [28]; c) Tarot 4006/620KV 24N22P motor performance [28].

- **no-load voltage and current.**
- **maximum withstand current/maximum withstand power.**
- **internal armature resistance** - this is an important parameter as it generates heat during motor operation and can reduce motor efficiency.
- **motor efficiency.**

In addition to these motor parameters, it is necessary to determine the specific tractive force developed by the propulsion system. This parameter is measured in g/W and is the defining factor in choosing the best motor-propeller combination so that the hexacopter operates in optimal parameters. The *xcopterCalc* platform presents aspects of specific thrust for drone at hover, which is interpreted as follows: specific thrust $\geq 6\text{g/W}$ - high efficiency drone, between $4\text{--}6\text{g/W}$ - low efficiency drone, $< 4\text{g/W}$ - inefficient drone.

3.4.2 The propeller

When choosing the propeller, all its parameters must be considered, as follows:

- **diameter** (see Fig. 3.4a). The propeller diameter refers to the diameter of the circle created by the blade tips during rotation. The use of a propeller with a certain diameter is primarily limited by the size of the drone frame. Fig. 3.4b shows the propeller equipping the hexacopter.
- **pitch** (see Fig. 3.4a). The pitch of the propeller is the distance the propeller travels in one complete rotation through a fluid. It may be fixed or variable. A smaller pitch propeller will always move faster, but will generate less thrust, compared to a larger pitch propeller which will generate more thrust, thus increasing the speed of the drone, but will generate more current consumption and increase heat release losses.
- **the number of blades** (see Figure 3.4a). The number of blades affects both the flight and the efficiency of the hexacopter. Thus, more blades produce more thrust but have higher losses through heat release and lower efficiency. Using propellers with fewer blades gives higher speed, higher efficiency, and lower current consumption, but lower thrust.
- **propeller mass and material.** The mass of the propeller depends on its size and the material it is made of. Most drone propellers are made of polymer composite materials that have a good balance of strength and weight, such as carbon fiber, nylon, fiberglass and stainless titanium.

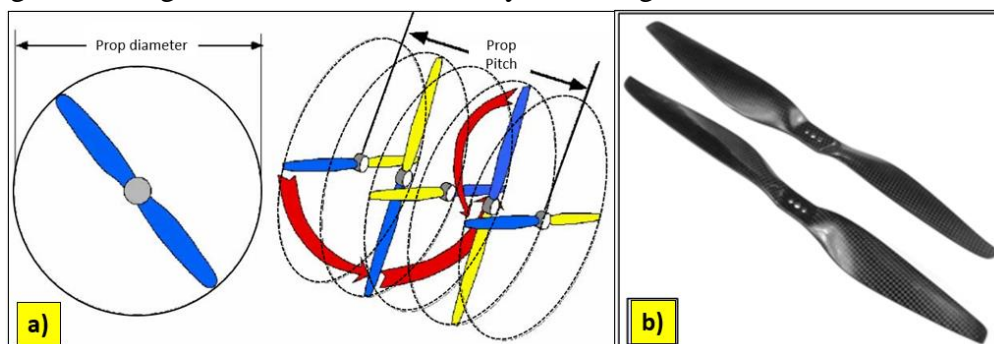


Fig. 3.4 a) Diameter and pitch of a 2-bladed propeller; b) Tarot 1355 propeller.

Propeller performance is described by the following parameters: traction force T (N), power P (W) and torque M (Nm).

3.4.3 ESC – Electronic Speed Controller

The basic function of an ESC is to control the motor speed based on the PWM signal that the autopilot sends to the motor, which is too weak to drive the brushless DC motor directly. This is done by the driver operating the speed stick in the range 0%-100%, and the ESC will send the driver commanded power to the motor. In addition, some ESCs also perform other functions: dynamic braking, battery short-circuit protection, motor start protection, power supply (battery disposal circuit) for the radio remote control receiver or servomotors, and determination of the direction of rotation of the motor.

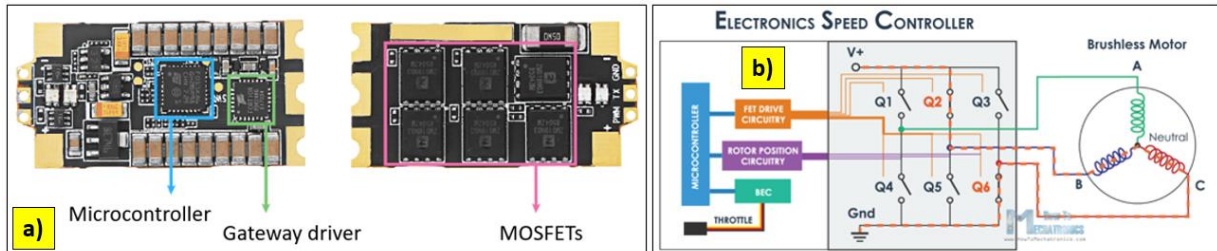


Fig. 3.5 a) General structure of an ESC; b) Simplified scheme of ESC operation [16].

The most important components of the ESC (Fig. 3.5a) are: the microcontroller, the driver for the gate between the autopilot (AP) and the MOSFETs, respectively. There are several types of protocols through which the PA sends the signals controlling this process to the ESC, each with different performance and signal frequencies. In Fig. 3.6a illustrates the type of ESC that equips the hexacopter, model Hobbywing XRotor 40A, which uses the PWM protocol.

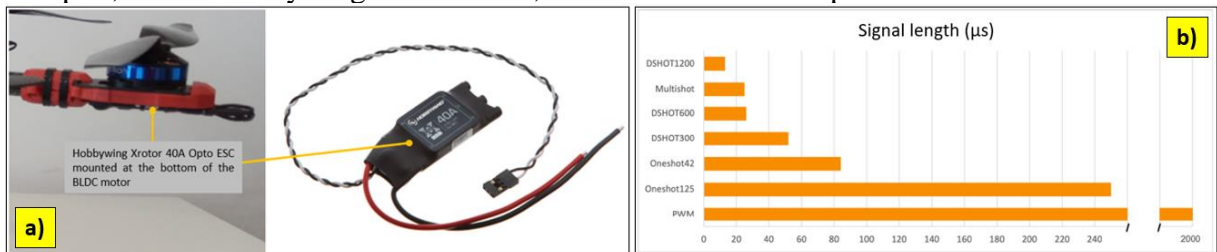


Fig. 3.6 a) ESC powering the Hobbywing XRotor 40A Opto hexacopter; b) Control signal length for the main communication protocols [29].

Fig. 3.6b shows a comparison of command signal lengths (μs) for the main communication protocols used by the ESC. In the case of the Hobbywing XRotor 40A using the Pulse Width Modulation (PWM) protocol, it has the longest response time in μs , with the range 1000-2000 μs being used for operator commands.

ESC parameters:

- **maximum continuous current/maximum instantaneous current (peak).** The first parameter represents the maximum continuous current under normal operating conditions, while the second parameter represents the maximum instantaneous current that the ESC can withstand for very short periods.

- **operating voltage.** The voltage range that allows the ESC to operate correctly is a very important parameter, indicating the types of batteries it supports ("3-4S LiPo" means that this ESC can operate with a 3-4 cell 3.7V LiPo battery, i.e., 11.1-14.8V).

- **endurance.** Since all ESCs have resistance, their heating cannot be neglected as the current flowing through them can sometimes reach tens of amps. Taking heat dissipation into account, the resistance of ESCs operating at high currents is always designed to be low.

- **refresh rate.** Motor response is closely related to the ESC's refresh rate, so a high refresh rate will result in faster motor response to pilot commands.

- **programmability.** ESC performance can be optimized by adjusting internal parameters. Parameters that can be set include throttle range calibration, low voltage protection, power cut-off

value, current limiting, braking mode, throttle control mode, timing setting, start mode and PWM mode setting.

3.4.4 The battery

The energy density of LiPo batteries ranges from 140 to 265 Wh/kg in terms of weight and 250 - 730 Wh/L in terms of volume. For LiPo batteries the nominal voltage is 3.7V/cell, with a maximum voltage of 4.2V/cell. (fig. 3.7ab)

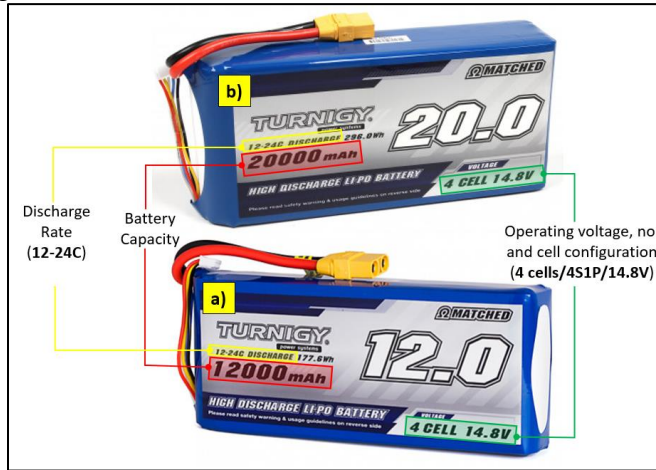


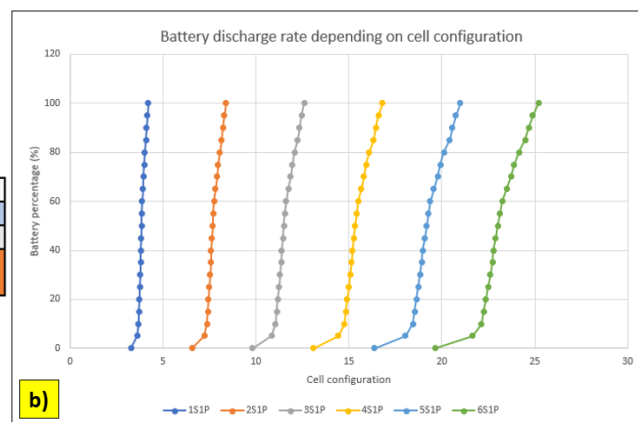
Fig. 3.7 LiPo batteries: a) Turnigy 12000mAh 4S1P 12C-24C, 14.8 V; b) Turnigy 20000mAh 4S1P 12C-24C, 14.8 V.

Battery parameters:

- **capacity**. It is expressed in mAh/Ah or watt-hours (Wh) and can be used to estimate flight duration using the relationship.
- **rated voltage**. It is an important parameter that helps to determine the motor speed and current consumption. Considering the KV parameter of the motor, which indicates its speed at every 1V applied (RPM/V) the nominal battery voltage will determine the motor speed.
- **discharge rate (C-Rating)**. The discharge rate or C-Rating is a measure of the safe discharge rate of the battery.
- **cell configuration**. It is usually listed on the battery label and describes the number and arrangement of LiPo cells in the pack. They can exist in several configurations, the most common being 1S1P÷6S1P. (fig. 3.8a)

LiPo batteries - Configurations and voltages						
Configuration	1S	2S	3S	4S	5S	6S
Nominal voltage	3.7V	7.4V	11.1V	14.8V	18.5V	22.2V
Voltage of fully charged cell	4.2V	8.4V	12.6V	16.8V	21V	25.2V

a)



b)

Fig. 3.8 a) Configurations and voltages for LiPo batteries; b) Relationship between battery discharge percentage and cell configuration

Fig. 3.8b illustrates the relationship between battery discharge percentage and cell configuration for batteries in configurations with up to 6 cells in series.

- **internal resistance (mΩ)**, which changes over time depending on how the battery is used.

3.5 Simulations carried out using specialized online platforms.

In the following section several variants for equipping the hexacopter are presented. Using the online dedicated platforms like *xcopterCalc* [30], *flyeval.com* [12], and *drivecalc.de* [11] respectively, simulations were performed, with the aim of finding an optimal configuration that increases the range and payload carrying capacity of the drone. Simulations with the aforementioned platforms were also carried out in the paper by **Stamate et. al** [24], from which elements of interest regarding the performance of the drone and the propulsion system were extracted.

3.5.1 Simulations carried out with the *xcopterCalc* platform.

3.5.1.1 Hexacopter in equipment version 1 (HUT v.1)

In the first stage, the theoretically achievable range, with its margin of error, of the test hexacopter (HUT) will be analyzed in its initial configuration:

General	Model Weight: 1211 g 42.7 oz	# of Rotors: 6 flat	Frame Size: 695 mm 27.36 inch	FCU Tilt Limit: 35°	Field Elevation: 85 m.ASL 279 ft.ASL	Air Temperature: 22 °C 72 °F	Pressure (QNH): 1010 hPa 29.83 inHg	
Battery Cell	Type (Cont. / max. C) - charge state: custom - normal	Configuration: 4 S 1 P	Cell Capacity: 6600 mAh 6600 mAh total	max. discharge: 80%	Resistance: 0.0038 Ohm	Voltage: 3.7 V	C-Rate: 10 C cont. 20 C max	Weight: 134.25 g 4.7 oz
Controller	Type: custom	Current: 40 A cont. 40 A max	Resistance: 0.006 Ohm	Weight: 26 g 0.9 oz	Accessories	Current drain: 0.35 A	Weight: 290 g 10.2 oz	
Motor	Manufacturer - Type (Kv) - Cooling: Tarot - 4006/620KV (620) good	KV (w/o torque): 620 rpm/V	no-load Current: 0.8 A @ 14.8 V	Limit (up to 15s): 426 W	Resistance: 0.126 Ohm	Case Length: 30 mm 1.18 inch	# mag. Poles: 22 Weight: 82 g 2.9 oz	
Propeller	Type - yoke twist: custom - 0°	Diameter: 13 inch 330.2 mm	Pitch: 5.5 inch 139.7 mm	# Blades: 2	PConst / TConst: 1.2 / 1.0	Gear Ratio: 1 : 1	calculate	

Fig. 3.9 Input data for HUT v.1

The input data for HUT v1 are (fig. 3.9):

- ✓ the HUT frame (the motor support arms, the upper and lower plates between which the arms are mounted, the battery support plate, the landing gear, and the support plates on which the motors are mounted) is made of carbon fiber, with a total mass of only 833g, while providing increased shock and vibration resistance. The frame size (distance between the centers of two motors) is 695mm.
- ✓ the 13" propellers that equip the HUT are made of carbon fiber, with a mass of only 16g each and a pitch of 5.5".
- ✓ the flight controller (autopilot) limits the HUT's pitch to a maximum of 35°; this, together with the PMU (Power Module Unit) and LED module consume about 0.3A.
- ✓ flight testing of the HUT is done at an altitude of about 85m above sea level (Bucharest altitude), at a temperature of 22°C and an atmospheric pressure of 1010hPa (757.5 mmHg);
- ✓ the battery mounted on the HUT is a 4-cell LiPo type (each cell having 3.7V and a mass of 134.25g - total battery mass is 537g) in 4S1P configuration (4 cells in series/1 cell in parallel), with an internal resistance of about 0.0038Ohm, nominal voltage - 14.8V. C Rating - 10C (10*6.6A = 66A - in continuous operation) with a maximum of 20C (20*6.6A = 132A - for short periods of 10-15 seconds). As mentioned above, it is recommended that the battery is not discharged to more than 80% of its capacity.
- ✓ electronic motor speed controllers (ESCs) can withstand a maximum current of 40A, have an internal resistance of approximately 0.0006Ohm and a mass of 26g each.
- ✓ the HUT is also fitted with the three-axis rotating and stabilizing gimbal, which is also battery powered, so this is also a consumer, which will be included in the Accessories category; it has a mass of 178g and consumes approximately 0.05A.
- ✓ Tarot 4006/620KV motors produce 620 rpm/V, have an internal resistance of 0.126 Ohm, have a mass of 82g each.

After running the program, the following results and conclusions are obtained (fig. 3.10):

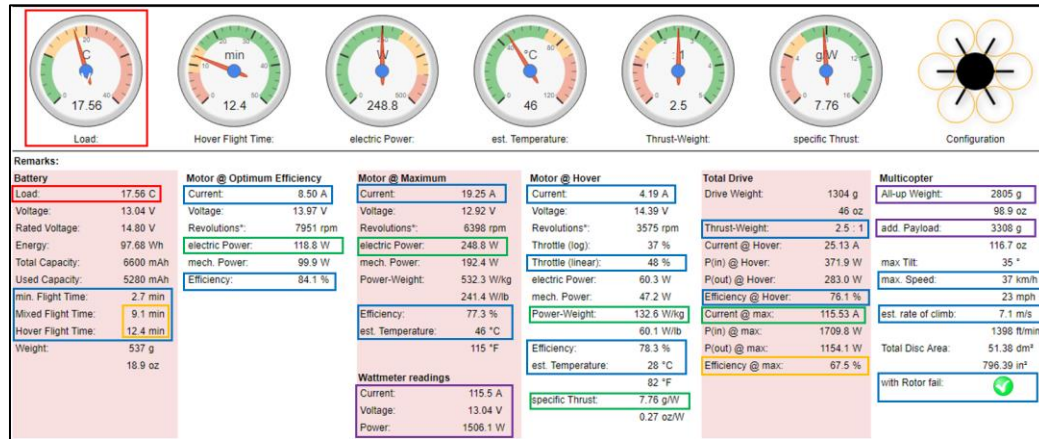


Fig. 3.10 Results of running the HUT v.1 program with the *xcopterCalc* platform.

- ✓ first of all, it can be noticed that the load on the battery (load) is 17.56C (which means a continuous load of $17.56 * 6.6A \approx 116A$). On the indicator the value obtained is positioned in the orange area. Considering the characteristics of the battery (continuous load of 10C and maximum of 20C for short periods) it means that the battery will be mostly overcharged, with a tendency to work more towards the maximum zone, which can lead to damage. Although there are no warning messages on the results page, a battery with a higher C-Rating is recommended.
- ✓ gives a flight time of 9.1 minutes for combined flight (hover, forward, reverse, climb, descent) and 12.4 minutes for hover.
- ✓ for optimum motor performance, 7951 rpm and 84.1% efficiency are achieved: for hovering, 3575 rpm. Motor speed is at 48% of capacity (which is a pretty good result - preferably around 50% to allow the drone to perform other maneuvers in flight that will overheat the motors, and therefore increase the temperature of the motor casing), a power-to-mass ratio of 132.6 W/kg (a good result - the most efficient systems get this down to 80W/kg), an efficiency of 78.3% and a temperature of just 28°C.
- ✓ another very important aspect is the thrust-to-mass ratio, which in our case is 2.5:1 (a standard ratio is 2:1, but the higher this ratio, the better the drone responds to commands. For values equal to or greater than 1.8 the motor speed will be less than or equal to 60% of its capacity. For values between 1.2÷1.8 the motor speed will be between 60÷80% of their capacity and the maneuverability of the drone will be limited. Below 1.2 the stability of the drone at a hover cannot be ensured).
- ✓ in the case of specific traction, a ratio of 7.76g/W is obtained - high efficiency.
- ✓ it is noted that additional equipment can be attached which cannot exceed a mass of 3.3 kg, which is more than generous.
- ✓ the maximum speed achieved is 37 km/h and the ascent rate is about 7.1 m/s.
- ✓ a very important aspect to bear in mind in this case, in the case of hexacopters and octocopters, is that in the event of a motor failure, the drone continues its flight and can be brought safely to a landing.
- ✓ on a frame size of 695 mm (distance between the centers of two motors on opposite arms), the maximum size of propellers that can be mounted is 13.6" and their pitch can be a maximum of 8.6" (in the case studied we are close to the maximum value with the Tarot 1355 propellers - diameter 13" and pitch 5.5").
- ✓ also notes the type of motors recommended (the motors equipping the hexacopter have 620 rpm/V, so they fall within the recommended range of 470÷680 rpm/V), and the ESCs mounted on the drone support a maximum of 40A, which also complies with the recommended values of minimum 20÷35 A.

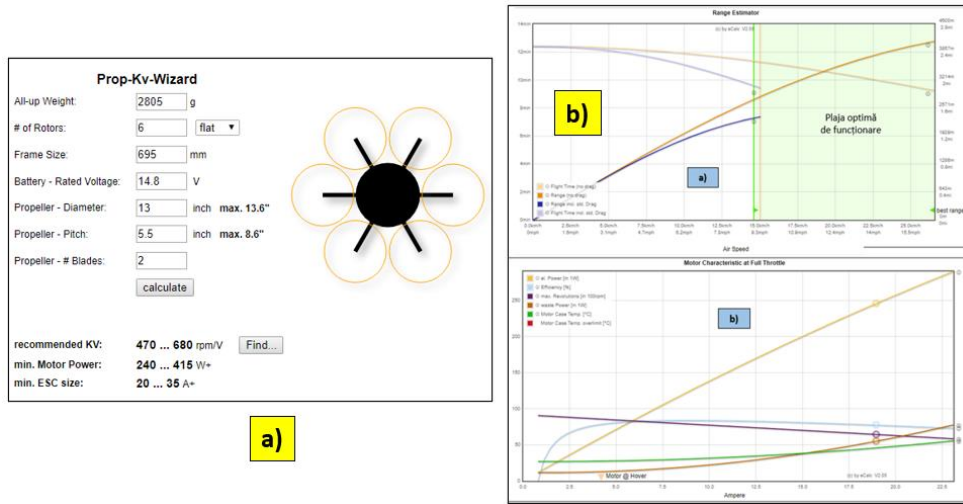


Fig. 3.11 a) Choice of motor-ESC-propeller propulsion package according to frame size, total drone mass and battery voltage; b) Estimated flight distance (a) and motor characteristics at maximum speed (b) for HUT v.1

After running the program, two graphs showing the data on flight distance, speed, and motor characteristics at maximum speed are also obtained (Fig. 3.11b):

- ✓ maximum flight time (without drag) is about 12 minutes.
- ✓ maximum flight time (with drag) drops below 10 minutes.
- ✓ maximum flight distance (without drag) is about 4000 m.
- ✓ maximum flight distance (with drag) is about 2300 m.
- ✓ the best performance of the hexacopter is obtained in the speed range 15÷27,5 km/h;
- ✓ it is noticed that the motors manage to operate in all speed ranges at a temperature of maximum 60°C. Care must be taken during motors operation because the temperature must not exceed 80°C as this factor may lead to their permanent damage!

Simulation scenarios are carried out for the Hexacopter in versions 2, 3, 4 of equipment, respectively for a quadcopter and an octocopter, in order to illustrate what happens and how the modification of certain parameters (frame size, propeller, motors, ESCs, batteries, avionics components) influences the dynamic hexacopter behavior.

3.5.2 Simulations on flyeval.com platform

For the comparative analysis of the results obtained from the calculations and using the xcopterCalc utility, input data were entered, and the calculation algorithms were also run using the flyeval.com platform. The following results show the simulation runs for the first 3 hexacopter equipment variants. The results analysis illustrated in Fig. 3.12 emphasize following values for HUT v.1: a flight time of 12.9 minutes for the flight in normal, combined conditions (forward, reverse, climb, descent maneuvers) and 13.57 minutes for the stationary flight at a hover. At maximum speed, a flight time of only 5.6 minutes is achieved.



Fig. 3.12 HUT (v1) performance using the flyeval.com platform.

In the case of HUT v.2, the results shown in Fig. 3.13 can be summarized as follows: a flight time of 20.8 minutes for flight in normal, combined conditions (forward, reverse, climb, descent

maneuvers) and 21.95 minutes for stationary flight at a hover. At maximum speed, a flight time of 12 minutes is achieved.



Fig. 3.13 a) HUT performance (v2) using the *flyeval.com* platform; b) HUT performance (v5) using the *flyeval.com* platform.

For HUT v.5 (Fig. 3.13b) the following results are obtained: a flight time of 31 minutes for normal, combined flight (forward, reverse, climb, descent maneuvers) and 32.18 minutes for stationary flight at a hover. At maximum speed, a flight time of 9.9 minutes is achieved.

3.5.3 Simulations employing the *drivecalc.de* platform.

A useful platform for choosing optimal combinations of the propulsion system is *drivecalc.de*, which can help the user to select several different arrangements based on the different types of components preloaded in the database provided on the platform or based on the user's option on how to define new components with their corresponding parameters. Fig. 3.14 depicts the performance of a APC 13x5.5 MR propeller model, from the APC manufacturer, being similar in size and geometric pitch to the one mounted on the hexacopter.

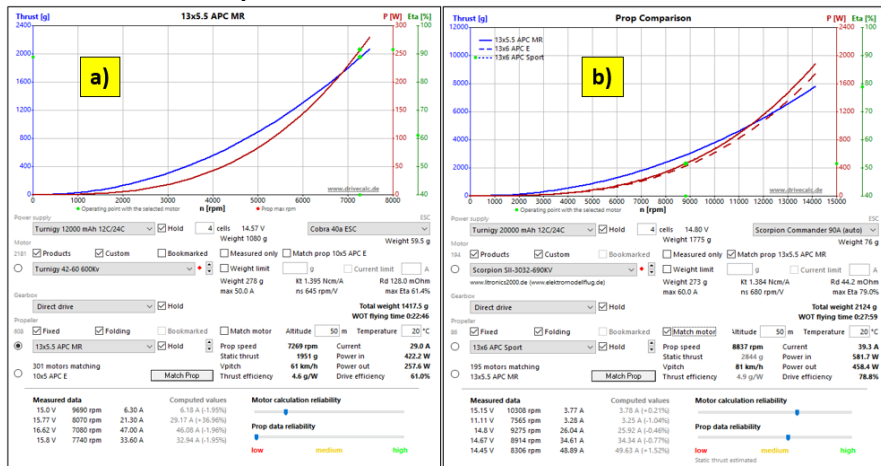


Fig. 3.14 a) APC 13x55 MR propeller performance; b) APC 13x6 Sport propeller performance

For this study, a motor with a KV 600 index close to that of the Tarot 4006 620KV motor and a Turnigy 12000 mAh battery, similar to one of the batteries employed in the tests, was used. It can be seen that in this configuration the propeller reaches a maximum speed of 7269 RPM, develops a thrust of 1951 g and an efficiency of only 4.6 g/W. Therefore, the propulsion system efficiency is only 61%. Fig. 3.14b shows the performance of a propeller model APC 13x6 Sport, from the same APC manufacturer, with the same 13-inch diameter as the one on the hexacopter, but with a 6-inch geometric pitch. At the same time, the 20000 mAh battery was introduced during the tests. The motor employed is the ScorpionSII-3032-690KV, slightly faster than the Tarot 620 KV, together with a high-performance Scorpion Commander 90A ESC. In this case one can see an improvement of the propeller and the propulsion system parameters: the propeller reaches a maximum speed of 8837 RPM, develops a thrust of 2844 g and a specific efficiency of only 4.9 g/W. Overall, the efficiency of the propulsion system has increased to 78.8%. The results on the flight time estimation of the hexacopter, as well as of the comparative quadcopter and octocopter variants, respectively, obtained

from the simulations, calculations and from several other calculations performed but not included in this chapter are summarized as presented in Fig. 3.15ad:

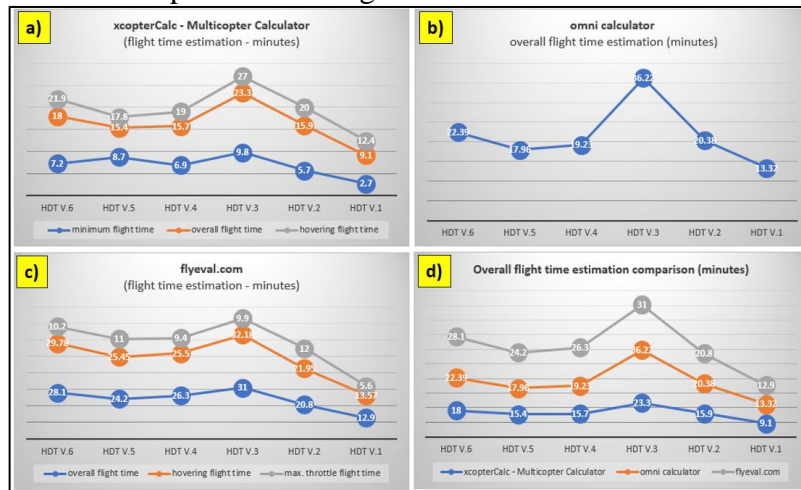


Fig. 3.15 a) Estimation of flight autonomy using xcopterCalc platform; b) Estimation of flight autonomy using omni calc platform; c) Estimation of flight autonomy using flyeval.com platform; d) Comparison of flight autonomy results

Although there are differences between the different simulation results, we can conclude that they follow the same trend for the best flight time. The data obtained and presented are not 100% reliable, although the platforms follow mathematical models with different approaches to determine the best configurations with the highest possible flight range. In conclusion, in order to determine the real performance of a drone, it is necessary to measure, verify and test the components before mounting them on the drone frame, after which it is necessary to perform ground tests. After confirming the operation within the parameters, flight tests are required, in different operating modes and atmospheric conditions.

3.6 Laboratory tests carried out to determine propulsion system performance.

3.6.1 Determination of the traction force

In order to determine the tractive force, and therefore the efficiency of the propulsion system, laboratory tests were carried out using the Mayatech MT10PRO 10KG test stand. A Turnigy LiPo battery with a capacity of 20000 mAh, 4 cells in 4S1P configuration, voltage 14.8V, was used to power the ESC-motor-propeller assembly. The Tx-Rx chain was provided by a 2.4GHz radio remote control, model RadioLink AT10II, and a 12-channel receiver, model RadioLink R12DS. The test configuration is illustrated in Fig. 3.16a.



Fig. 3.16 a) Propulsion system efficiency test stand configuration; b) Measurement of rotor speed

3.6.2 Determination of maximum rotor speed

Using a tachometer, in the same test configuration, the maximum speed of the motor-propeller assembly was determined, giving a maximum value of 13418 RPM (Fig. 3.16b). Tractive force,

current draw, battery voltage and mechanical power were measured using the test stand (Fig. 3.16) and rotational speed using the tachometer (Fig. 3.16b). The results are shown in Fig. 3.17ad and were as follows:

- **the maximum tractive force developed by the motor-propeller assembly**, measured on the stand, was approximately **1,718 Kgf \approx 16,84 N**.
- **maximum speed measured by tachometer - 13418 RPM**.
- the efficiency of the propulsion system decreases with the increase of the rpm. In the idling zone, at 30-40% rpm the efficiency reaches a value of **13-14 g/W (\geq 6g/W - high efficiency drone)**. In the 50-75% rpm range, which is equivalent to operating the drone in hover and light horizontal maneuvers, the efficiency decreases to a value of **6.49 g/W (\geq 6g/W - high-efficiency drone)**. In the speed range 85-100%, the efficiency further decreases to a minimum value of **4.96 g/W (\div 6g/W - low efficiency drone)**.
- with increasing speed, the current consumption increases proportionally, reaching a measured **current** value of **21.6Ah** at 100% speed.
- the **mechanical power** developed also increases to a value of **346.2 W** at 100% speed.

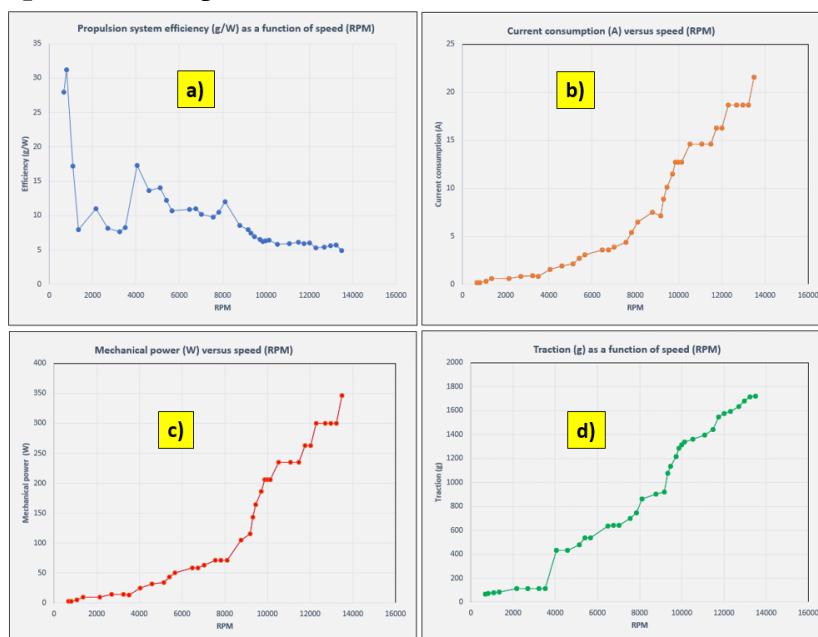


Fig. 3.17 a) Efficiency of the propulsion system with which the hexacopter is equipped; b) Current consumption (A) as a function of speed; c) Mechanical power (W) as a function of speed; d) Traction (g) as a function of speed.

3.6.3 Determination of the motor operating temperature range

During the tests on the test stand, motor temperatures at different motor speeds and rpm ranges were measured using a FLIR E86 thermal imaging camera (Fig. 3.18). The following points of interest were found:

- at idle, with the rev stick at 30% for 3-5 minutes, the motor temperature reached 40°C.
- at hover, with the speed stick at 50%, for 3-5 minutes, the motor temperature reached 60°C.
- in maximum mode, with the speed stick at 100%, for 3-5 minutes, the temperature reached over 200°C, which means that it is only desirable to operate the drone in maximum mode for very short periods, around 10-15s, to avoid these temperature increases in the motor windings, which can eventually lead to burn-out.

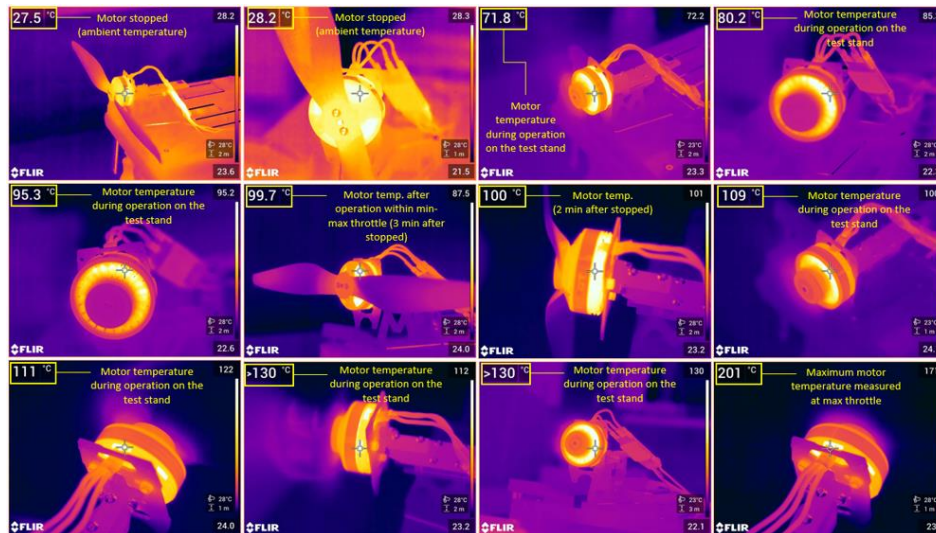


Fig. 3.18 Motor temperature measurement during operation on the test stand, in the speed range 5%-100%

3.7 Interpretation of results obtained from analytical calculations.

After the laboratory tests have been carried out, the results obtained from the analytical calculations based on the equations presented at the beginning of the chapter are interpreted and the required thrust force of the drone is determined for the fixed-point stationing for the 6600 mAh battery variant, when the total mass of the drone is 2.77 kg, and for the HUT v2 variant, when the mass of the hexacopter changes to 3.716 kg. Although the total mass of the drone has increased from 2.77 kg to 3.716 kg, the flight range has also increased from 13.32 min to 20.38 min, because of the 16 Ah capacity battery, compared to the initial value of 6.6 Ah. Depending on the missions the drone performs, the calculated times can vary as follows, according to *xcopterCalc*: for flights that do not involve movement, but more stationary at a hover (aerial photography), the flight time is approximately **75%** of the calculated one; if the drone is moving in areas with strong winds or performing frequent movements, the flight time is approximately **50%** of the calculated time; for drones used in FPV (First Person View) aerial races or flights with high motor revolutions, the flight time dramatically drops to approximately **25-30%** of that calculated value.

3.8 Interpretation of the results on choosing of the optimal motor-propeller combination

Motors with a low KV index have lower revs than those with a high KV index but produce much more torque (traction) and are more economical. On the other hand, motors with a high KV index tend to turn faster and are capable of higher speeds, but at the cost of reduced efficiency. Therefore, motors with a small KV index are more suitable for turning large propellers at low speeds and motors with a large KV index for turning small propellers at high speeds. The larger the propeller diameter, the more efficiently the drone flies in a fixed-point hover, but *the less efficiently it responds to operator commands*. A propeller with a pitch-diameter ratio greater than 0.667 tends to lose lift as the load on it increases, leading to loss of control of the drone. As a general rule, according to *xcopterCalc* it is better to *choose a propeller with a pitch-diameter ratio less than 2/3*.

3.9 Conclusions, original contributions and published article.

Conclusions

- laboratory tests carried out on the test stand to determine the thrust force resulted in a maximum thrust force developed by the propeller-motor assembly of 1,718 Kgf. A maximum take-off mass that the hexacopter can lift of 10,308 kg was obtained.
- tachometer tests to determine the maximum rotor speed revealed a maximum speed of 13418 rpm.
- due to the limitation of the hexacopter frame size (695 mm) it is not possible to mount propellers with diameters larger than 13.6" in order to obtain a higher thrust than the Tarot 1355 propellers.

- the simulations performed with the *xcopterCalc* utility shown above were carried out with the following input data for atmospheric conditions: temperature - 22°C, atmospheric pressure - 1012 hPa (759 mmHg). Further simulations were performed, changing the temperature conditions, implicitly atmospheric pressure, i.e., temperature - 32°C, respectively atmospheric pressure - 1010 hPa (757.5 mmHg), at the same altitude above sea level of 85 m (Bucharest altitude). The reason why they were not presented in the thesis is that the differences arising from the simulations are not significant compared to those tested under initial conditions (22°C/759 mmHg/85 m).
- simulations have proved that the platforms give autonomy results 10-25% higher than the results obtained in reality.
- although preliminary theoretical realistic data were obtained, in the case of the octocopter and quadcopter, in terms of their autonomy, other negative aspects of critical importance for their operation in flight (high motor operating temperatures, low thrust-to-mass ratio, etc.) have emerged, which confirms the statements made so far in this report (***higher does not always mean more efficient***).
- other scenarios have been carried out to equip the drone with different battery variants in order to increase the drone's capacity, but equipping the drone with high mass batteries reduces the thrust-to-mass ratio so that at some point the drone can no longer be optimally controlled.
- an important aspect is the maximum flight distance of the drone (distance to the operator - home location). The data provided by the *xcopterCalc* utility provides ***theoretical*** distances that the drone can fly. In reality, the maximum distance is limited by the performance of the remote control (transmitter - Tx) and the receiver (Rx), i.e., the communication protocols between Tx - Rx and Rx - flight controller (autopilot). According to the RadioLink manufacturer's specifications, the RadioLink AT10II radio control has a maximum range of up to 4 km. This parameter was not tested in the thesis.
- methods to extend the maximum flight range are acquisition of Tx with signal amplification, respectively, and perhaps the most efficient method, command, and control of the drone via 3G/4G, respectively 5G communication networks (currently under study).

Original contributions

- experimental determination of the maximum tractive force developed by the motor-propeller assembly using the Mayatech MT10PRO 10KG test stand.
- experimental determination of the maximum rotor speed using the tachometer.
- experimental determination of motor operating temperatures using the FLIR E86 thermal imaging camera.
- presentation of the technical characteristics of the propulsion system components and remarks on their compatibility, including aspects related to the design of the drone structure.
- analytical calculations of the hexacopter range for various LiPo battery different capacities.
- simulations of the hexacopter performance compared with quadcopter or octocopter variants using specialized online platforms.

Published article.

- **Stamate, M. A.**, Nicolescu, A. F., Pupăză, C., 2020, *Study regarding flight autonomy estimation for hexacopter drones in various equipment configurations*, Proceedings in Manufacturing Systems (icmas.eu), Volume 15, Issue 2, 81-90, ISSN 2067-9238, [Copernicus](#).

Chapter 4. Experimental tests on hexacopter behavior during hover flight

4.1 Introduction

Chapter 4 describes the results of tests carried out both in the laboratory and in the field for the motor start-stop maneuvers, to check if the motors are operating at optimum parameters during stationary flight maneuvers at hover and roll, pitch, and yaw maneuvers. The hexacopter has moved in different flight directions, under atmospheric conditions suitable for these types of actions (temperature: 10°-30°, wind: 1-2 m/s, no precipitation). The flight parameters extracted from the tests were analyzed and corrective action was taken where necessary, as identified in **Stamate et. al [26]**. All these tests were performed employing the physically realized hexacopter platform used in the thesis. Finally, conclusions were drawn, and the flight parameters were analyzed. **Solutions have been found for improving the drone parameters.**

4.2 Chapter objectives

- upgrading of the hexacopter for the second version of the equipment.
- ground tests on the hexacopter in the two equipment variants.
- flight tests with the hexacopter in the two equipment variants to determine its optimum performance during hover flight in certain atmospheric conditions.
- ground and in-flight check of the command and control chain using the Mission Planner ground control station.
- flight autonomy assessment of the hexacopter by carrying out flights in open area for different equipment variants with batteries of different capacities.
- analysis and explanations regarding the parameters received from the hexacopter to ensure optimal operation during hover flight.

4.3 Equipment variants of the hexacopter developed and tested.

The built hexacopter is presented in two equipment variants (v1 and v2), with two different sets of avionics. Variant 1 (v1) (Fig. 4.1) illustrates the Tarot ZYX-M avionics kit consisting of: Tarot ZYX-M flight controller (FP), 5V/12V voltage distribution module, GPS antenna, LED for status indication, Turnigy 9X 8C v2 8-channel radio receiver, 2.4 GHz frequency. A Turnigy Multistar 4-cell LiPo battery, 4S1P configuration, 6600 mAh capacity, was used to power the drone.

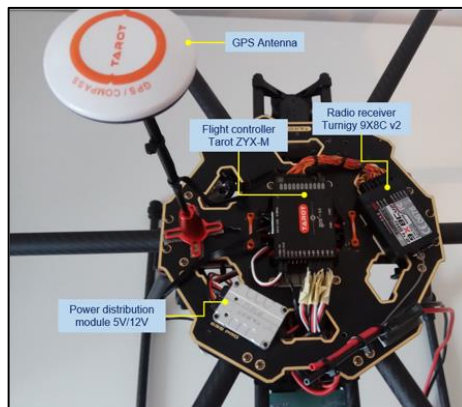


Fig. 4.1 Hexacopter equipped in version v1.

Fig. 4.2a depicts the radio control employed to transmit the control signal to the motors, model Turnigy TGY 9X, mode 2 (on the left side is the stick for the turn and yaw commands and on the right side is the stick for roll and pitch maneuvers) with 9 transmission channels, which is paired with the Turnigy 9X 8C v2 radio receiver mounted on the drone. In the v1 version no telemetry data and video signal transceiver equipment were used from the drone to the operator. This version aims only the preliminary testing of the normal ground and flight operation modes of the hexacopter without a detailed analysis of the flight parameters.

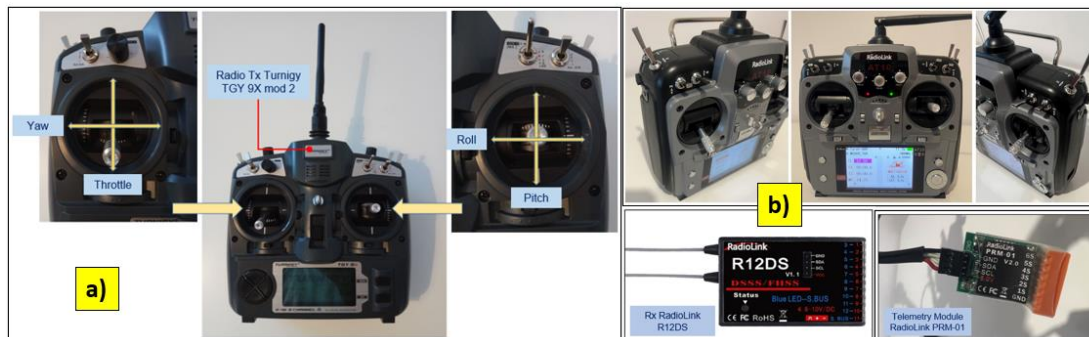


Fig. 4.2 a) Turnigy TGY 9X radio control, mode 2, with illustration of the controls on the 3 axes (pitch, roll, yaw, and rpm); b) Tx (RadioLink AT10II) + Rx (RadioLink R12DS) assembly + PRM-01 telemetry module

In Fig. 4.3, version 2 (v2) is illustrated, consisting of: flight controller (autopilot - AP) Pixhawk 2.4.8, PPM protocol encoder (allows encoding of 8 signals using the Pulse Width Modulation (PWM) protocol into a single signal using the Pulse Position Modulation (PPM) protocol), loudspeaker (for emitting PA status beeps), safety on/off switch (for the protection against accidental starting of the motors), YRRC telemetry data transmitter, 433 MHz frequency, 1000 mW power (for the transmission of the ground telemetry data), paired with ground telemetry signal receiver, model YRCC, video signal transmitter, 32 channels, frequency 5.8 GHz, 600 mW power (for video signal transmission) from the GoPro Hero 4 camera mounted on the Tarot T4-3D three-axis rotating gimbal, RadioLink R12DS 12-channel 2.4 GHz radio receiver (for radio control reception from the transmitter built into the control box at the ground controller), ReadytoSky GPS signal receiver antenna, as identified in **Stamate et. al [26]**.

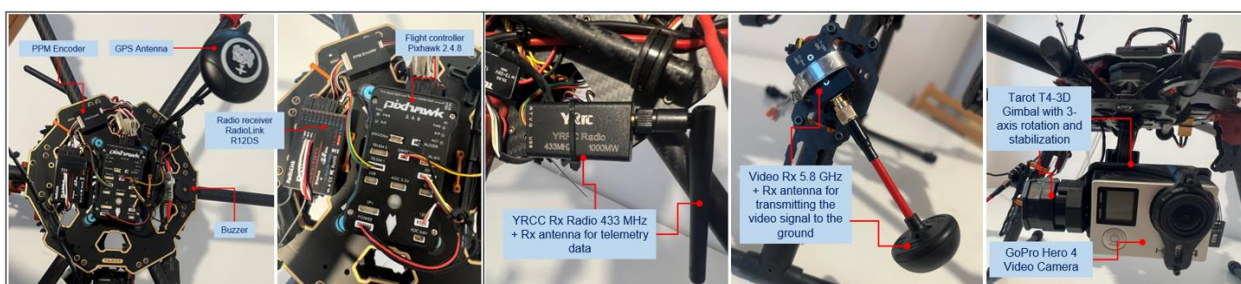


Fig. 4.3 Hexacopter in v2 version

Fig. 4.2b shows the RadioLink AT10II, mode 2 (Tx) radio control used to transmit the ground command to the drone, together with the drone-mounted RadioLink R12DS (Rx) receiver, which obtains the ground command and transmits it to the autopilot, and the PRM-01 telemetry module, which allows the voltage of the drone's on-board battery to be displayed on its screen. Both versions, v1 and v2, were mounted on the same hexacopter frame structure. It is made of a carbon fiber structure, consisting of two plates, upper and lower, for the central part of the frame, between which six support arms are fixed, at the end of which the motors and electronic speed controllers (at the

bottom part of the motors) are mounted on six dedicated mounts. The landing gear is composed of two tubular structures mounted at an angle to the bottom plate of the frame. At the bottom of the bottom plate a bracket is mounted for attaching the battery pack. In the v1 version, an additional bracket is mounted on the right arm of the landing gear for mounting the video transmitter. Carbon fiber ensures the drone frame elasticity, i.e., increased resistance to deformation, stress, bending and a reduced mass of the overall structure. However, a drawback of the carbon fiber is that it attenuates the strength of the radio signal transmitted/received. That is why the location of the radio/video transmitting/receiving equipment must be carefully chosen, either on the frame of the drone or in its vicinity by fitting spacers.

Fig. 4.4-4.5 illustrates the presented design features, focusing on components and in an overall view, for equipment variants v1 and v2.



Fig. 4.4 Hexacopter structure, by component

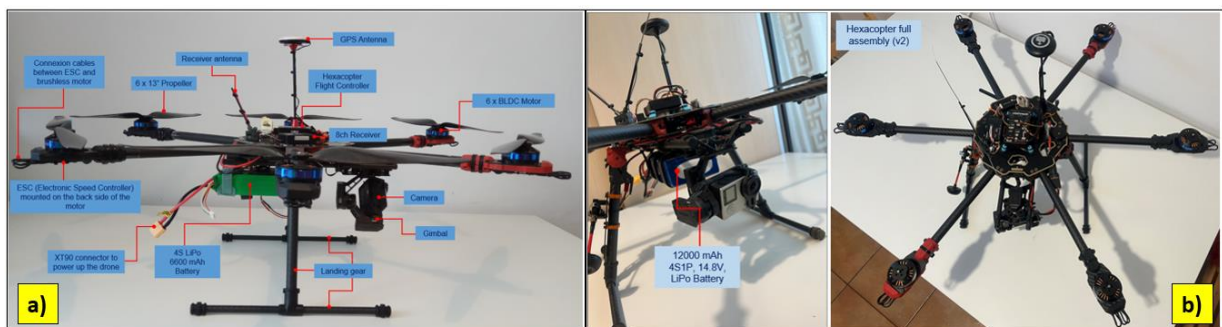


Fig. 4.5 a) Structure of the assembled hexacopter in version v1.
b) Structure of the assembled hexacopter in version v2.

Fig. 4.6 depicts the block diagram of the hexacopter platform architecture, illustrating the main components of the drone, and the command-and-control ground station together with their relationships.

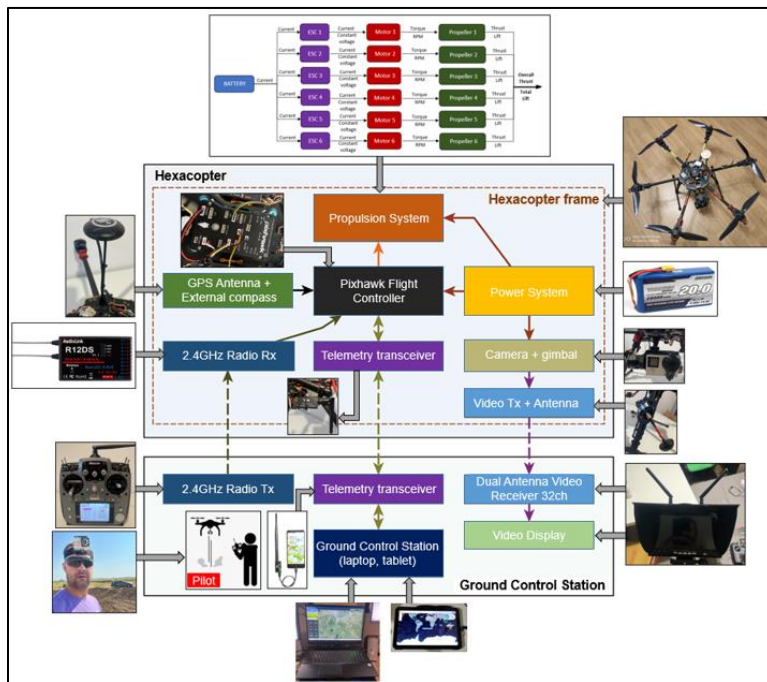


Fig. 4.6 Block diagram of the hexacopter platform architecture

Telemetry data from the drone is transmitted via a YRCC transmitter equipped with an antenna that operates at 433 MHz frequency. The signal is received on the ground by a YRCC receiver equipped with a receive antenna, paired with the one on the drone, and at the same operating frequency (433 MHz). The receiver can be connected to a mobile device (tablet or smartphone) or a laptop on which a GCS (Ground Control Station) platform is installed. In Fig. 4.7 the two components of the telemetry kit are presented: the transmitter mounted on the drone and the receiver in two connection variants (Samsung tablet and HP Omen laptop), on which the Mission Planner GCS has been installed.

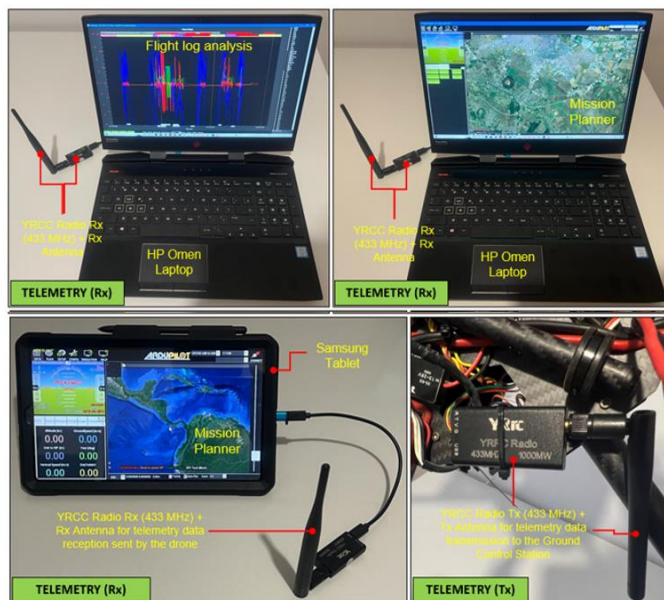


Fig. 4.7 Telemetry (transceiver) kit layout on the drone and on the ground

The video signal from the hexacopter is either stored on the GoPro camera's internal microSD card (to operate in record mode) or transmitted in real time to the ground via the following chain: the

GoPro camera is connected to the Tarot T4-3D gimbal via a dedicated connector. The video signal is then transmitted to a 32-channel transmit antenna operating in the 5645-5945 MHz frequency range. This communicates with a dual receiver (2 built-in antennas for better signal reception) on 32 channels, on the same frequency of 5.8 GHz, and the image is displayed on a 7" HD monitor. Following laboratory tests, for the optimal operation of the transceiver chain, the transmitter was set to channel 4 (5645 MHz) and the receiver was set to channel 5 (5885 MHz), according to the frequency matrices in the specifications of each component. Fig. 4.8 shows the configuration and location of the video transceiver system, from the hexacopter to the operator. The HD video monitor with built-in receiver is shown in the tripod-mounted version, but it can also be mounted on the operator's radio remote control for easy observation of real-time images and gimbal control to obtain the desired frame during the surveillance, reconnaissance, investigation, shooting mission.

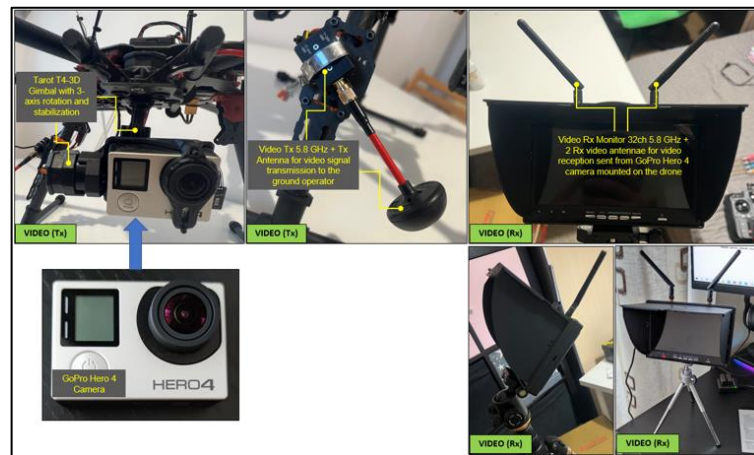


Fig. 4.8 Video signal transmission-reception chain from drone to operator

Fig. 4.9 illustrates the Pixhawk 2.4.8 flight controller (FMUv2 version) installed on the drone, in v2 version, with the interfaces to various avionics/peripheral equipment highlighted.

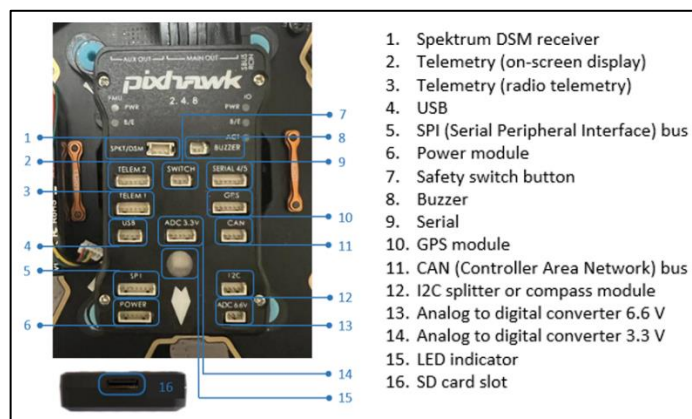


Fig. 4.9 Pixhawk 2.4.8 (FMUv2 version) automatic pilot and peripheral connection interfaces

The hardware components of the AP are as follows:

- STMicroelectronics STM32F427 Cortex-M4F 32-bit system-on-chip main microcontroller, operating frequency 180 MHz, RAM: 256 KB SRAM (L1), 2 MB Flash memory for writing instructions.
- System-on-Chip STMicroelectronics STM32F100 Cortex-M3 32-bit, 24 MHz operating frequency, 8 KB SRAM (L1), 64 KB Flash memory for writing instructions.
- embedded sensors on the motherboard:

- a 3-axis STMicroelectronics L3GD20H 16-bit gyroscope.
- a 14-bit STMicroelectronics LSM303D accelerometer/magnetometer.
- an Invensense MPU-6000 3-axis accelerometer/gyroscope.
- a TE Connectivity MEAS MS5611 barometer.

An external GPS antenna/bus antenna module consisting of:

- Ublox M8N GPS receiver.
- Honeywell HMC5883L digital compass.

In order to carry out the tests both on the ground and in flight, the ArduCopter firmware, version v4.x, was installed on the Pixhawk 2.4.8 PA motherboard. A laptop and a tablet were used for the ground control station, on which the Mission Planner platform was installed. In the v2 version the drone powering was done with three Turnigy batteries, LiPo type with 4 cells, in 4S1P and 4S2P configurations, maximum supported current 12-24C, with capacities: 12000 mAh, 16000 mAh, respectively 20000 mAh (fig. 4.10).



Fig. 4.10 Turnigy LiPo batteries with capacities of 12Ah, 16Ah, 20Ah respectively [48].

4.4 Hexacopter tests and results analysis

The results were obtained from tests carried out in the v2 configuration, equipped with the Turnigy 12000 mAh 12-24C LiPo 4S1P battery. For the GCS variant, the Mission Planner platform was used, whose interface is illustrated in Fig. 4.11.

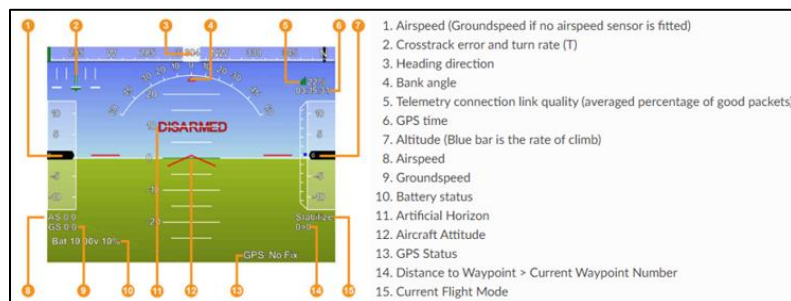


Fig. 4.11 Mission Planner HUD window

The purpose of these tests is to ensure, verify and prove the functioning of the drone in the configuration physically realized in the thesis, both in terms of the structure adopted and the avionics components, especially the flight controller used. These tests are divided into two main tests: the ground test and the flight test. The purpose of the ground test is to ensure that the drone's structure and avionics systems comply with the requirements, so that the hexacopter will perform the flight as expected.

4.4.1 Ground tests

The ground test consists of:

- inspection of the structural integrity of the drone. Each joint of the structural elements is checked and must be securely fastened to ensure its rigidity.
- checking the weight and balance of the drone. This provides information on the location of the actual center of gravity in all three axes X, Y and Z. The location of the center of gravity affects the performance and stability of the drone in flight.
- the operation of avionics systems (controller, navigation, power supply, video system, telemetry data transmission system and wiring). All data concerning the operating limits of the equipment making up the subsystems composing the avionics system (when known or obtained from measurements/tests) must be memorized/noted by the operator in order to avoid undesirable events (maximum range of the drone, range of the drone, maximum operating range of the radio controls, battery capacity, power consumption of the various electronic components, maximum authorized flight altitude, legislative aspects concerning the operation of the drone in certain areas, depending on the geographical layout). The flight controller has programmed the flight scenario (in the case of autonomous flight, following a pre-programmed route), the flight parameters and the failsafe measures required in the event of emergencies (loss of radio link between the drone and the operator, battery voltage falling close to the critical value, a motor shutdown).
- test on the operation of the motors by simple on/off commands to ensure the rated static performance of the motors. Increasing the speed incrementally up to 10-15% and checking their operation, oscillations, noises, proper propeller rotation directions.
- testing the telemetry data link between the drone and the Mission Planner ground control station. This ensures the stability of the radio link between the drone and the operator, with the help of the control station the operator can either plan autonomous flights on pre-programmed routes or intervene in the control of the drone in emergency situations, if radio control is not used.
- weather conditions check (wind speed, temperature, precipitation, atmospheric pressure) - this is an extremely important step in planning a flight, as there are limitations to operating the hexacopter.

Fig. 4.12 shows a map of the location of the tests using the Mission Planner platform.

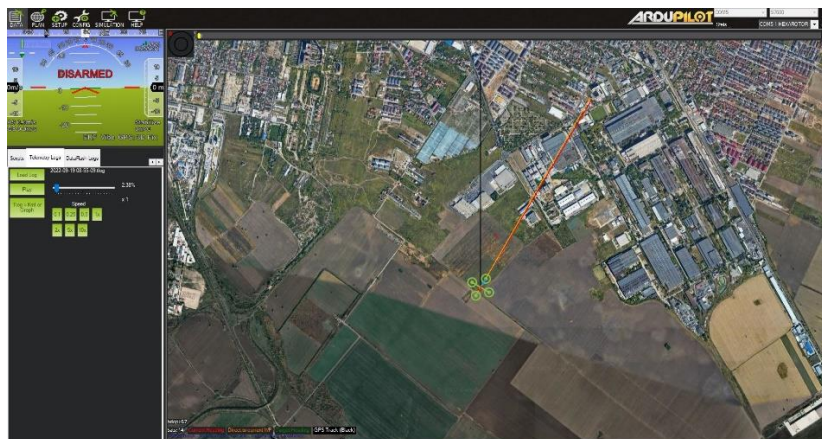


Fig. 4.12 Main window of the Mission Planner platform

The test stands, the ground control station, and the test location are illustrated on Fig. 4.13, and in Fig. 4.15 the details during the execution of the hexacopter maneuvers (take-off, climb, stationary, descent, landing) are shown.



Fig. 4.13 Test stands

4.4.2 Hover flight tests

After completion of the ground test, the hexacopter flight test is carried out in a stationary position at hover (Fig. 4.15). The tests were carried out in a plain area without obstacles around the test area, within a radius of 5 km, in order to avoid unpleasant events, such as: drone crash, i.e., destruction of property or injury to persons. Regarding the wind speed at the test site, days with low wind speed 1-2 m/s were chosen, measured with an anemometer (Fig. 4.14).



Fig. 4.14 Measuring wind speed with an anemometer

In the case of hovering, after the operator has given the command to increase the motor speed, the speed stick is kept in the 50-75% rpm range (for the hexacopter configuration) and the lift force required to lift the drone off the ground and kept it stationary. The lift force is created by the rotation of the six rotors, which rotate at the same rpm during the vertical climb, while the hexacopter tries to stabilize its attitude (position on the three coordinate axes). During the vertical climb, until the altitude set by the operator is reached and in respect to the command given by the operator, the hexacopter attitude PID regulators apply corrections to maintain the drone's position within the values of the commanded parameters. When stabilizing the hexacopter at a given altitude, the operator keeps the speed stick in the appropriate speed range and the PID altitude controller applies the necessary corrections to the thrust of the motors to maintain the drone at the desired altitude.



Fig. 4.15 Testing the drone in stationary flight at a hover - stages of flight.

Fig. 4.16a depicts images of the drone on the ground and in flight received from the GoPro Hero 4 camera mounted on the drone, and Fig. 4.16b shows the Mission Planner interface with the layout of the hexacopter on the map of the test location, and the video received from the GoPro camera on the built-in dual receiver monitor.



Fig. 4.16 a) Drone-mounted GoPro camera images, on the ground and in flight; b) Mission Planner interface/drone-mounted GoPro camera images

4.4.3 Interpretation of the results

In the case of the built hexacopter equipped with a three-axis gimbal and a photo/video camera, the drone must be able to maintain its position at a hover in order to carry out surveillance, reconnaissance, and photography missions. For this purpose, when using the manual radio control by the ground operator, it is recommended to operate it in the following modes: Stabilize (PID controllers automatically adjust pitch and roll) and Alt Hold (PID controllers automatically adjust pitch and roll and maintain drone altitude), respectively RTL (Return to Land) for emergency cases. Loiter can also be employed (semi-autonomous flight - the PID controllers automatically adjust the drone's altitude and position; the drone uses GPS for movement), PosHold (similar to Loiter mode but when the roll

and pitch sticks are not centered, the operator controls the two movements) and Land (the drone descends and lands directly, without returning to the take-off point). Auto mode is employed for autonomous movement along a predefined flight path. For PID controller tuning procedures, ATUTOTUNE mode is used, after sensor calibration procedures (accelerometers, gyroscopes, magnetometers) and initial tuning. In the case of the hover tests the take-off was performed in Stabilize mode, after which it was switched to Alt Hold mode, and then to RTL mode. The drone was lifted to an altitude of 8.5 m (Fig. 4.17). The EKF subsystem is responsible for generating attitude, velocity, position, and altitude estimates for the drone so that the navigation and control systems can operate correctly. EKF takes the inputs from IMU, GPS and BARO sensors and integrates them to provide these assessments, one of which is the estimated altitude. This is then passed to the vehicle's altitude control system, which attempts to align to the target altitude in altitude-controlled flight modes.

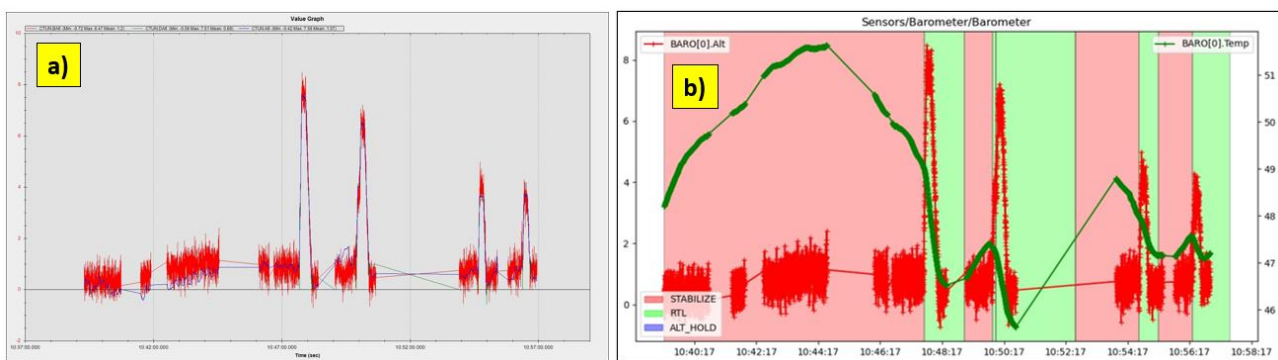


Fig. 4.17 a) Drone altitude; b) Drone altitude and ambient temperature

Fig. 4.17a shows the altitude reached by the drone in blue, the commanded altitude in red and the altitude measured by the barometer in green. It can be seen that there are no significant differences between the three values, the largest of these values being less than 1 m.

In Fig. 4.17b, using the MAVExplorer platform [4], the graph is extracted also showing the altitude at which the drone was lifted, respectively the ambient temperature at the test site, in degrees Fahrenheit ($46-51^{\circ}\text{F} = 7.8-11.1^{\circ}\text{C}$).

Fig. 4.18a illustrates the graph showing the atmospheric pressure (Pa) extracted from the data measured by the barometer with which the drone autopilot is equipped.

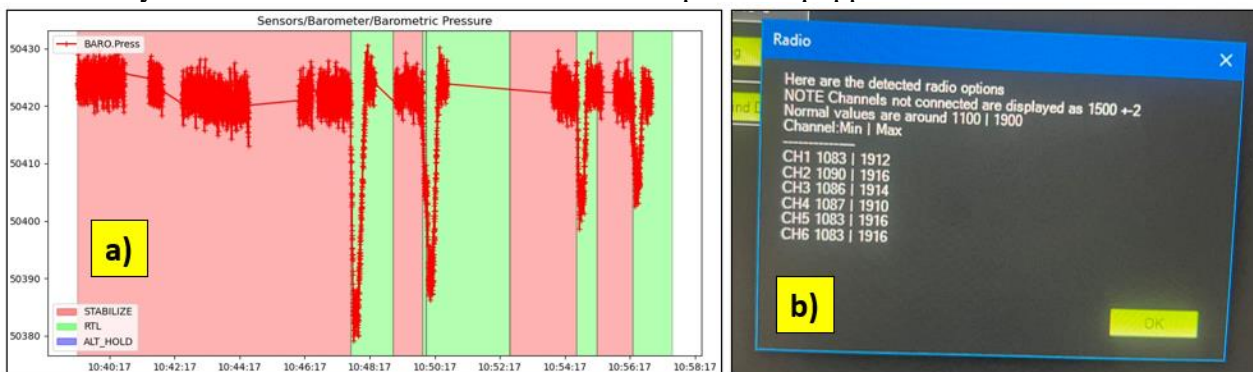


Fig. 4.18 a) Ambient atmospheric pressure; b) Fig. 4.32 RadioLink AT10II radio control calibration

For optimal operation of the drone, radio control calibration was initially performed using the GCS Mission Planner. Fig. 4.18b illustrates the minimum-maximum PWM (Pulse Width Modulation) signal duration limits for the channels used by the RadioLink AT10II radio control, mode 2 (motor stick is located on the left side), as follows: Channel 1 (CH1) - roll, Channel 2 (CH2) - pitch, Channel 3 (CH3) - throttle, Channel 4 (CH4) - yaw, Channel 5 (CH5) - flight modes (Stabilize, Alt Hold and

RTL), Channel 6 (CH6) - motor kill switch. In general, these channels operate in the range 1000-2000 μ s. The PWM signal is used to control the pulse width modulation signal for each electronic speed controller that is connected to each of the 6 motors. The PWM signal is a periodic square wave signal with a period of 20ms, which means it has a refresh rate of 50Hz. Each cycle of the PWM signal lasts for 1-2ms high level (1000 μ s - 2000 μ s), which is the control value of that channel. In the case of speed, 1000-1100 μ s corresponds to 0 speed of the hexacopter and 1900-2000 μ s corresponds to maximum speed.

Prior to ground and flight tests at the test site, the motors were checked in the laboratory without fitted propellers, to test their operation within the parameters. Fig. 4.19a illustrates the command given by the operator from the radio control, in the range 1083-1916 μ s, as calibrated previously. In Fig. 4.19b the response of the ESC-controlled motors in response to the operator's command to increase the speed is shown.

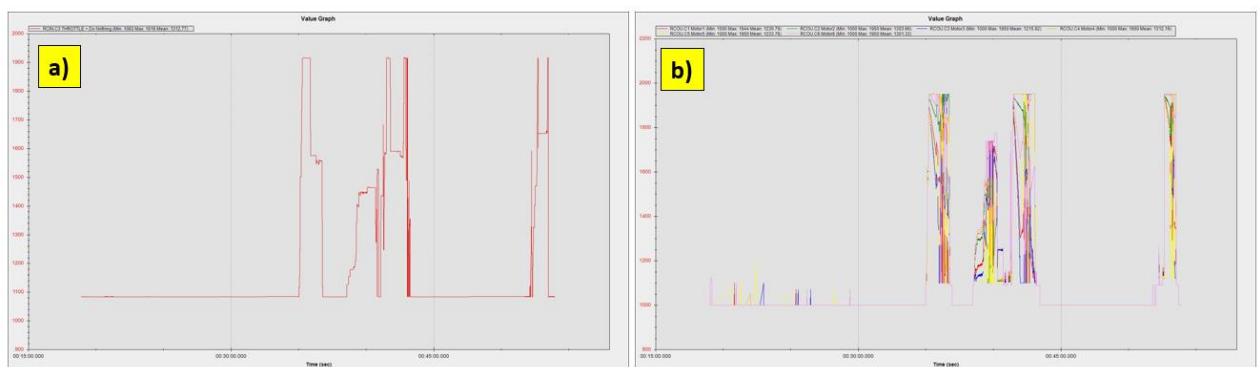


Fig. 4.19 a) Speed command given by the operator; b) Response of the motors to the command given by the operator.

It can be seen from Fig. 4.19b that they operate within the appropriate parameters, with values between 1000-1950 μ s and respond proportionally to the command given by the operator.

Fig. 4.20a illustrates the altitude of the test site (79-80 m above sea level). The peaks of the graph represent the altitudes to which the hexacopter was lifted during the maneuvers, and Fig. 4.20b show the geographic coordinates of the location (maximum altitude of the hexacopter stationary at the hover - 8.5 m).

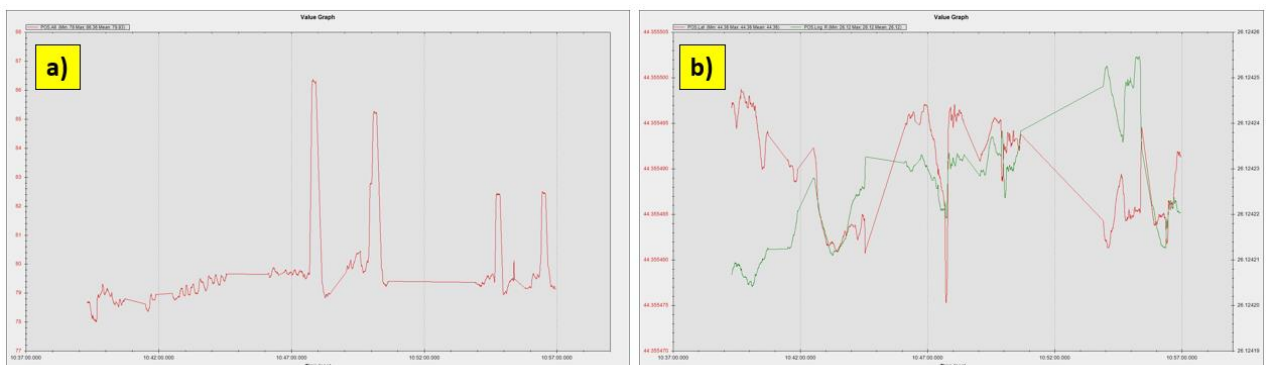


Fig. 4.20 a) Operating altitude of the drone in hover flight; b) Test location

The interpretation of the presented results has been performed with the Mission Planner and MAVExplorer platforms because each offers similar functionalities, but also brings features that are not found on both platforms.

Fig. 4.21a shows the command given by the ESCs to the motors in response to the operator throttle stick move in the 50-75% range. The motor rpm increases to a value at which the drone detaches from

the ground and begins to climb until the operator holds the rpm stick at a certain percentage. The operation of the motors is observed in the range 1000-1725 μs , as the rpm range does not reach 100%, leaving room for additional maneuvering if needed. It is observed that there are differences in the response time between 100-200 μs , possibly due to the eigen frequencies of the motors or of the structural elements on which they are mounted.

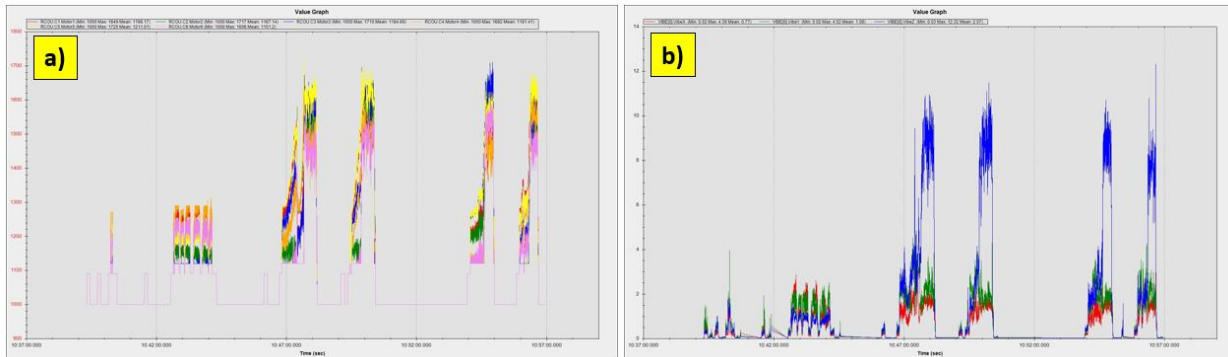


Fig. 4.21 a) Motor response to climb command; b) Accelerometer vibration (0)

Strong vibrations can cause accelerometer erroneous assessment of the drone's altitude and horizontal position, leading to problems to maintain the altitude (the hexacopter may start an uncontrolled climb maneuver without the operator being able to intervene) or position control problems in flight modes such as Loiter, PosHold, Auto etc.

Vibrations are best visualized by plotting the VibeX, VibeY and VibeZ values in the VIBE menu. These represent the raw vibration values before being filtered by the accelerometers. Vibration levels below 30 m/s^2 are normally acceptable. Levels above 30 m/s^2 can induce problems, and levels above 60 m/s^2 almost always are caused by problems with position or altitude maintenance [3]. The graph below shows acceptable vibration levels that are consistently below 30 m/s^2 , around 13 m/s^2 (Fig. 4.21b).

Similar results in terms of accelerometer vibration (0) were obtained when performing another flight under similar conditions with the hexacopter, as shown in Fig. 4.22.

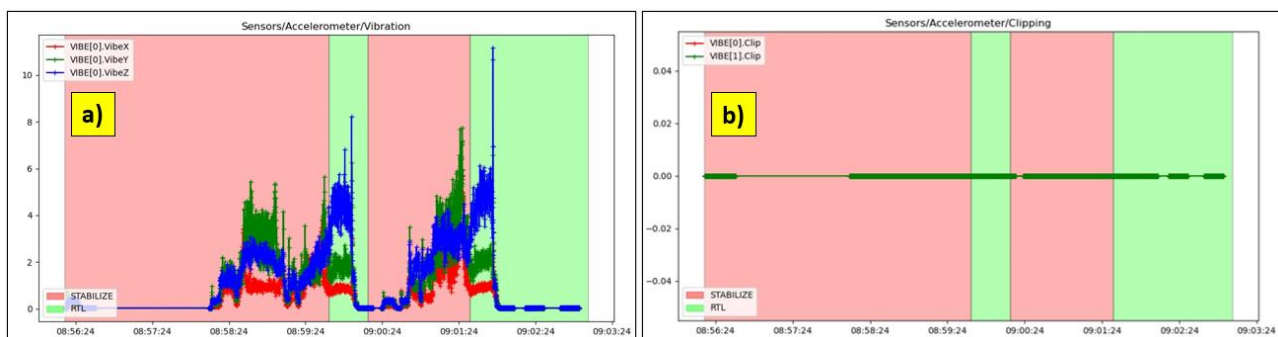


Fig. 4.22 a) Vibrations of accelerometer (0); b) Clipping phenomenon of accelerometers (0) and (1)

Fig. 4.22b shows the phenomenon of accelerometer clipping, which means that the accelerometers have been exposed to a level of vibration that exceeds their full measurement range. These are feedback signals to the control loop, so if they are not operating in optimal parameters then attitude control cannot be maintained. This phenomenon usually occurs when the drone collides with a hard object, such as crashing or landing hard on a surface. If the value increases during flight, it is recommended to rebuild the damping system by fitting double adhesive strips or soft rubber mounts to allow 3-axis movement and avoid inducing vibrations in the autopilot housing, which are then transmitted to the on-board sensors. In the case of the hexacopter it is observed to have a value of 0,

so we can conclude on this point that the accelerometers are not significantly affected by vibrations during operation. To illustrate the operation of the gyroscopes, in Fig. 4.23a-b the raw values measured by the gyroscopes of the rotational speeds in rad/s are shown. It can be seen that very low values are recorded because the hexacopter does not pitch, roll, or gyrate during the climb to the fixed-point hover altitude, but only compensates in very small increments to maintain attitude. Because the autopilot has two IMUs (Inertial Measurement Unit), namely (0) and (1), two graphs with data from both subsystems are shown.

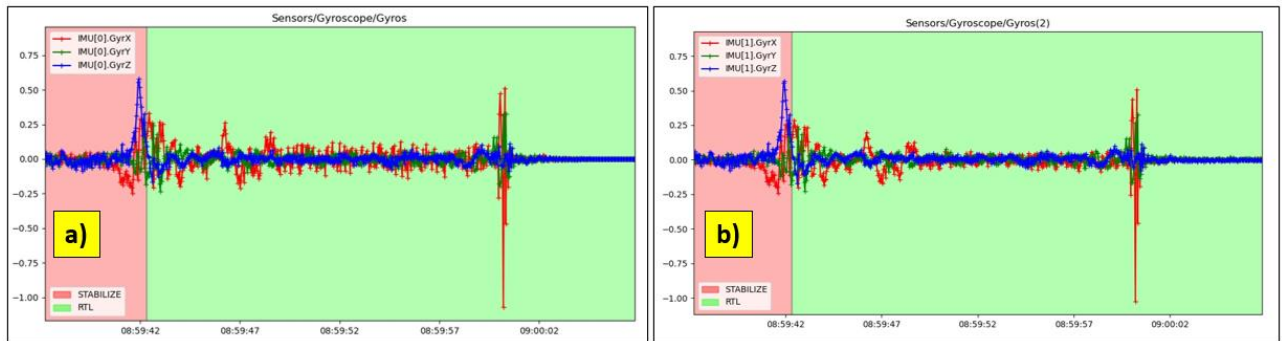


Fig. 4.23 a) Raw values of gyro rotational speeds in rad/s for IMU (0).
b) Raw values of gyroscope rotational speeds in rad/s for IMU (1).

As expected, the values measured by the gyroscopes of both IMUs are identical, indicating that they are functioning properly. In Fig. 4.24a the received GPS signal accuracy data is illustrated, in the case of the GPS signal received using the GPS antenna, which has the Ublox M8N GPS receiver incorporated. HAcc indicates a horizontal positioning accuracy of 0.5-1.2 m, VAcc indicates a vertical positioning accuracy of 0.55-1.45 m, and SAcc indicates a velocity measurement accuracy of up to 0.2-0.4 m/s. NSats indicates the number of satellites received, up to a maximum of 15.

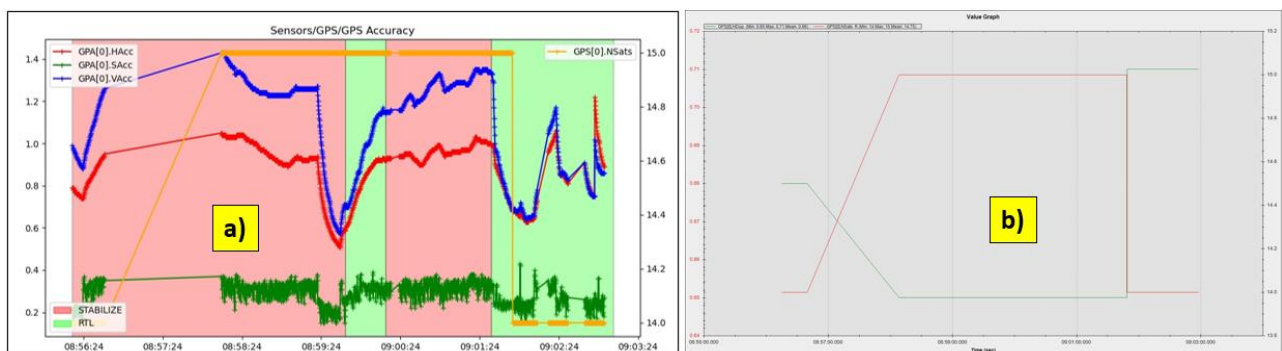


Fig. 4.24 a) Accuracy of data received from GPS satellites; b) Accuracy of HDop positioning data received from GPS satellites.

While operating in one of the autonomous modes (Loiter, RTL, Auto, etc.) GPS position errors can cause the hexacopter to “believe” it is in a different location than the correct one, which can lead to the drone flying aggressively to correct its perceived erroneous location information. These “errors” appear in both *tlogs* and data flash logs as a decrease in the number of visible satellites and an increase in the horizontal HDop accuracy value.

Hdop values less than 1.5 are very good, and values above 2 could indicate that GPS positions are not correct. Decreasing the number of satellites below 12 leads to erroneous measurements of the drone's position and speed relative to the ground. A significant change in these two values often accompanies a change in GPS position. Fig. 4.24b shows that the number of satellites received is 15,

and the horizontal position accuracy is 0.65-0.71 m, so both values correspond to a parameterized operation of the GPS satellite reception equipment.

Fig. 4.25a depicts a graph showing the relative speed of the drone to the ground, based on the information received from the GPS. Given that the drone performs the climb and hover maneuver at the hover with small position adjustments, it is observed that the value of this velocity is mostly close to 0 m/s.

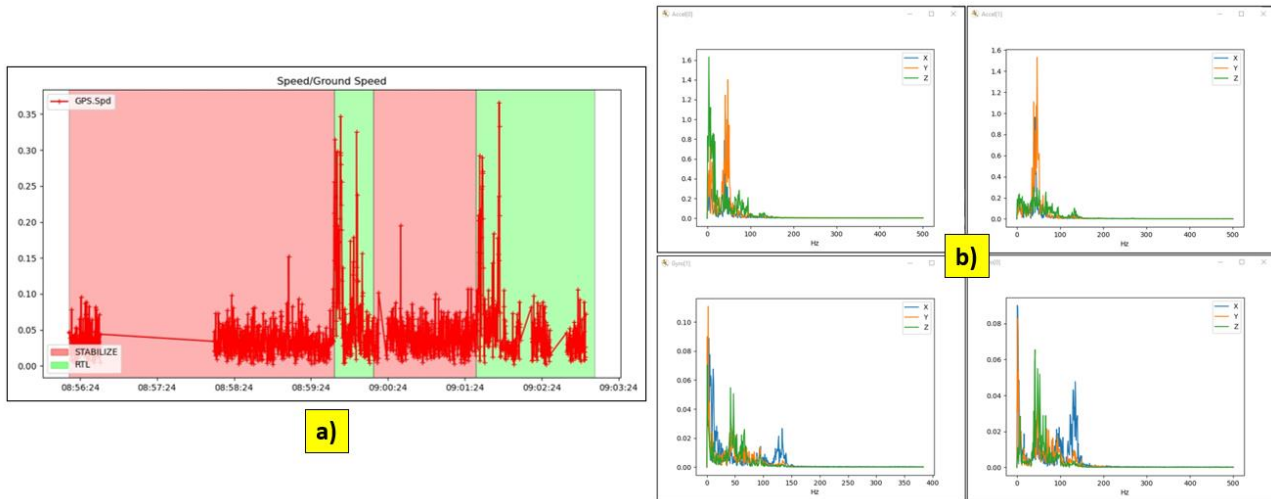


Fig. 4.25 a) Relative speed of the drone to the ground; b) Vibration frequencies introduced by the rotation of the motors.

Mission Planner, via the IMU Batch Sampler menu has the option to record high frequency data from IMU sensors to the flash data log on the autopilot. This data can be analyzed after the flight to diagnose vibration-related problems using graphs created from Fast Fourier Transforms (FFT) of the data. FFT transforms data from the time domain to the frequency domain. In other words, accelerometer data recorded over time (e.g., a flight) can be converted into a graph showing vibration frequencies. A common feature of these plots is a peak at the "propeller blade crossing frequency" (the frequency at which the blade passes over the arms), which causes an acceleration in the airframe. In the graphs illustrated in Fig. 4.25b it can be seen from the data collected from accelerometers and gyros that there are, however, certain noises corresponding to the natural rotational frequencies of the motors. The accelerometer and gyroscope data show on the vertical axis the amplitude and on the horizontal axis the natural rotational frequency of the motors. The amplitude is not scaled to a useful value, which means that we cannot state whether the levels of these values are high or low, which means that the graph is only useful for determining the vibration frequency. Vibrations at frequencies higher than 300 Hz can lead to attitude or position control problems. In this case, frequency peaks are observed at 40 Hz/2400 rpm, 47 Hz/2820 rpm, 95 Hz/5700 rpm, 130 Hz/7800 rpm and 153 Hz/9180 rpm. It is possible to filter out some of these noises to increase performance and allow better parameter tuning by activating the harmonic notch filter(s). The harmonic notch filter is designed to match the frequency of the noise introduced by motor rotation. Its value changes as the motor rotates by interpreting the value of the motor acceleration. The frequency is scaled up from the hover frequency and will never drop below this frequency. However, in dynamic flight it is quite common to reach low motor operating frequencies during propeller rotation. To solve this, it is possible to modify the reference value to scale the filter to a lower frequency.

4.5 Conclusions, original contributions and published article.

Conclusions

- tests have proved that the drone operates within the correct parameters during fixed-point flight maneuvers.
- the test flights were carried out in stationary flight at a hover, with four LiPo batteries in 4S1P configuration, rated voltage 14.8V, of different capacities: 6600 mAh, 12000 mAh, 16000

mAh and 20000 mAh respectively. The simulations show the versions with 6600 mAh and 16000 mAh batteries (Figure 4.10).

- the tests carried out illustrated an increase in autonomy with the higher capacity battery.
- following the tests carried out with the HUT in the equipment shown in v.1, the hexacopter could be kept in the air for about 10 minutes in the case of hover1 flight. By comparison, in the case of the results provided in chap. 3, following the simulations performed with the *xcopterCalc* utility, the range of the drone was 12.4 minutes, **resulting a 20% increase** and from the analytical calculation relationships presented in chap. 3 resulted in a range of 13.32 min, **resulting a 25% increase** in autonomy.
- in the case of the 12000 mAh battery the autonomy of the drone was 15.8 minutes, **resulting a 37% increase** in autonomy and in the case of the 20000 mAh battery the autonomy obtained was approximately 20 minutes, **resulting a 50% increase** in autonomy.
- after replacing the battery with a 16000 mAh battery / 4S2P / 14.8V / 4 cell configuration, in the case of hover flight the HUT could be kept in the air for about 18 minutes, **resulting a 45% increase** in autonomy. By comparison, for the data provided by the *xcopterCalc* utility, the drone range was 20 minutes, **resulting a 50% increase** in autonomy and, following the introduction of the new battery capacity into the analytical calculation relationships in chap. 3, a range of 20.38 min resulted, **resulting a 51% increase** in autonomy.
- the performance of the drone can be improved by eliminating of translating as far as possible the natural vibration frequencies introduced by the rotation of the motors using dynamic harmonic notch filters.
- for the operation of the drone beyond visual line of sight (BVLOS), the necessary components for implementation on the drone have been purchased and ground and flight tests can be carried out to demonstrate their capability to control the hexacopter over 3G/4G LTE mobile networks. These include Raspberry Pi 3B board, IR camera + EO camera, 4G LTE modem.
- other drone flights in different flight regimes, both manual and autonomous, can be carried out to test its limits, but the author considered of interest the behavior of the drone in stationary flight at a hover, a maneuver that will also be studied in chapter 5, in the FEM/CFD analysis, where wind speed and direction will be considered.

Original contributions

- the new hexacopter platform built in two versions, equipped with avionics components for the command and control of the drone, including the transmission-reception system of drone-ground-drone telemetry data.
- equipping the hexacopter with a video transmission-reception system.
- laboratory, ground and flight tests were performed to verify the compatibility of the components and the optimum functioning of the drone.
- conducting flights on the ground to determine the flight autonomy of the hexacopter, with different battery capacities.
- making the necessary corrections/adjustments for stable operation of the drone during stationary flight at a hover.

Published articles:

- **Stamate, M. A.**; Pupăză, C.; Nicolescu, F. A.; Moldoveanu, C. E. Improvement of Hexacopter UAVs Attitude Parameters Employing Control and Decision Support Systems. *Sensors* **2023**, 23, 1446. <https://doi.org/10.3390/s23031446>.

Chapter 5. FEM analysis of the hexacopter drone using advanced simulation procedures

5.1 Introduction

As demonstrated in Chap. 1, great efforts and attempts have been made in recent decades to improve the design solutions of Unmanned Aerial Vehicles (UAVs) using numerical and computer aided engineering methods, due to their remarkable usefulness in a very wide range of applications in many fields.

The hexacopter has been analyzed to provide a robust structure for carrying a large payload. Recent studies have also analyzed by numerical methods (FEM) the stable attitude of the drone during flight, according to the work of Suprpto et. al [27]. The evaluation focused on frame displacement and frame stress analysis to ensure the capability of transporting the desired payload. In the work of Lei et. al [17], an experimental and CFD simulation investigation of a very small UAV model under light wind influences was recently performed. The study is comprehensive, but the geometry of the prototype, as well as the flow regimes of the fluid in this case were found to be below the level of common applications where UAVs are used. The downward flow areas of airfoils at different glide altitudes have also been simulated and analyzed in the work of Zheng et. al [31] for plant protection applications. Although the study is convincing, the achievements are strictly related to agricultural engineering applications. Although many studies have been undertaken on hexacopters from different perspectives, CFD analysis for this type of UAVs has mostly been presented by software development companies to prove the capabilities of the simulation platforms, as it is still considered a challenging modelling and simulation problem. FEM is still not widely used for drone design purposes. Model reduction, tuning the model mesh parameters according to the available computational resources and choosing appropriate computational models are considered difficult to be achieved. In the case of six rotors, the rotating domains of the propellers are so close to each other that the narrow space causes even more modelling problems.

The novelty of the research lies in combining the CFD approach with structural evaluation to provide useful knowledge to the hexacopter drone developer in order to achieve stable, fixed-point hovering. The effect of wind interference (air fillets) between the rotors was also investigated, elements identified in the work of Stamate et. al. [25], respectively in the work of Stamate et. al. [26].

This chapter is structured as follows: after a brief introduction, the next section presents an aerodynamic study of the hexacopter using CFD simulations. The computational model and the adopted hypotheses are confirmed by extracting from the numerical simulation results the same values of the forces calculated analytically. The research strategy and the mathematical model employed for the turbulence study have also been presented. CFD simulation scenarios for three different wind speeds and directions are analyzed and the simulation results are examined. In the next section the results of the CFD simulations are transferred to the structural elements of the drone and the displacements that occur as a result of the velocities and pressures created by the turbulence occurring when the drone is stationary at a hover are analyzed. The next section includes a study of the free vibrations of the hexacopter with consequences for the drone stability. The good synchronization of the values obtained by simulation and those determined experimentally by FFT analysis of the accelerations were also emphasized. Finally, a dynamic impact analysis is performed for a scenario of the hexacopter falling from a height of 20m. The results are analyzed in relation to experimental observations during flight tests.

The studied hexacopter is equipped with six rotors, each rotor assembly consisting of a Brushless Direct Current Motor (BLDC) and a 2-bladed, fixed pitch propeller mounted on top of the motor. The drone has Short Vertical Takeoff and Landing (SVTOL) capabilities.



Fig. 5.1. Hexacopter developed and used in the CFD study.

Fig. 5.1 shows the improved version and the design employed in the FEM simulation. Each rotor assembly is positioned at the end of a support arm, set at 60 degrees to each other, with all six rotors lying in a plane parallel to the ground around the main axis of rotation of the drone (the vertical z-axis in this case). The drone also has two arms, in the shape of an inverted T, attached to it for the landing gear, in order to bring the drone safely to the ground and to protect the equipment from damage or destruction.

5.2 Chapter objectives

- ensuring the stability of the hexacopter drone during stationary flight maneuvers;
- development of a complete and complex simulation model for all types of CAE analyses;
- validation of the FEM computational model;
- synchronization of analytical, experimental, and numerical results;
- using the results obtained from the FEM study to optimize the flight parameters (e.g., rotor speeds).

5.3 Aerodynamic study of the hexacopter drone employing numerical methods (CFD)

Hexacopter drones have a stable flight behavior at high wind speeds and an increased capacity to carry large payloads. However, the most common problems occur when the drone is out of its nominal operating range (hovering) or when attempting aggressive maneuvers in flight. The lack of horizontal force control makes it almost impossible to independently intervene on the position of the vehicle attitude, limiting possible drone control solutions. This is why Computational Fluid Dynamics (CFD) combined with structural analysis (FEM) of propeller behavior during flight can help the researcher to gather valuable information that, combined with different flight regimes/altitudes, can contribute to the development of appropriate control solutions. This chapter focuses on a practical combination of computer-aided engineering techniques leading to innovative CAE development of hexacopter drones. Stationary fixed-point flight is one of the most important flight regimes of the hexacopter, in this case the UAV having maximum stability requirements. The fixed-point turbulence regime is also important, as it may be in close proximity to buildings, other targets or even the ground, in a package delivery situation, especially in urban areas. This was considered when creating the flow domain around the hexacopter. The air pressure under the hexacopter is higher the closer the drone is to the ground. It is therefore important to know the air pressure values so that the hexacopter remains stable. Also, on the frame of the drone the pressure increases correspondingly as it approaches the ground or a target. Some of the turbulences that are created return and also act on the drone components and rotors. The hexacopter can work in areas with dust, sand and even snow, which can then interact with the drone. This is why CFD study is essential to ensure the stability and safe operation of the

hexacopter. Another important aspect of CFD simulations is the power requirements and the evaluation of the lift forces. These must be understood in the sense that the modelling simplifications required to create flow domains may result in values slightly lower than the experimental, real values.

5.3.1 CFD Simulation

The proposed CFD approach consists of three main steps (Fig. 5.2a): a modeling phase of defeaturing and geometry simplification to create the computational model, followed by the CFD runs to calculate the thrust forces on each propeller and to evaluate the total deformation on the mechanical structure of the hexacopter for one of the simulation cases. The rotors are arranged on a 343 mm radius as illustrated in detail. The propeller faces were mapped, and the model topology was edited and verified to ensure the quality of the discretization. The final step is a new fluid-structure interaction strategy to evaluate the effect of airfoil turbulence on the glide flight of the hexacopter, *Stamate et. al.* [25].

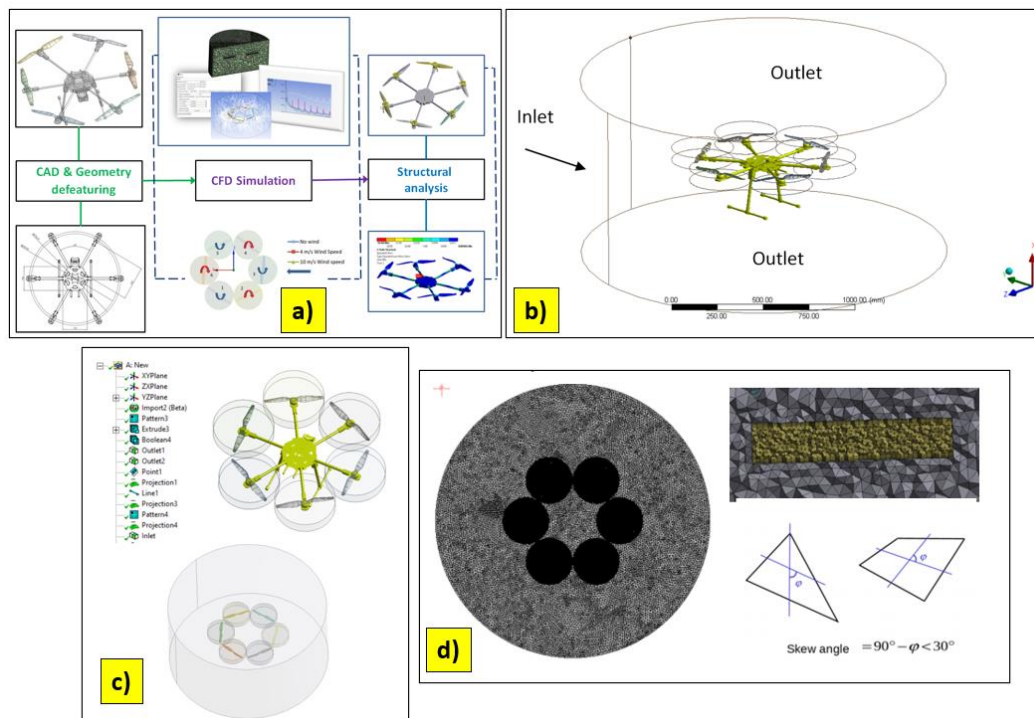


Fig. 5.2 a) CFD approach in the context of hexacopter concept development; b) Geometry prepared for CFD calculations; c) Extracting the computational model from the overall hexacopter geometry; d) Discretization. Global model, detail, and skewness criterion

The improved UAV model was designed in SolidWorks, imported in STEP format, and simplified (Fig. 5.2b). The flow domains were constructed with respect to discretization that materializes the rotation of the air fillets around each propeller, where a particularly fine grid was generated. For this, inflation layers were constructed built around the propeller faces, and the size of the elements was reduced to avoid continuity problems during iterative calculations. Due to the relatively small proximity of the six rotors and the fine discretization of the rotors domain, contact regions between the discretization domains of each rotor have to be avoided (Fig. 5.2c). The modelling for the CFD simulations considered that the analysis is performed in a transient regime, in which case the size of the discretization is determined by the Courant number. In order to avoid numerical instability problems this number must be $\cong 1$ [8].

$$Co = v_{max} \cdot \frac{dt}{dx} = 10 \cdot \frac{0.03}{300 \cdot 10^{-3}} = 1 \quad (5.1)$$

where v_{\max} is the maximum velocity in the flow domain, dt - the time increment, and dx is the finite element size. For the worst case scenario, the velocity is 10 m/s, $dt = 0.03$ s (from the computation settings), and the discretization size is 300 mm. Both for the individual rotor enclosures and in the vicinity of their surfaces, where boundary conditions may result in large velocity flow gradients, five successive gradually discretized layers (inflation layers) were created. Finally, a discretized model was obtained as illustrated in Fig. 5.2d with 602317 nodes and 2865347 elements. The quality of the discretization was checked by employing the "skewness" criterion, which measures the difference between the element shape and perfect shape. Finite elements with high skewness coefficient may decrease the accuracy of the results and destabilize the numerical solution. The general rule is that the maximum skewness for a tetrahedral mesh should be kept below 0.95, with an average value less than 0.33. In the case of the developed model these parameters were: maximum skewness coefficient 0.94, and mean value 0.216.

5.3.2 The flow model.

In numerical fluid dynamics the conservation of mass and momentum equations are employed to solve the equations of motion. When the flow regime is turbulent, for the k - ϵ enhanced turbulence model, additional equations for fluid mass transport, are added to these equations. The solver calculates the fluid flow equations by default in a stationary, or inertial, reference frame. In practice, however, there are many problems where one must solve the equations in a moving or non-inertial reference frame, such as rotors and moving walls, where engineers are particularly interested in the behavior of the model around moving parts. In most cases, these moving parts make the problem unstable when viewed from a stationary frame. That is why the transient regime and/or so-called "reference frames" are employed. In these cases, the equations of motion are modified to incorporate the additional terms given by the acceleration, which arise as a result of the transformation from the stationary to the moving regime. The K -epsilon (k - ϵ) turbulence model is the most commonly used model for simulating turbulent flows. The description of fluid flow is given by two equations: the kinetic energy (k) and the kinetic energy dissipation coefficient (of turbulence - ϵ). The assumption made is that viscosity is isotropic and the relationship between specific stresses and strains is constant in all directions for Newtonian fluids. It is the most general turbulence model that can describe a wide range of flow phenomena. Disadvantages of this model are related to the fact that the model is essentially a Reynolds model with problems related to boundary conditions around the walls and which from a mathematical point of view causes a so-called "numerical stiffness", requiring high degree nonlinear functions for solving, which are difficult to handle in linear computational algorithms.

Another disadvantage is *the lack of sensitivity of the model to large pressure gradients. It has been observed that under such conditions the model overestimates the shear stress and thereby delays the separation of the flow layers.* For these reasons in the thesis the k - ϵ realizable flow model was used according to [7].

5.3.3 Simulation scenarios and discussion of results

The CAE study has been performed on five simulation scenarios, considering wind speed in the horizontal direction: no wind, wind speed of 0 m/s, 4 m/s, 10 m/s, 15 m/s, 20 m/s respectively. For all cases the angular velocity of the rotors had a maximum value of 6500 rpm. Fig. 5.3a-e depicts the velocity and pressure contours in the vertical plane, for the turbulent flows. The influence of the wind on the turbulent flow of the propellers occurring in this section of the hexacopter plane can be observed, and the dissipation of the central turbulence is significant, the air-fillets being deflected by the crosswind (for the cases $v = 4$ m/s, $v = 10$ m/s, $v = 15$ m/s, respectively $v = 20$ m/s).

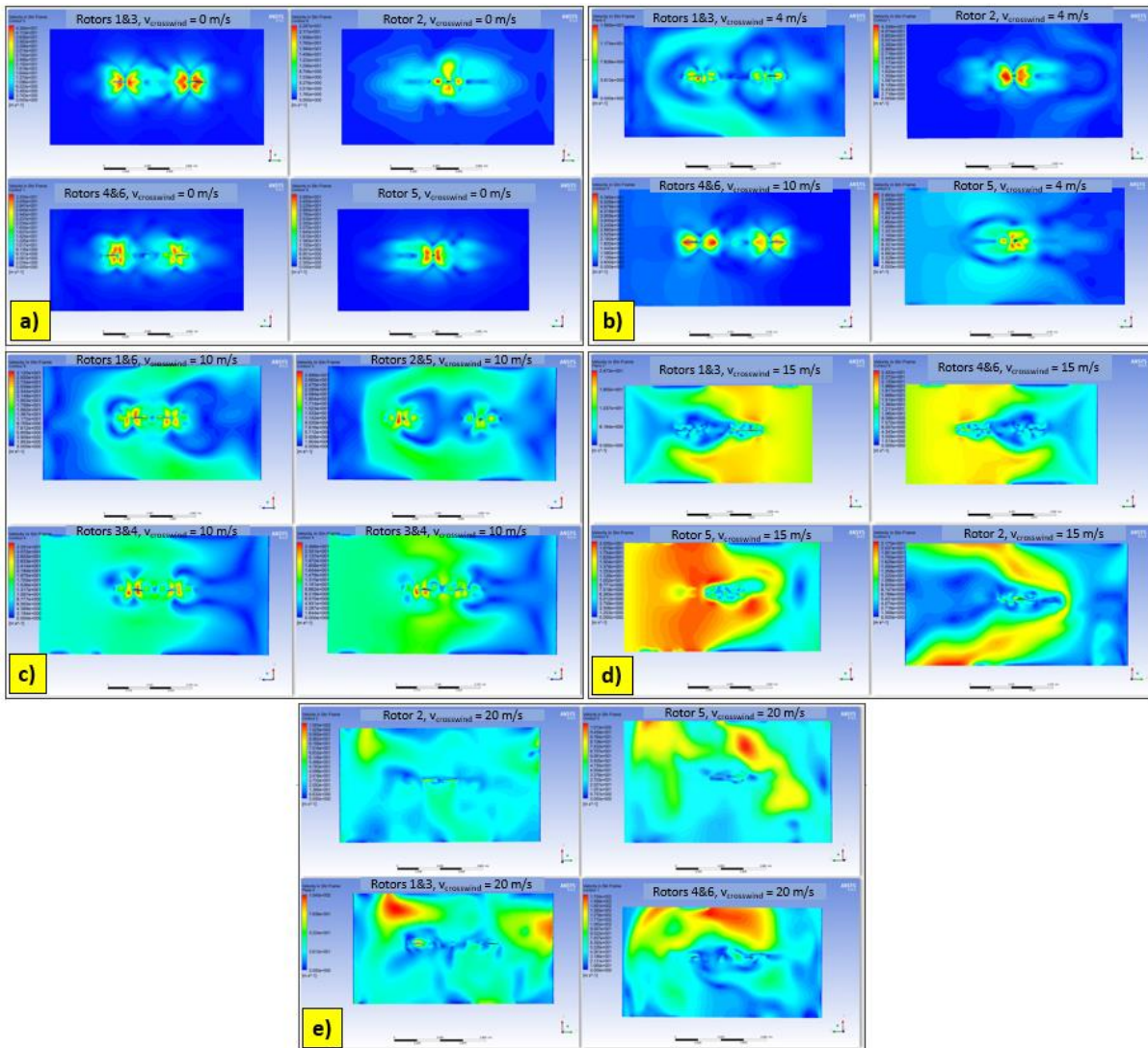


Fig. 5.3. a) Speed contours for crosswind $v = 0$ m/s; b) Speed contours for crosswind $v = 4$ m/s; c) Speed contours for crosswind $v = 10$ m/s; d) Speed contours for crosswind $v = 15$ m/s. e) Speed contours for crosswind $v = 20$ m/s

The values of the reaction thrust forces of the six propellers were between 0 and 38 N in absolute values (Fig. 5.4-5.6). The thrust forces were exported in a static analysis and the spatial orientation of the hexacopter structure was evaluated as a function of the air pressure caused by the turbulence created, the rotational speed of the six rotors and the acceleration of the hexacopter. Finally, a static analysis was performed and the total deformation of the rotors at different times during the simulation was processed.

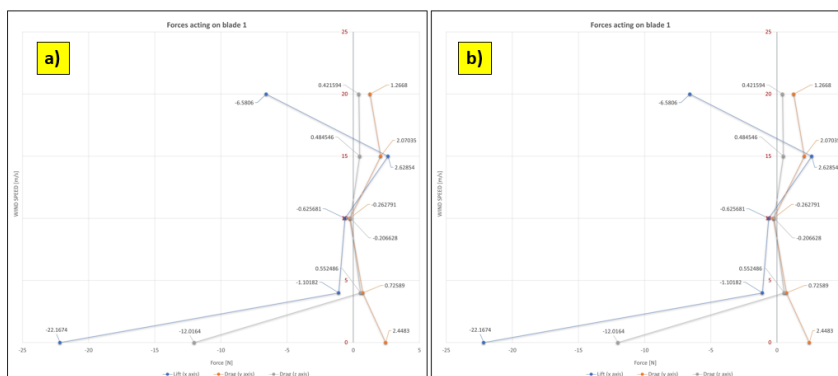


Fig. 5.4. a) Forces acting on propeller 1; b) Forces acting on propeller 2

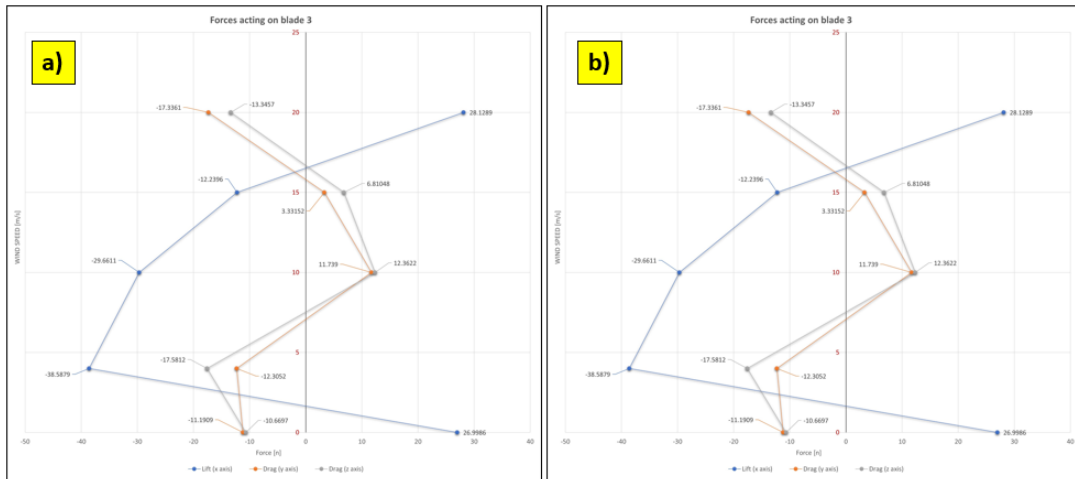


Fig. 5.5. a) Forces acting on propeller 3; b) Forces acting on propeller 4

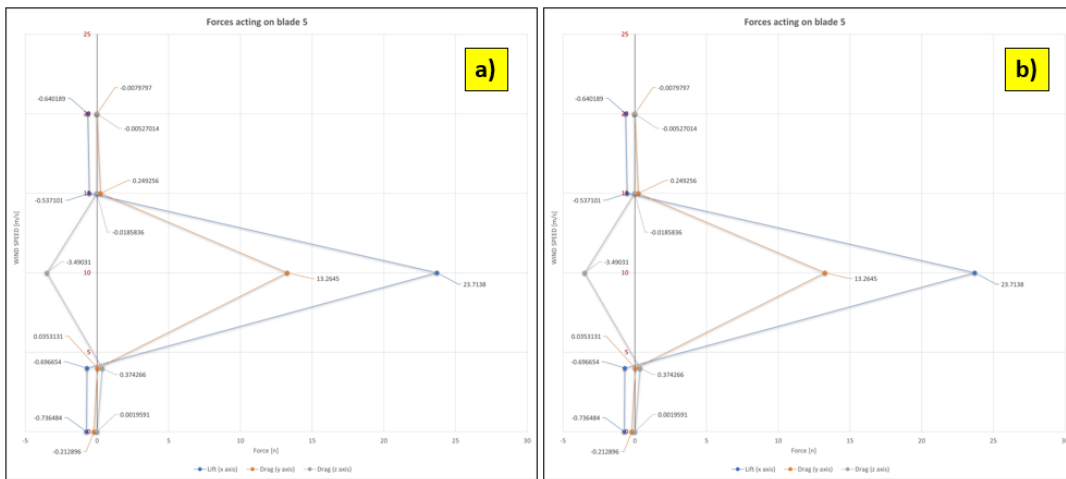


Fig. 5.6. a) Forces acting on propeller 5; b) Forces acting on propeller 6

5.4 Static analysis of hexacopter structural elements

The pressure distribution and thrust forces from the CFD simulations were exported to a structural analysis of the propeller assembly to capture the influence of the CFD response parameters on the stability and maneuverability of the hexacopter. Fig. 5.7 illustrates the deformed structure of the hexacopter overlapped on the undeformed shape in the YZ plane. The directional deformation at 0.25s demonstrates a low maximum value of 0.5 mm and ensures the stability of the hexacopter during hover.

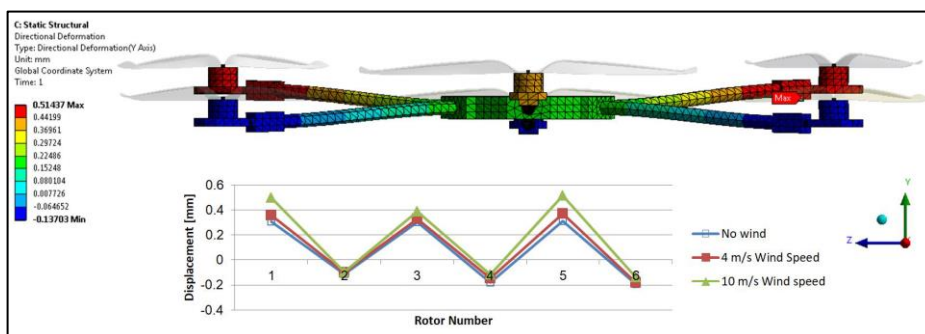


Fig. 5.7 Maximum displacements in the Y-direction of the hexacopter mechanical structure after 0.25s hover

The displacements are observed to have low values (0.4-0.5 mm) even under strong side winds, the drone structure being robust from this point of view.

5.5 Dynamic analysis and hover stability conditions

The dynamic analysis focused on the study of free vibration (modal analysis) and impact vibration (drop test) of the rotors and the whole drone (Fig. 5.20) to verify the stability and the structural integrity of the hexacopter.

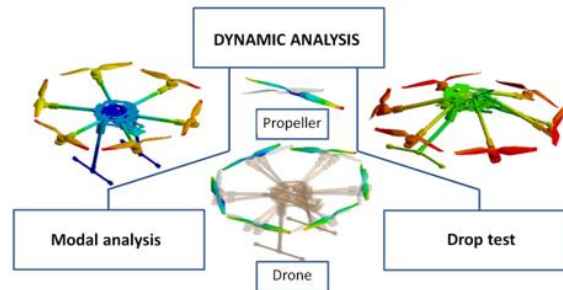


Fig. 5.8. Dynamic analysis of the hexacopter by FEM

The purpose of the modal analysis is to determine the eigenvalues for the drone structure and for the propeller and to design the drone control system to ensure the structural stability of the drone for certain fixed-point velocities in case of surveillance operations. Generally, all FEM structural analysis programs provide good accuracy for the first six natural frequencies and the corresponding mode shapes. An orthotropic elastic Epoxy Carbon Woven (230 GPa) Prepreg material was employed for the drone's structure and rotors (Tables 5.1-5.3). In order to ensure during the simulation a similar behaviour of the model to the real drone, all the masses of the assemblies and individual components of the drone were controlled and synchronised.

Table 5.1. Material properties for static and modal analysis

Material property	Value	Material property	Value
Density	1420 [Kg/m ³]	XY Poisson Coefficient	0.05
Coefficient of thermal expansion in X direction	2.5 · 10 ⁻⁶ [C ⁻¹]	YZ Poisson Coefficient	0.3
Coefficient of thermal expansion in Y direction	2.5 · 10 ⁻⁶ [C ⁻¹]	XZ Poisson Coefficient	0.3
Coefficient of thermal expansion in Z direction	1 · 10 ⁻⁵ [C ⁻¹]	XY Shear Modulus	1500 [MPa]
Young Modulus in the X direction	61340 [MPa]	YZ Shear Modulus	3000 [MPa]
Young Modulus in the Y direction	61340 [MPa]	XZ Shear Modulus	3000 [MPa]
Young Modulus in the Z direction	6900 [MPa]		

Table 5.2. Stress limits

Material property	Value	Material property	Value
Tensile stress X	892 [MPa]	Shear stress XY	120 [MPa]
Tensile stress Y	892 [MPa]	Shear stress YZ	50 [MPa]
Tensile stress Z	50 [MPa]	Shear stress XZ	50 [MPa]
Compression stress X	-439 [MPa]		
Compression stress Y	-439 [MPa]		
Compression stress Z	-140 [MPa]		

Table 5.3. Strains limit and Tsai-Wu coefficients

Material properties	Value	Material properties	Value
Strain X	0.0086	Shear XY	0.022
Strain Y	0.0086	Shear YZ	0.018
Strain Z	0.007	Shear XZ	0.018
Compression X	-0.0055	Tsai-Wu Coefficient XY	-1
Compression Y	-0.0055	Tsai-Wu Coefficient YZ	-1
Compression Z	-0.012	Tsai-Wu Coefficient XZ	-1

The computational model was built based on beams and plates, with the full control of the components weight and of the assembly (Fig. 5.9). An efficient model in terms of the computational time was achieved. The mesh was processed in an advanced ANSA Preprocessing System to combine several discretization strategies.



Fig. 5.9. Discretization for structural analysis

5.5.1 Discussion of the modal analysis results

The modal analysis aimed to determine the natural frequencies, the mode shapes and to identify possible dynamic "weak points" of the drone's structure. For this purpose, the rotors and the drives were replaced by concentrated masses simulating their presence. Since the drone structure and the propellers have different frequency domains, distinct modal analyses were performed on specific frequency domains. The structure is symmetric, and this is also reflected in the modal structural response. Similar modes have been removed and only representative modes for the vibrational response have been processed. Thus, the first modes are bending modes in the vertical plane, followed by bending modes in the vertical combined with share in the horizontal plane, after which dominant share modes occur (Tables 5.4-5.5). Participation factors were employed to select the dominant vibration modes. For this purpose, the first 10 eigenvalues were calculated, with the normalization of the mass matrix in respect to the unit matrix.

Table 5.4. Vibration modes of the drone's structure

<p>D1 Modal Total Deformation Type: Total Deformation Frequency: 8.2564 Hz Unit: mm</p>	<p>D1 Modal Total Deformation 2 Type: Total Deformation Frequency: 14.246 Hz Unit: mm</p>	<p>D1 Modal Total Deformation 4 Type: Total Deformation Frequency: 14.769 Hz Unit: mm</p>
<p>Mode 1 $f_1=8.256$ Hz/495.36 rpm vertical bending vibrations of the rotor arm support</p>	<p>Mode 2 $f_2=14.246$ Hz/854.76 rpm bending vibrations of two arms</p>	<p>Mode 4 $f_4=14.27$ Hz/856.2 rpm bending vibrations for four arms of the drone</p>
<p>D1 Modal Total Deformation 5 Type: Total Deformation Frequency: 15.275 Hz Unit: mm</p>	<p>D1 Modal Total Deformation 6 Type: Total Deformation Frequency: 15.478 Hz Unit: mm</p>	<p>D1 Modal Total Deformation 7 Type: Total Deformation Frequency: 16.639 Hz Unit: mm</p>
<p>Mode 5 $f_5=15.275$ Hz/916.5 rpm bending and share vibrations of the drone arms</p>	<p>Mode 6 $f_6=15.478$ Hz/928.68 rpm Y-plane bending vibrations</p>	<p>Mode 7 $f_7=16.639$ Hz/998.36 rpm Z-plane bending vibrations of the vertical legs of the drone</p>

The analysis of the mode shapes of the hexacopter structure shows that there are no frequencies that create problems regarding the attitude or position control of the drone. Significant propeller frequencies are shown in Table 5.5.

Table 5.5. Rotor vibration modes

<p>F1 Modal Total Deformation Type: Total Deformation Frequency: 45.866 Hz Unit: mm</p>	<p>F1 Modal Total Deformation 2 Type: Total Deformation Frequency: 47.13 Hz Unit: mm</p>	<p>F1 Modal Total Deformation 3 Type: Total Deformation Frequency: 111.48 Hz Unit: mm</p>
<p>Mode 1 $f_1= 45.866$ Hz/2751.96 rpm vibrations in the vertical</p>	<p>Mode 2 $f_2=47$Hz/2820 rpm "Flapping wings"</p>	<p>Mode 3 $f_3=111$ Hz/6660 rpm horizontal share vibrations.</p>
<p>F1 Modal Total Deformation 4 Type: Total Deformation Frequency: 113.66 Hz Unit: mm</p>	<p>F1 Modal Total Deformation 5 Type: Total Deformation Frequency: 362.19 Hz Unit: mm</p>	
<p>Mode 4 $f_4=113$ Hz/6780 rpm horizontal twisting vibrations.</p>	<p>Mode 5 $f_5=362$ Hz/21720 rpm combinations of bending and twisting vibrations.</p>	<p>Mode 6 $f_6=367$ Hz/22020 rpm combinations of bending and twisting vibrations.</p>

While the structural elements of the drone do not pose any problems in respect to the natural frequencies, regarding the rotors, as anticipated in Chapter 4 it is confirmed that the amplitude peak at 47 Hz/2820 rpm is due to the natural frequency of the rotor that is the same with the operational frequency. This speed should be avoided and can be considered for the flight parameters control at fixed-point. See Fig. 4.25b and the comments on it in the previous chapter. Higher order frequencies influence flight parameters during maneuvering, but they do not overlap with the rotational speed employed during the experiments. However, they have to be known and avoided.

5.6 Impact analysis of the hexacopter

5.6.1 Objectives.

The aim of this analysis was to assess possible damage of the drone structural elements in the event of a crash, or an accidental landing on a rigid plate from a height of 20 m. All contacts between the components were considered rigid to mitigate potential impact mitigation effects.

5.6.2 Drop test.

This simulation is performed by explicitly solving the equations of motion. It is employed for transient phenomena with short time duration and extreme nonlinearities, such as the UAV crash test. This analysis involves phenomena with extremely large strains, breakage, material damage, and non-linear material behavior. During the simulation, the time is sampled, and the resolution depends on the results of the previous time step. The duration of the impact is very small (microseconds), the time step is also very small, assuming a large number of complete calculation cycles for the entire model. The time step is set in respect to the element size. The explicit solver has the advantage that it does not compute the stiffness matrix of the structure. This significantly reduces the computational time for transient dynamic regimes. The algorithm also allows the computation error control. The equations of motion express the conservation laws of mass, momentum, and energy in Lagrange coordinates. These, together with a given material model and a set of initial data (e.g., height from which the object falls or the initial velocity) and boundary conditions completely define the dynamic phenomenon to be solved.

The explicit solver uses a differential time integration scheme called the Leapfrog method. There is no requirement for iterations during time integration; no convergence checks are needed since the equations are decoupled. All nonlinearities including contact are included in the vector of internal forces. During the computation the internal energy, kinetic energy and contact energy were monitored (Fig. 5.10a). The effect of the mesh distortion, the Hourglass-effect, was also recorded. The low values of this parameter confirmed the good mesh quality.

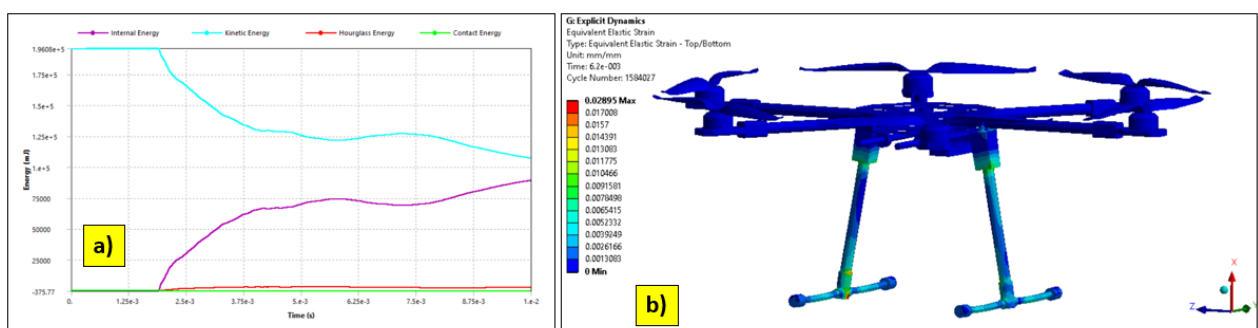


Fig. 5.10. a) Energy and Hourglass effect during calculations; b) Maximum equivalent elastic strain after impact

In Fig. 5.10b the equivalent elastic strain of the structural elements at impact are processed. It can be noticed that the highest strain value (2.8%) occurs on the vertical beams, in the jointed area with the horizontal supports, but also on the upper part of the vertical supports. These values mark the areas on the structure where impact damage will occur. Failure may occur if the fall height is higher, or if there are elements that can lead to strain augmentation such as terrain obstacles. As observed during the experiments, when the drone fell to the ground from a 3m height (Fig. 5.11a), the drone

structure didn't fail, but large displacements of the drone arms and large strains of the vertical supports occurred, as illustrated in Fig. 5.11b and 5.11c.

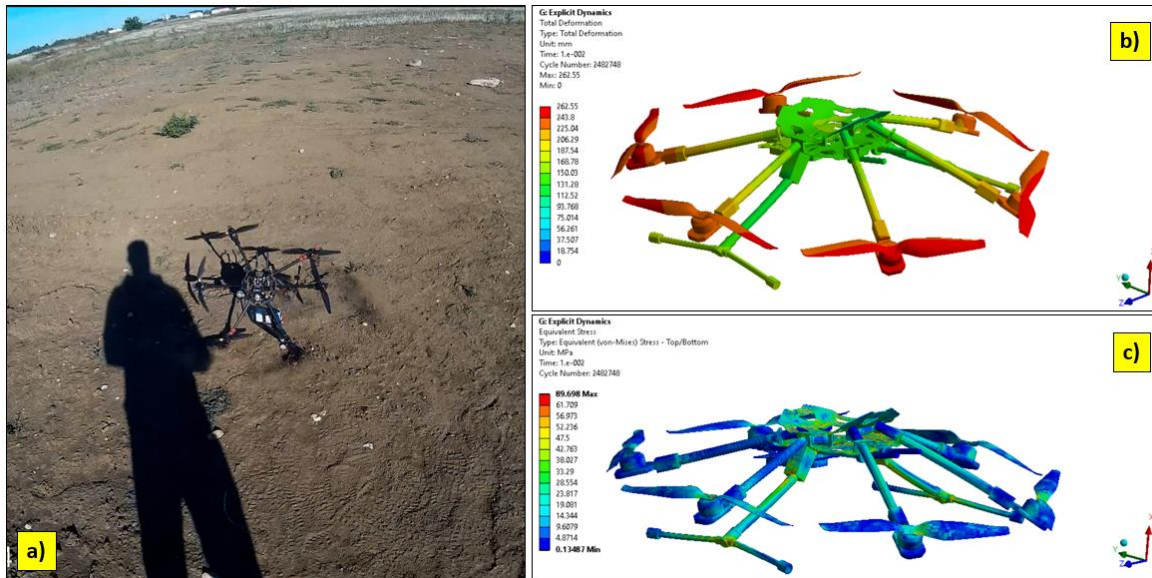


Fig. 5.11. a) Drone impact with the ground from a height of 3 m; b) Maximum total deformation at 0.1s after impact; c) Maximum von Mises equivalent stresses at 0.1s after impact

The maximum equivalent strain of 0.0289 are above the limit imposed on Epoxy Carbon Woven material (see Table 5.3). In order to be sure of these concluding remarks, the maximum deformation and stress for bending, compression and share were processed for the whole model. The maximum values were however recorded at a small number of points in the joint area, as shown in Fig. 5.10b. The large displacements are due to the design solution imposed by the presence of the 6 rotors. (Fig. 5.11b). The deformations of the rotors are very small. They have a robust construction, as can be seen in Fig. 5.11b and Fig. 5.11c processed at 0.1s after impact.

The post-impact stresses are small (Fig. 5.11c), and are tuned with the experiments, appropriately reflecting the drone's behavior at impact. The hexacopter deforms sharply but can be brought back to its original shape after impact, even if large deformations occur at impact (see maximum stresses in Table 5.2).

5.7 Conclusions, original contributions and published articles.

Conclusions

- CFD simulation is essential for understanding the aerodynamic stability, ensuring low power consumption, stable flight behavior at high wind speeds, and the capability to carry high payloads, i.e., increased drone range. All these are mandatory requirements when launching a new, powerful hexacopter on the market.
- the chapter presents a novel approach for modelling and simulation of a high-performance UAV system, considering the maximum rotational speed of the rotors and the influence of two strong wind scenarios acting in the horizontal plane.
- optimization of flight control parameters can be performed in connection with the results of the CFD analysis, namely: the lift forces on the rotors (Z-axis) as well as the forces in the Z and Y directions during hover. The study can be continued by considering the forward speed of the hexacopter and adjusting the rotational speeds of the propellers according to the experimental data.

- certain values of the lift and drag forces obtained from the simulations were calculated in Chapter 2, thus validating the simulation model used.
- Fig. 5.12a shows the graph of the drag force (0.552486 N) obtained from the CFD simulation on propeller 1 and the same value of this force calculated in Chapter 2 (0.5605 N). It can be seen that the error is 1.4% between the two methods.
- Fig. 5.12b depicts the plot of the absolute value, in mode, of the thrust force, (29.6611 N) obtained from the CFD simulation on propeller 3, respectively the same value of this force calculated in Chapter 2 (29.1486 N). It can be seen that the error is 1.72% between the two methods.
- in the case of modal analysis, the drive speeds that have to be avoided are marked red in Table 5.5 corresponding to the dominant natural frequencies of the rotors. These can lead to high stresses at the base of the rotors and could cause the yield strength to be exceeded or increase the fatigue of the propellers. Considering that the maneuvering speeds [58.34 Hz/3500rpm 66.67 Hz/4000rpm] are at least 24% higher than the dominant rotor eigenvalues, it can be assumed that no resonances can occur for the maneuvering regime of the hexacopter, but only for the stationary fixed-point regime. The maximum engine speeds for different flight conditions in the range [6500-8000 rpm] should be chosen with care, as resonances may occur in the 3rd and 4th rotor modes. If the natural frequencies of the drone are in the range of the operating frequencies the dynamic study should be continued with a frequency response analysis to determine the deformations and stresses at resonances in case of the hexacopter structural stability loss.

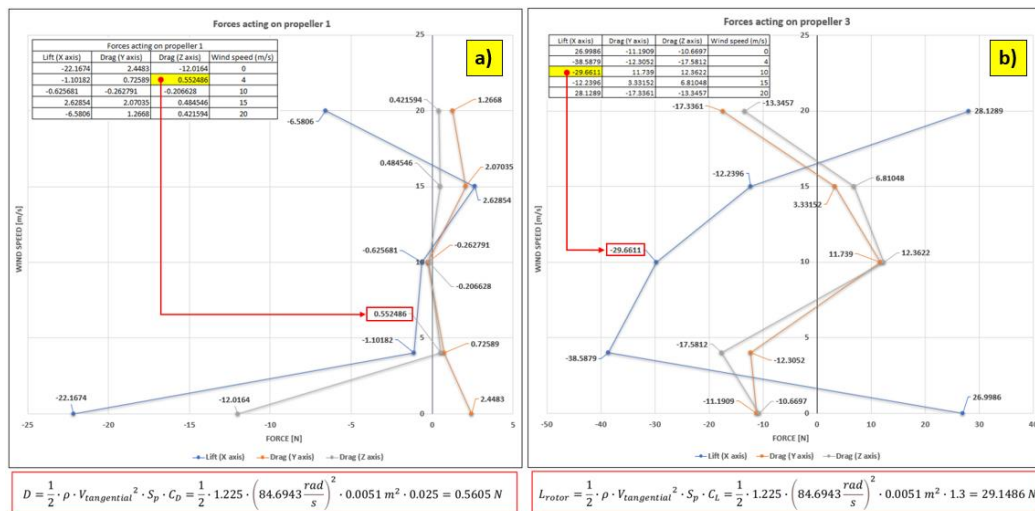


Fig. 5.12 a) Drag (numerical model vs. analytical calculation);
 b) Lift (numerical model vs. analytical calculation)

- impact simulations confirmed that when the hexacopter accidentally falls from a height of 20 m, the drone's structure undergoes significant deformation but is not destroyed and can be straightened and recovered.
- maximum deformations occur on the vertical and horizontal beams in the joint areas. Due to the fact that the maximum strains are not large, the hexacopter structure can be straightened, as observed during field experiments. In this study, it was not considered the hexacopter rigging. Only the behavior of the structural elements was studied.
- it was also observed that the rotors are much stiffer than the design found in recent articles and reported solutions [20], [21], confirming the robust design of the structural elements of the drone.

Original contributions:

- development of an original solution for extracting CFD parameters to obtain the necessary data for the control system.
- development of a synchronized calculation model for all FEM simulations
- verification of hexacopter stability by numerical methods
- verification of resonances
- verification of the impact behavior of the hexacopter.
- verification of the stability of the hexacopter drone during stationary flight maneuvers at a hover.
- validation of the FEM model by means of experiments and analytic computations.
- synchronization of analytical, experimental, and numerical results.
- use of the results obtained from the FEM study to optimize certain flight parameters (e.g., rotor speeds)

Published articles:

- **Stamate, M.A.**, Nicolescu, A.F., Pupăză, C., 2020, *Hexacopter model development using advanced simulation procedures*, Proceedings of the 34th International Business Information Management Association Conference (IBIMA) 4-5 November 2020, Granada, Spain, **ISBN: 978-0-9998551-5-7**, Innovation Management and Education Excellence through Vision 2020, Editor Khalid S. Soliman International Business Information Management Association (IBIMA), Conference Paper.
- **Stamate, M. A.**; Pupăză, C.; Nicolescu, F. A.; Moldoveanu, C. E. (2023) *Improvement of Hexacopter UAVs Attitude Parameters Employing Control and Decision Support Systems*. *Sensors*, Special Issue “Advanced Intelligent Control in Robots”, 23(3), IF 3.847, Q2, pp. 1446, <https://doi.org/10.3390/s23031446>.

Chapter 6. Final conclusions, original contributions, and directions for further research

6.1 Final conclusions

The Doctoral Thesis studied the category of hexacopter drones with the rotors arranged in a plane parallel to the ground (flat configuration). Due to their low-cost efficiency and numerous possibilities of being used in a wide range of civil, commercial, and industrial applications (inspection of power lines, inspection of road infrastructure, bridges, inspection of oil pipelines, inspection of industrial installations of strategic interest - oil refineries, nuclear power plants, inspection of disaster areas), multicopter unmanned aerial vehicles have already been the subject of study for more than a decade. Since then, numerous research studies have been carried out on the modelling and development of actuation, command and control systems and the development of various design solutions for them.

The State-of-art chapter has made a detailed review of research in the field of multicopter drones, on topics concerning: mathematical modelling, development, based on derived equations, of controllers and command and control systems for multicopter drones in general, with emphasis on hexacopter platforms; constructive solutions of hexacopter platforms; command and control of drones out of direct line-of-sight, some solutions to improve the autonomy of drones, respectively FEM/CFD analysis with the help of ANSYS FLUENT environment. *This study emphasized the gaps in the scientific literature regarding hexacopter dynamic stability.*

In the first part of Chapter 2 I outlined **the mechanical structure of the physically developed hexacopter**, together with its equipment with the avionics components for command and control of the drone, the video subsystem consisting of the gimbal with three-axis stabilization and the photo-video camera, respectively the radio control used by the operator to send commands from the ground to the hexacopter. At the end of the Thesis, the technical data sheets of these components are presented. In the second part of this section, **elements of mathematical modelling theory, based on matrix formalization, adapted for a hexacopter drone with rotors mounted in a plane parallel to the ground (flat configuration)**, mathematical relations describing the movements performed in three-dimensional space by the drone, forces and aerodynamic moments occurring during the flight were described. In the case of the hexacopter studied in this thesis, operation is based solely on the rotor speed variation. Fundamentals of rotor dynamics have been explained, in order to highlight the main forces and moments that develop on the propeller blade, respectively the geometrical elements of the propeller, which are required for further calculation presented in the third subchapter. **An analytical calculation algorithm** has been tuned with the realized hexacopter variant, starting from the input data of the hexacopter up to the results concerning the dynamic characteristics of the drone (lift force, drag force, moments) during the fixed-point hover flight. The study focuses exclusively on the behavior of the drone in stationary flight at a fixed point. These results are then employed in Chapter 5, in the FEM/CFD analysis of the hexacopter.

Chapter 3 presented in a new and practical approach, through comparative analyses, the performance of a hexacopter drone for different equipment variants using specialized online platforms: www.ecalc.ch/, www.omnicalculator.com/, <https://flyeval.com/>, www.drivecalc.de/. Starting from the hexacopter design developed in the thesis, four different equipment variants were analyzed in terms of battery, propellers or engines used. For comparison, simulations were also carried out for two variants of quadcopter and octocopter multicopter drones. With the help of theoretical computational elements, analytical calculations were performed to determine the theoretical performance of the hexacopter, mainly: flight range, thrust developed by the propeller, maximum rpm, motor efficiency, motor operating temperature, propeller efficiency. Some of the

parameters were determined using a propulsion system test stand, in particular the thrust force, the maximum rotor rpm and the operating temperature range of the motors.

Chapter 4 presents the results of tests carried out both in the laboratory and in the field, during engine start-stop maneuvers, to check that the engines are operating at optimum parameters, for stationary flight maneuvers at a fixed point, and roll, pitch and yaw maneuvers, when moving in different flight directions. The atmospheric conditions suitable for these types of activities were temperature: 10°-30°, wind speed: 1-2 m/s and no precipitation. The flight parameters extracted from the tests were analyzed and corrective actions were taken when necessary. All these tests were performed using the physically realized hexacopter platform employed in the thesis. Conclusions were drawn from the performed tests and **solutions for improving the drone parameters were found**. In order to analyze the flight range flights with the hexacopter equipped with batteries of different capacities were carried out.

Chapter 5 dealt with a FEM/CFD analysis of the hexacopter, aiming to improve its stability during stationary fixed-point flight. Thus, a CFD aerodynamic study of the hexacopter was performed. The computational model and the all the hypotheses considered were confirmed by comparing the simulation results with the analytically calculated forces. A perfect match was found. The modeling strategy and the mathematical model of the turbulences have also been described. The CFD simulation scenarios for five different wind speeds and directions were analyzed and the simulation results were examined from different perspectives. Subsequently, the results of the CFD simulation were transferred to the structural elements of the drone and the displacements, stresses, strains caused by the air-fillets were determined. A free vibration FEM study of the hexacopter with consequences for the stability of the drone was performed. It was also noticed the perfect synchronization of the natural frequencies obtained by simulation and those determined experimentally by means of a FFT analysis. Finally, a dynamic impact analysis was completed, and the results were analyzed in relation to the remarks during flight tests.

6.2 Original contributions

6.2.1 Theoretical contributions

- in Chapter 2, the **dynamic characteristics of the hexacopter** conceived in the thesis were determined, with a view to further study of the possibilities of improving the constructional-functional characteristics, a subject dealt with in Chapter 3.
- regarding the hexacopter equations of motion, **the forces and moments acting on the drone in hover flight were calculated**, without considering disturbing factors, in particular wind speed and direction. This issue has been studied separately in Chapter 5 in the FEM/CFD analysis.
- the computational model for the drone equations of motion study for climbing flight, forward flight, sideways flight, and rotational motion about the z-axis (gyration), respectively is formally written. Information of experimental nature, which is not the subject of this thesis can be further included.

6.2.2 Experimental contributions

A. Laboratory experiments

- tests carried out in the laboratory on the test stand determined the thrust force, the **maximum thrust force developed by the propeller-engine assembly was 1,718 Kgf**, resulting in a **maximum take-off mass that the hexacopter could lift of 10,308 kg**.
- tachometer tests determined the maximum rotor speed of 13418 rpm.
- due to the limitation of the hexacopter frame size (695 mm) it is not possible to mount propellers with diameters larger than 13.6" in order to obtain a higher thrust than the Tarot 1355 propellers.

B. Experiments on flight simulators

- **simulations with the *xcopterCalc* utility** were performed with the following input data for atmospheric conditions: temperature - 22°C, atmospheric pressure - 1012 hPa (759 mmHg). Further simulations were performed, changing the temperature conditions, implicitly atmospheric pressure, namely, temperature - 32°C, respectively atmospheric pressure - 1010 hPa (757.5 mmHg), at the same altitude above sea level of 85 m (Bucharest altitude). The reason why they were not presented in the thesis is that the differences arising from the simulations are not significant compared to those tested under initial conditions (22°C/759 mmHg/85 m).
- it was demonstrated that the simulations on **the platforms give 10-25% higher autonomy results than the results obtained in reality.**
- the test flights were carried out in stationary flight at a fixed point, with four LiPo batteries, in 4S1P configuration, nominal voltage 14.8V, of different capacities: 6600 mAh, 12000 mAh, 16000 mAh and 20000 mAh respectively. The simulations show the versions with 6600 mAh and 16000 mAh batteries.
- **the tests carried out proved an increase in the autonomy with a higher battery capacity.**
- although preliminary data were obtained for the octocopter and quadcopter in terms of their autonomy, other negative aspects of critical importance for their flight operation (high motor operating temperatures, low thrust-to-mass ratio, etc.) emerged, in safe conditions, confirming the statements made so far in this work (larger does not always mean more efficient).
- **other scenarios of equipping the drone with different battery variants have been studied** to increase the drone's capacity but equipping the drone with high mass batteries reduces the thrust-to-mass ratio so that at some point the drone can no longer be optimally controlled.
- an important aspect to mention here is the maximum flight distance of the drone (distance to the operator - home location). The data provided by the *xcopterCalc* utility have given the theoretical distances that the drone can fly, but in reality, the maximum distance is limited by the performance of the remote control (transmitter - Tx) and the receiver (Rx), i.e. the communication protocols between Tx - Rx on the one hand and Rx - flight controller (autopilot) on the other. According to the RadioLink manufacturer's specifications, the RadioLink AT10II radio control has a maximum range of up to 4 km. This parameter was not tested in the thesis.
- **methods to extend the maximum flight range have been identified, such as:** the following can be mentioned: acquisition of Tx with signal amplification, respectively, and perhaps the most efficient method, command, and control of the drone via 3G/4G, respectively 5G communication networks (currently under study).
- **research has been carried out to increase drone autonomy, as follows:**
- following the tests carried out with the HUT in the equipment shown in v.1, in the case of fixed-point flight, the hexacopter could be kept in the air for about 10 minutes. In comparison, in the case of the results provided in chapter 3, following the simulations performed with the *xcopterCalc* utility, the range of the drone was 12.4 minutes, showing an **increase of 20% of flight autonomy** and from the analytical calculation relationships presented in chap. 3 resulted in a range of 13.32 min, showing an **increase of 25% of flight autonomy**.
- in the case of the 12000 mAh battery the drone autonomy was 15.8 minutes, showing an **increase of 37%** and in the case of the 20000 mAh battery the autonomy was approximately 20 minutes, showing an **increase of 50%**, compared to the simulations performed with the 6600 mAh battery.
- after replacing the battery with a 16000 mAh battery / 4S2P / 14.8V / 4 cell configuration, in the case of hover flight the HUT could be kept in the air for about 18 minutes, showing an **increase of 45%**. In comparison, for the data provided by the *xcopterCalc* utility, the drone range was 20 minutes, showing an **increase of 50%** and, following the introduction of the

new battery capacity into the analytical calculation relationships in chap. 3, a range of 20.38 min resulted, showing an **increase of 51%**.

C. Field tests

- field tests with the hexacopter demonstrated that the drone operates with appropriate parameters during fixed-point flight maneuvers.
- it has been demonstrated that the performance of the drone can be improved by eliminating as far as possible the resonances introduced by the rotation of the motors using *dynamic harmonic notch filters*.
- for the operation of the drone beyond the visual line of sight (BVLOS), the necessary components been purchased, and ground and flight tests can be carried out to demonstrate their capability to control the hexacopter over 3G/4G LTE mobile networks. These include Raspberry Pi 3B board, IR camera + EO camera, 4G LTE modem.
- further drone flights in different flight regimes, both manual and autonomous, can be performed to test its limitations, but in this thesis only the behavior of the drone in stationary flight at a fixed point was studied. This maneuver was also studied in chapter 5, in the FEM/CFD analysis, where wind speed and direction were considered.

6.2.3 Contributions regarding FEM/CFD modelling and simulation.

- CFD simulation is essential for aerodynamic stability, ensuring low power consumption, stable flight behavior at high wind speeds, and the ability to carry high payloads, i.e., increased drone range, all of which are mandatory requirements when launching a new, powerful hexacopter on the market.
- **the FEM/CFD analysis presented a novel, original approach for modelling and simulating a high-performance UAV system**, considering the maximum rotational speed of the rotors and the influence of two strong wind scenarios acting in the horizontal plane.
- **it has been demonstrated that the optimization of flight control parameters can be performed in correlation with the results of CFD analysis, namely:** the lift forces on the rotors (Z-axis) as well as the forces in the Z and Y directions during hover. The study can be continued by considering the forward speed of the hexacopter and adjusting the rotational speeds of the propellers according to the experimental data.
- **the numerical FEM/CFD model was validated** by the values of lift and drag obtained from the FEM/CFD simulations, which were found to be consistent with the analytical calculated values. The error between the FEM results and the analytical values was 1.4-1.7%, which means that the simulation model was reliable.
- in the case of modal analysis, the drive motor speeds that have to be avoided were found, corresponding to the dominant natural frequencies of the rotors. Resonances can lead to high stresses at the base of the rotors and could cause the material yield strength to be exceeded or reduce the fatigue strength of the propellers. Considering that the maneuvering speeds [58.34 Hz/3500rpm 66.67 Hz/4000rpm] are at least 24% higher than the dominant eigenvalues of the rotors, it can be assumed that no resonances can occur for the maneuvering regime of the hexacopter, but only for the stationary fixed-point regime. The maximum engine speeds for different flight conditions in the range [6500-8000 rpm] should be chosen with care, as resonances may occur in the 3rd and 4th rotor modes. If the natural frequencies of the drone are in the range of the operational frequencies the dynamic study has to be continued with a frequency analysis, to determine the strain and stresses at resonance. This is a case of structural stability loss of the hexacopter.
- **drop test simulations confirmed that when the hexacopter accidentally falls from a height of 20 m, the drone's structure undergoes significant deformation but is not destroyed** and can be straightened and recovered. This was also observed during the field

tests. It was also observed that the rotors are much stiffer than in the solutions reported in recent articles and postings [89], [90], confirming the robust design of the structural elements of the drone.

6.3 Other original contributions

- development of the CAD model of the hexacopter drone prototype.
- development of the original design solution of the hexacopter platform, in version 1 of the equipment.
- employing a mathematical model based on matrix formalization, the equations of motion of the hexacopter and the rotor dynamics equations were determined.
- the analytical calculation methodology was tuned to the mechanical structure of the hexacopter developed in the thesis, as follows:
 - the experimental mass that an engine can lift.
 - the maximum rotor speeds.
 - the maximum theoretical mass that an engine, i.e., the hexacopter, can lift has been determined.
 - lift coefficient CL and drag coefficient CD - were obtained from the NACA 4412 (naca4412-il) airfoil polar for an incidence angle of 10° . The NACA 4412 airfoil (naca4412-il) has similar characteristics to the APC12 airfoil of an APC 13x55 MR propeller, which is constructively similar to the Tarot 1355 propeller with which the hexacopter is equipped (diameter - 13", pitch - 5.5").
 - lift force and drag force were determined analytically.
 - total drag coefficient CX and power coefficient CP were determined analytically, based on previously obtained CL and CD .
 - the (theoretical) rate of climb of the hexacopter at ground level was determined analytically.
 - the forces and moments acting on the rotor during hover flight of the drone were determined analytically.
 - the maximum thrust force developed by the motor-propeller assembly was determined experimentally using the Mayatech MT10PRO 10KG test stand.
 - the maximum rotor speed was experimentally determined using the tachometer.
 - the operating temperature range of the motors was experimentally determined using the FLIR E86 thermal imaging camera.
 - the technical characteristics of the propulsion system components and their compatibility aspects were presented, including features related to the sizing of the drone structure.
 - analytical calculations of the range of the hexacopter, with different LiPo battery capacities.
 - simulations of hexacopter performance compared to a quadcopter or octocopter variant were performed using specialized online platforms.
 - the flight autonomy of the hexacopter was determined conducting field flights with three different battery capacities.
 - the practical implementation of the hexacopter platform in two versions, equipped with avionics components for command and control of the drone, including a system for transmitting and receiving drone-ground-drone telemetry data has been completed.
 - the hexacopter has been equipped with a video transmission-reception system.
 - laboratory, ground, and flight tests to verify the compatibility of the components and the optimal operation of the drone were performed.
 - parameter adjustment for a stable operation of the drone during hover flight were done.
 - development of an original solution for extracting CFD parameters to obtain the necessary data for the control system has been accomplished.
 - development of a synchronized calculation model for all FEM analyses.
 - verification of hexacopter stability by numerical methods.

- resonance verification.
- verification of the impact behavior of the hexacopter.
- ensuring the stability of the hexacopter drone during stationary flight maneuvers at a fixed point.
- the development of a complete and complex simulation model for all types of CAE analysis.
- validation of the FEM computation model.
- synchronization of analytical, experimental, and numerical results.
- the use of the simulation results to optimize certain flight parameters (e.g., rotor speeds).

6.4 Future research topics

- the implementation of the command-and-control chain of the hexacopter via 3G UMTS/4G LTE/5G NR mobile phone networks for operation beyond visual line-of-sight (BVLOS).
- study of other equipment variants with different types of propellers, engines, speed controllers to identify the optimal hexacopter equipment variant according to the desired purpose.
- study of other types of mechanical structures of hexacopter platforms with SVTOL (Short Vertical Takeoff and Landing) capabilities, to increase the carrying capacity of large payloads.
- study of other methods for improving flight autonomy by equipping with hybrid propulsion systems (electric + thermal engine), thermal engine or other innovative battery technologies.

References

- [1] Airfoil Tools, accessed in august 2022, link: <http://airfoiltools.com/airfoil/details?airfoil=naca4412-il#polars>.
- [2] APC Propellers, accessed in august 2022, link: <https://www.apcprop.com/technical-information/performance-data/>.
- [3] Ardupilot Diagnosing Logs, accessed in august 2022, link: <https://ardupilot.org/planner/docs/common-diagnosing-problems-using-logs.html>
- [4] Ardupilot Mavexplorer, accessed in august 2022, link: <https://ardupilot.org/dev/docs/using-mavexplorer-for-log-analysis.html>.
- [5] Bershadsky, D., Haviland, S. (2016) *Electric Multirotor Propulsion System Sizing for Performance Prediction and Design Optimization*, AIAA SciTech, 4-8 January 2016, San Diego, California, USA, 57th AIAA/ASCE/AHS/ASC Structures, Structural Dynamics, and Materials Conference, <http://arc.aiaa.org>, DOI: 10.2514/6.2016-0581.
- [6] Biczyski, M., Sehab, R., Whidborne, J. F., Krebs, G., Luk, P. (2020) *Multirotor Sizing Methodology with Flight Time Estimation*, Hindawi Journal of Advanced Transportation Volume 2020, Article ID 9689604, 14 pages, <https://doi.org/10.1155/2020/9689604>.
- [7] CFD Israel, accessed in august 2022, link: <https://cfdisrael.blog/2018/04/23/understanding-realizability-for-the-k-%CE%B5-turbulence-model/>.
- [8] Courant, R., Friedrichs, K., Lewy, H. (March 1967), "On the partial difference equations of mathematical physics", *IBM Journal of Research and Development*, **11** (2): 215234, [Bibcode:1967IBMJ...11..215C](https://doi.org/10.1147/rd.112.0215), [doi:10.1147/rd.112.0215](https://doi.org/10.1147/rd.112.0215), [MR 0213764](https://doi.org/10.1147/rd.112.0215), [Zbl 0145.40402](https://doi.org/10.1147/rd.112.0215).
- [9] Dai, X., Quan, Q., Ren, J., Cai, K. Y. (2018) *An Analytical Design Optimization Method for Electric Propulsion Systems of Multicopter UAVs with Desired Hovering Endurance*, DOI 10.1109/TMECH.2019.2890901, IEEE/ASME Transactions on Mechatronics, 1083-4435 (c) 2018 IEEE.
- [10] Dai, X., Quan, Q., Ren, J., Cai, K. Y. (2018), *Efficiency Optimization and Component Selection for Propulsion Systems of Electric Multicopters*, DOI 10.1109/TIE.2018.2885715, IEEE Transactions on Industrial Electronics, 0278-0046 (c) 2018 IEEE.
- [11] Drivecalc, accessed in august 2022, link: <http://drivecalc.de/>
- [12] Flyeval, accessed in 2022, link: <https://flyeval.com/>.
- [13] Fogelberg, J. (2013) *Navigation and Autonomous Control of a Hexacopter in Indoor Environments*, Lund University, Department of Automatic Control.
- [14] Gatti, M., Ph.D. (2017) *Complete Preliminary Design Methodology for Electric Multirotor*, Journal of Aerospace Engineering, ASCE, ISSN 0893-1321, DOI: 10.1061/(ASCE)AS.1943-5525.0000752.
- [15] Highend, accessed in august 2022, link: <https://microlinearactuator.com/brushed-vs-brushless-dc-motors/>.
- [16] Howtomechatronics, accessed in august 2022, link: <https://howtomechatronics.com/how-it-works/how-brushless-motor-and-esc-work/>.
- [17] Lei, Y., Cheng, Mingxin (2019), *Aerodynamic Performance of Hex-Rotor UAV Considering the Horizontal Airflow*, in Applied Sciences, MDPI, 9, 4797; doi: 10.3390/app9224797.
- [18] Omnicalculator, accessed in august 2022, link: <https://www.omnicalculator.com/other/drone-flight-time#drone-flight-time-formula>.
- [19] Rotaru, C. (2009) *Aerodinamică-Elemente teoretice și aplicații*, Editura Academiei Tehnice Militare, ISBN 978- 973-640-186-2, 272 pagini.
- [20] Simscale Drop Test, accessed in august 2022, link: <https://www.simscale.com/forum/t/drop-test-of-a-drone/64430>.

- [21] Simscale Webinars, accessed in august 2022, link: <https://www.simscale.com/webinars-workshops/get-into-the-drone-simulation-zone/>.
- [22] **Stamate, M. A.**, Nicolescu, A. F. (2017) *Conceptual and functional study of a multicopter drone prototype used for security applications*, *Research and Science Today, Supplement No. 2/2017*, p. 155-164, ISSN-p: 2247-4455 / ISSN-e: 2285-9632 / ISSN-e supplement: 2344-0007.
- [23] **Stamate, M. A.**, Nicolescu, A. F., Pupăză, C. (2017) *Mathematical model of a multi-rotor drone prototype and calculation algorithm for motor selection*, *Proceedings in Manufacturing Systems*, Volume 12, Issue 3, 2017, p. 119-128, ISSN 2067-9238.
- [24] **Stamate, M. A.**, Nicolescu, A. F., Pupăză, C. (2018), *Study regarding flight autonomy estimation for hexacopter drones in various equipment configurations*, *Proceedings in Manufacturing Systems*, Volume 13, Issue 1, 2018, ISSN 2067-9238.
- [25] **Stamate, M.A.**, Nicolescu, A.F., Pupăză, C. (2020) - *Hexacopter model development using advanced simulation procedures*, *Proceedings of the 314th International Business Information Management Association Conference (IBIMA) 4-5 November 2020, Granada, Spain, ISBN: 978-0-9998551-5-7*, Innovation Management and Education Excellence through Vision 2020, Editor Khalid S. Soliman International Business Information Management Association (IBIMA), Conference Paper
- [26] **Stamate, M. A.**; Pupăză, C.; Nicolescu, F. A.; Moldoveanu, C. E. (2023) *Improvement of Hexacopter UAVs Attitude Parameters Employing Control and Decision Support Systems*. *Sensors*, Special Issue "Advanced Intelligent Control in Robots", 23(3), IF 3.847, Q2, pp. 1446, <https://doi.org/10.3390/s23031446>.
- [27] Suprpto, B. Y., Heryanto, A., Suprijono, H., Muliadi, J., Kusumoputro, B. (2017) *Design and Development of Heavy-lift Hexacopter for Heavy Payload*, 2017 International Seminar on Application for Technology of information and communication (iSemantic), p. 242-247, doi: 10.1109/isemantic.2017.8251877.
- [28] Tarotrc, accessed in august 2022, link: <http://www.tarotrc.com/>.
- [29] Tytorobotics Lab Coursewares, accessed in august 2022, link: <https://www.tytorobotics.com/pages/lab-coursewares>.
- [30] xcopterCalc, accessed in august 2022, link : <https://www.ecalc.ch/xcopterCalc.php>.
- [31] Zheng, Y., Yang, S., Liu, X., Wang, J., Norton, T., Chen, J., Tan, Y. (2018), *The computational fluid dynamic modeling of downwash flow field for a six-rotor UAV*, *Frontiers of Agricultural Science and Engineering*, 5(2), p. 159-167.